Machine Learning in Ocean Applications: Wave Prediction for Advanced Controls of Renewable Energy and Modeling Nonlinear Viscous Hydrodynamics

by

Yu Ma

B.S., Shanghai Jiao Tong University (2011)
S.M., Shanghai Jiao Tong University (2014)

Submitted to the Department of Mechanical Engineering
in partial fulfillment of the requirements for the degree of

Doctor of Philosophy in Mechanical Engineering

at the

MASSACHUSETTS INSTITUTE OF TECHNOLOGY

May 2020

Author .....
Department of Mechanical Engineering
May 1, 2020

Certified by .....
Paul D. Sclavounos
Professor of Mechanical Engineering
Thesis Supervisor

Accepted by .....
Nicolas Hadjiconstantinou
Chairman, Department Committee on Graduate Theses

Machine Learning in Ocean Applications: Wave Prediction for Advanced Controls of Renewable Energy and Modeling Nonlinear Viscous Hydrodynamics

by

Yu Ma

Submitted to the Department of Mechanical Engineering
on May 1, 2020, in partial fulfillment of the
requirements for the degree of
Doctor of Philosophy in Mechanical Engineering

Abstract

Many conventional problems in ocean engineering remain challenging due to the stochastic nature of ocean waves, viscous effects of the flow, nonlinear resonance, etc., and the combination of these factors. Data-driven techniques is an prospective approach complementary to traditional methods to model physical problems since data from experiments, field tests or high-fidelity simulations are mostly informative about actual physical systems. Machine learning algorithms, especially kernel based methods have very good generalization capability as well as statistical inference. This thesis targets to establish a framework that how we can use data from real-time measurements or data gathered from experiments and field tests and simulations to provide an alternative approach for physical modeling or practical engineering solutions. In this thesis, we mainly target two different types of problems–mapping highly nonlinear physical relations and predicting time series, to prove the feasibility of such a framework.

More specifically, one problem is the short-term wave prediction based on real-time measurements and its application to the advanced controls of renewable energy. The other one is the modeling of nonlinear viscous hydrodynamic loads of ships and offshore platforms. The Support Vector Machines (SVM) is used in solving both the problems. In the thesis, the SVM regression model are developed for the real-time short-term forecast of wave elevations and wave excitation forces. Optimal controllers aiming to reduce the structural loads or optimize energy capture with the knowledge of the forecasted wave force are established for offshore floating wind turbines and wave energy converters. A series of CFD simulations of a rectangular barge with bilge keels are conducted and validated, along with the experiment data of a fixed offshore cylindrical platform, to serve as the baseline data set to model the nonlinear viscous hydrodynamic loads. Using the wave elevations and ship roll kinematics as features, the SVM regression models are trained and tested to predict the nonlinear hydrodynamic loads. The influence of the stochastic effect and different

feature selections and kernel selections are discussed in the thesis as well.

Key words: Machine learning, SVM regression, short-term forecast, model predictive control, nonlinear viscous hydrodynamic loads

Thesis Supervisor: Paul D. Sclavounos
Title: Professor of Mechanical Engineering

Acknowledgments

I would like to express my sincere gratitude to my PhD advisor, Professor Paul D. Sclavounos, for his guidance and support during the past six years. His passion, talents and willingness to explore new areas, are all great inspiration to me. It has been great pleasure working with him and completed the research that we aimed. More importantly, he has inspired and guided me to be a better researcher with the passion, skills and vision towards our professon. Thank you and I am truly honored to have you as my advisor.

I am also sincerely grateful to my two committee members, Professor Pierre Lermusiaux and Professor Thomas Peacock. They have been very supportive to my research and given valuable advises to me. The committed meetings with them have been very good experiences along the way to this final thesis.

Many thanks to my labmates, Dr. Godian Chan, Dr. Yu Zhang and David F. Larson. They have made life in the Laboratory of Ship and Platform Flow very pleasant. The heated research discussions, the small chats and laughs, are all valuable memories to keep. Six years seem to be a very long yet very short journey. I cannot get through this during my ups and downs without the companion of my friends. Thank you all for being there, in MIT, or thousands of miles away.

I cannot express my gratitude and love enough to my parents, Yajing Niu and Lingxun Ma, for their unconditional love and endless support. They have always respected each decision of my life, and supported me through the way. They always have confidence in me, even when I was doubting myself. They are the source of my inner strength. My gratefulness and love to them are truly beyond words.

Finally, I dedicate this thesis to my beloved grandma in heaven. She was the most kind and loving person I have ever known. I know she would be very proud of me. May she rest in peace.

Contents

List of Figures

List of Tables

Chapter 1

Introduction

1.1 Data-driven methods in physical problems

Many conventional problems in ocean engineering remain challenging due to the stochastic nature of ocean waves, viscous effects of the flow, nonlinear resonance, etc., and the combination of these factors. Traditionally, to solve these problems, we mostly would explore theoretical and numerical methods and conduct experiments to understand the physics and provide engineering solutions. While traditional development of fluid/fluid-structure models has focused on incorporating more physics to improve model accuracy and predictive capabilities, an alternative approach is raising up recently, that is to utilize data directly [84]. Data-driven modeling is considered as a prospective approach since data from experiments, field tests or high-fidelity simulations are mostly informative about the actual physical systems.

The physical-related problems we are interested in can be categorized into two types, which are mapping highly nonlinear physical relations and predicting time series. Machine learning algorithms, either kernel based methods or deep neural networks, have very good generalization capability as well as statistical inference that makes them good at solving these types of problems. Raissi et. al. [71] used neural network to reconstruct the velocity and pressure field for vortex induced vibrations. Zhou et.al. [91] used Support Vector Machines (SVM) to predict wind velocity based on measurements. The exploit of machine learning methods in physical-related

problems can be also found in the works of many researchers through many domains [23] [70] [47].

Among various machine learning techniques mentioned above, SVM stands out as one of the most widely used algorithms to establish models connecting pertinent features to physical quantities of interest [18] [76]. The essence of SVM algorithms is to use kernels instead of an explicit set of basis functions in order to establish a more compact and generalized model based upon a set of explanatory variables or features. The selected kernel with optimized hyperparameters encodes the covariance structure between the features, which forms the basis of the learning algorithm that relates the quantity being modeled to the features, from the perspective of statistical learning theory.

1.2 Short-term wave prediction and model predictive control in renewable energy

The ocean provides enormous sources of renewable energy, among which two of the promising kind are ocean wind and wave energy (Fig.1-1, Fig.1-2). Research on ocean wind and wave energy systems has drawn a lot of attention over the past decades. One important element of the developing research is the control system. The development of advanced control algorithms for offshore wind and wave energy system focuses on two objectives, energy capture and load mitigation.

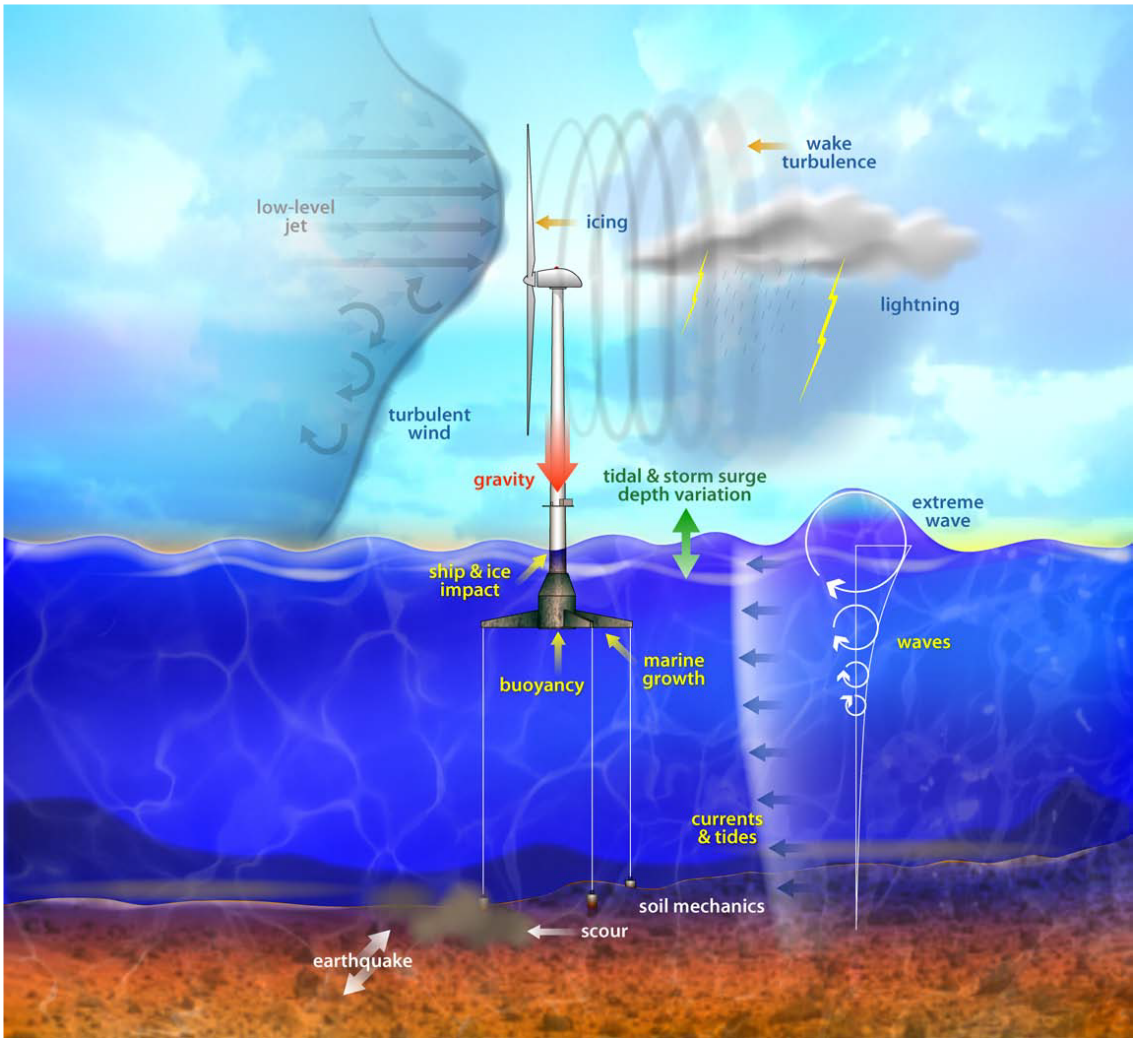

Figure 1-1: Offshore Floating Wind Turbine (OFWT): Integrated aero-hydro-elastic-servo system [51]

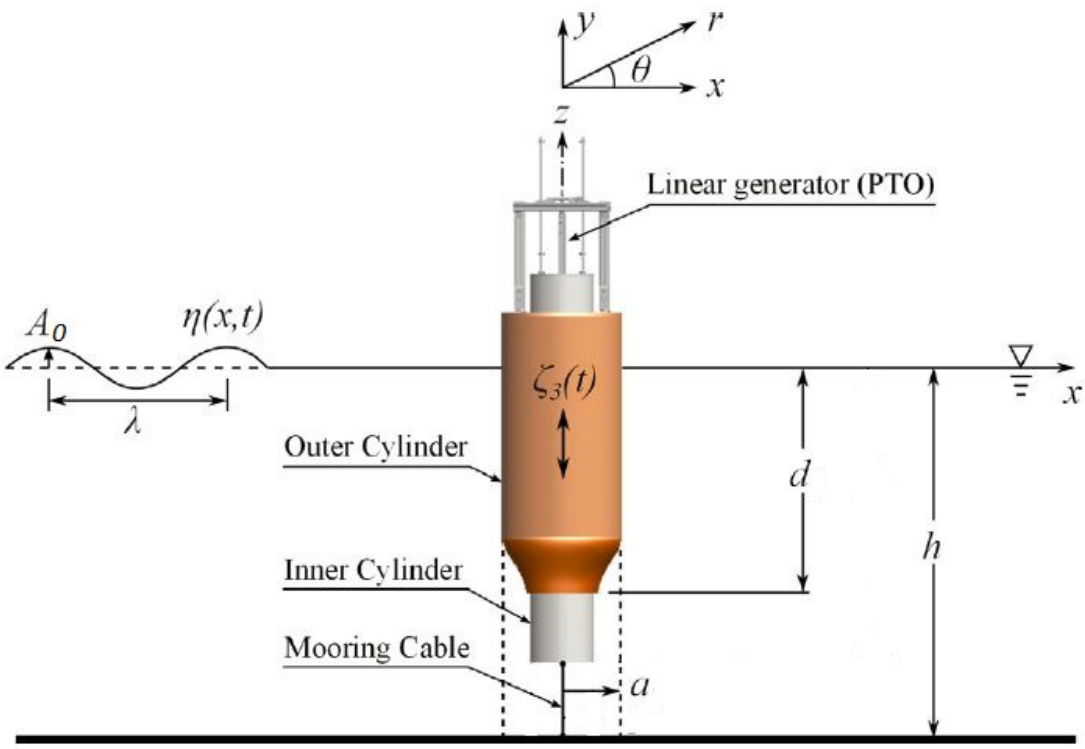

Figure 1-2: Schematic of an oscillating heaving point absorber [90]

Several advanced control approaches were proposed in the last decades to achieve load reduction or power optimization of onshore and offshore wind turbines. One promising approach is to use feedforward or model predictive control (MPC) to improve disturbance rejection. Extensive studies have been done on model predictive controls on onshore and offshore wind turbines with regard to wind induced loading [39] [41] [69]. These studies have shown that, with a model predictive controller, the fatigue loads at critical structural sections can be significantly reduced when wind speed predictions are provided to the controller. So far, the majority of studies on advanced control algorithms targets the mitigation of loads induced by incoming wind speed. For offshore floating wind turbines, wave excitation force is also a dominant persistent disturbance that excites dynamic and structural responses. Control issues for modelling floating wind turbines were mentioned earlier with regard to the coupling between the pitch controller and the platform motion [87] [43]. Without

adjustment, such coupling effects would cause negatively damped responses thus resulting in instability of the system. However, little research has been done aiming at resisting wave disturbance using similar advanced control approaches as MPC.

As for wave energy converters, the most concerning issue is to achieve optimal energy extraction under irregular sea states while reducing the risk of device damage, in which the control algorithm plays a critical role. Several studies have been carried out to explore the performance of model predictive controls on wave energy converters [32] [11] [17]. These studies have shown that it is possible to develop a controller that maximizes the energy capture within constraints if it is provided with a sufficiently accurate real-time prediction of the wave excitation force. Price et al. [68] discussed the need for knowledge of the future wave excitation forces in computation of the optimal control command.

As stated, the design of advanced model predictive controls requires a sufficiently accurate prediction of the wave elevations or wave excitation forces. Efforts have been made to predict wave elevations or wave excitation forces by various approaches. Hals et al. [32] used the augmented Kalman filter with a simple damped harmonic oscillator to model and predict the wave forces with a forecast horizon 2.2 seconds under an irregular sea state for their model predictive controller. Fusco & Ringwood [29] compared four different approaches for predicting short-term wave elevations, which were cyclical models, sinusoidal extrapolation with the Extended Kalman filter, autoregressive models, and the neutral networks. The prediction models were validated using field measurements from two sites. Casanovas [13] compared the performance of autoregressive models and ESPRIT (Estimation of Signal Parameters via Rotational Invariance Techniques) models to forecast wave elevations.

Although some work has been done on this issue, there are still gaps to achieve real-time implementation. Hals et al. [32] stated that the forecast horizon and accuracy had a great impact on the overall performance of the MPC algorithm. The augmented Kalman filter did not fulfil such requirements very well even though it was tested by simulated sea states. Fusco & Ringwood [29] used ideal non-causal filters to preprocess the raw wave elevations to get a better forecast performance which could

not be implemented in real-time. Casanovas [13] validated the AR and ESPRIT model using simulated wave elevations which contained no noise thus much easier to predict.

Therefore, more refined methods to predict real-time wave elevations and wave excitation forces need to be developed and validated. Also, the performance of optimal control algorithms for offshore floating wind turbines and wave energy converters need to be validated under real-time prediction of wave elevations or wave excitation forces instead of an assumption of perfect prediction.

1.3 Modeling of nonlinear hydrodynamic loads

Ships and offshore platforms are subject to the hydrodynamics loads excited by ocean waves. The modeling of hydrodynamics loads has developed for decades to understand the relevant physics and predict the wave-structure interaction. Linear frequency-domain analysis derived from the panel methods based on potential flow theory is one of the most popular tools because of its efficiency, reliability and conciseness [58]. However, in many scenarios, the nonlinear and viscous effects are not negligible due to large-amplitude body motions, nonlinear resonance and flow separations etc. To better model the nonlinear hydrodynamic loads for ships and offshore platforms, different methods have been developed using both potential flow theory and computational fluid dynamics (CFD).

For some problems where the nonlinearity is largely excited due to large-amplitude body motions or steep large-amplitude waves, the potential flow theory is sufficient as it is still dominated by inertia rather than viscous effects. The potential flow theory solves the boundary value problem (BVP) by applying the nonlinear boundary conditions on the free surface or the body wetted surface or both [75]. The most common computational method used in solving the problem is via boundary element methods (BEM) which can be formulated in two different ways: the Rankine panel method or the transient free surface Green function method. (e.g. [7]).

After having solved the fluid flow solution upon the nonlinear boundary conditions

for the wave-body interaction problems, the hydrodynamic pressure over the body surface can be obtained by the Bernoulli equation. However, since the direct integration of the pressure over the instantaneous body surface involves a partial temporal derivative and spatial derivative of the velocity potential over the body surface, it is usually challenging in terms of the computational cost [44]. Sclavounos [75] proposed another approach by applying the momentum conservation principle that does not involve the temporal and spatial derivatives of the potential to get the nonlinear hydrodynamic force and moment on the body. In addition, for slender bodies, the total hydrodynamic loads are usually corrected by Morison's equation to take account of the viscous effects [73].

These methods require the discretization of the body surface and some also require the discretization of the free surface, which can be very demanding in both delicate numerical treatment and computational cost. Meanwhile, depending on the surface and body boundary conditions imposed, the numerical schemes can only take account contributions from certain nonlinear aspects to a certain order. Therefore, establishing a direct generalized model for nonlinear wave loads from a data-driven perspective could be very prospective in terms of accuracy and efficiency, which could be further applied in various design and operation practises.

On the other hand, for some problems, the viscous effects are non-negligible and more complicated to model. Among these problems, the ship roll hydrodynamics is a classical topic. It is highly nonlinear and subjected to significant viscous effects arising from eddies shed from the hull, lift effect in case of a ship advancing with a forward speed and bilge keel damping, etc. [26] (Figure 1-3). While all other degrees of freedom motion can be predicted well by potential flow theory, the estimation of ship roll hydrodynamics remains a challenge. Numerous experiments and CFD simulations have been conducted to study the flow patterns and the modeling of roll hydrodynamics. Since experiments and CFD simulations are expensive in terms of budget, computational resources and computational time, such experiments and CFD simulations are mostly combined with existing semi-empirical models for further design purposes and the prediction of motion responses [86] [38] [54] [53]. The semi-

empirical models are usually based on polynomial approximations that connect the nonlinear damping and restoring forces with the ship velocities and displacements.

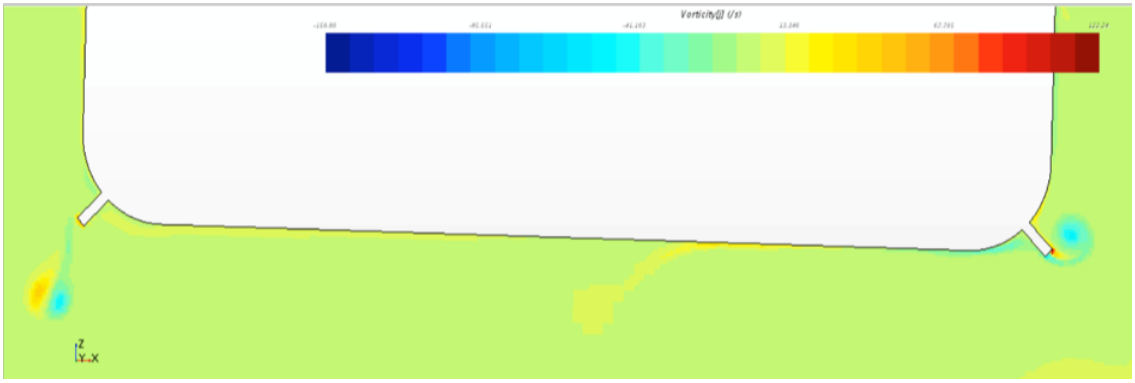

Figure 1-3: Vorticity around bilge keels

However, as discussed by many researchers, the widely-used semi-empirical models with constant coefficents and linear or quadratic damping terms cannot fully capture the characteristics of ship roll hydrodynamics. Memory effects, the behavior under a large roll amplitude, the stochastic nature of irregular wave conditions, etc., need to be carefully taken into account. Towards this objective, Bassler [6] proposed a piece-wise damping model to better predict large amplitude roll damping. However, we still lack a more general model that takes into account all pertinent features of this problem.

1.4 Outline of current work

In the present work, we are interested in establishing such a framework that how we can use data from real-time measurements or data gathered from experiments and simulations to provide an alternative SVM model for physical modeling and practical engineering solutions. This thesis will focus on two different types of problems in the ocean applications to prove the feasibility of such a framework: the short-term wave prediction based on real-time measurements and its application to the advanced controls of renewable energy; the modeling of nonlinear hydrodynamics of ships and offshore platforms.

The first contribution of this thesis is to fill the gaps in designing advanced model predictive controls taking the wave loading as targeted persistent disturbances for offshore wind and wave energy systems. To achieve this, it involves two tasks. The first one is the development of a SVM regression model for real-time short-term forecast of wave elevations and wave excitation forces [48]. The model is trained and validated using measurements from a wave tank test, which is considered as a good representative of the real ocean measurements. The SVM regression model is compared with a conventional subspace method ESPRIT and proved to have better generalization capability and consistently better performance.

Following the successful prediction of the wave force over a finite horizon into the future, two model predictive control algorithms are then designed for the offshore floating turbines and wave energy converters separately since they target different objectives and have different system characteristics.

For the offshore floating wind turbines, the model predictive control is formed as a finite-horizon linear-quadratic-regulator (LQR) controller based on its system characteristics. The controller is designed to reduce the fore-aft tower base bending moment, especially the components excited by the wave force. In the thesis, it has demonstrated that the performance of this optimal control is effective and robust for the aimed load reduction comparing to the baseline speed regulator.

For the wave energy converters, the objective is to maximize the energy capture under stochastic seas. A state-space model is derived for the causal impulse response function of the radiation problem and its non-causal counterpart in the diffraction problem. The objective along with the system dynamics as constraints have formed a convex quadratic programming problem to be optimized [77]. The cumulative power of the wave energy converter under two different sea states are shown increased significantly under this optimal control.

The second major contribution of this thesis is to provide an alternative approach using SVM regression to model the nonlinear hydrodynamic loads of ships and offshore platforms.

In the thesis, a series of CFD simulations of a rectangular barge with bilge keels

are conducted and validated to provide a baseline data set used to establish the SVM regression model. Using the wave elevations and ship roll kinematics as features, an SVM regression model is trained and tested to predict the nonlinear hydrodynamic loads. Furthermore, by comparing the two models using training data from free decay tests and from irregular wave cases, the influence of the stochastic effect is discussed. The study also compares and discusses the different feature and kernel selections used in the model.

Other than CFD simulations, experimental data are also a reliable source used to build the data-driven model. A set of experiments for a shallow water bottom fixed cylinder are studied in the thesis to develop the SVM regression model of the nonlinear wave loads. Different feature and target selections are discussed as well.

To summarize, the reminder of this thesis is organized as follows. In Chapter 2, the SVM regression methodology is thoroughly discussed. In Chapter 3, the study on short-term wave prediction is demonstrated. Following that, Chapter 4 and Chapter 5 show the modeling and performance of the model predictive control for offshore floating wind turbines and wave energy converters. Chapter 6 is devoted to the modeling of the nonlinear viscous ship roll hydrodynamics. The modeling of the nonlinear wave loads of a fixed cylinder is described in Chapter 7. The overall conclusions and possible future work are described in Chapter 8.

Chapter 2

Support Vector Machines Regression

2.1 Introduction

Support vector machines are supervised learning models which can be used in various of classification and regression problems [34] [33]. The original SVM was first proposed to construct a linear classifier based on the maximum-margin hyperplane principle and then extended to nonlinear classifiers using the kernel trick [9] [8]. Later it was introduced to solve regression problems as well [21].

SVM regression is a powerful machine learning method which has been successfully used for time-series prediction in various fields [81] [91] [72]. It uses a hypothesis space of linear functions in a high dimensional feature space, which is trained with a learning algorithm from optimization theory that implements a learning bias derived from statistical learning theory. An important property of support vector machines is that the determination of the model parameters corresponds to a convex optimization problem, and so any local solution is also a global optimum [8]. Following the general work of SVM, Suykens and Vandewalle [79] also proposed a least-squares version of SVM, which uses equality constraints and leads to solving a set of linear equations instead of a convex quadratic programming (QP) problem of classical SVM algorithms.

In this chapter, the theory of least-squares support vector machines regression is introduced, which would be applied to solve the proposed problems in ocean

application in the following chapters. Cross-validation is briefly described to optimize the hyperparameters. A more thorough discussion on general kernel selection is also included in this chapter.

2.2 Mathematical formulation of least-squares support vector machines regression

The LS-SVM regression model assumes the following functional dependence of a physical quantity y on relevant K-dimensional vector features $\mathbf{x} = (x_1, x_2, ..., x_K)^T$

$$y_f = \mathbf{w}^T \phi(\mathbf{x}) + b \tag{2.1}$$

The series expansion in (2.1) involves the unknown weight vector $\mathbf{w} = (w_1, w_2, ..., w_M)^T$ and vector basis functions $\phi(\mathbf{x}) = (\phi_1(\mathbf{x}), \phi_2(\mathbf{x}), ..., \phi_M(\mathbf{x}))$. The number of the basis functions M is a priori unknown and may be infinite. The constant b is the bias term. Given a sample of training data $\{(\mathbf{x_i}, y_i)\}_{i=1}^N$, LS-SVM determines the optimal weight vector and bias term by minimizing the cost function R:

$$\min_{\mathbf{w},\mathbf{e}} R(\mathbf{w}, \mathbf{e}) = \frac{1}{2}\|\mathbf{w}\|^2 + \frac{1}{2}\gamma\|\mathbf{e}\|^2 \tag{2.2}$$

subject to the equality constraints:

$$y_i = \mathbf{w}^T \phi(\mathbf{x_i}) + b + e_i, \quad i = 1, 2, ..., N \tag{2.3}$$

Where, $\|\cdot\|$ denotes the Euclidean norm. γ is the regularization parameter which controls the trade-off between the bias and variance of the LS-SVM model. $\mathbf{e}$ is the error vector, $\mathbf{e} = (e_1, e_2, ..., e_N)^T$.

The equations (2.2)-(2.3) form a standard optimization problem with equality

constraints. The Lagrangian of such a problem is:

$$L(\mathbf{w}, b, \mathbf{e}, \lambda) = R(\mathbf{w}, \mathbf{e}) - \sum_{i=1}^{N} \lambda_i (\mathbf{w}^T \phi(\mathbf{x_i}) + b + e_i - y_i) \tag{2.4}$$

Where, λ_i are the Lagrange multipliers.

According to the Karush-Kuhn-Tucker Theorem, the conditions of optimality are:

$$\begin{aligned}
&\frac{\partial L}{\partial w} = 0 \rightarrow \mathbf{w} = \sum_{i=1}^{N} \lambda_i \phi(\mathbf{x_i}) \\
&\frac{\partial L}{\partial b} = 0 \rightarrow \sum_{i=1}^{N} \lambda_i = 0 \\
&\frac{\partial L}{\partial e_i} = 0 \rightarrow \lambda_i = \gamma e_i \\
&\frac{\partial L}{\partial \lambda_i} = 0 \rightarrow \mathbf{w}\phi(\mathbf{x_i}) + b + e_i - y_i = 0
\end{aligned} \tag{2.5}$$

Cast (2.5) into a linear matrix equation:

$$\begin{bmatrix} 0 & \mathbf{1}^T \\ \mathbf{1}^T & \mathbf{K} + \gamma^{-1}\mathbf{I} \end{bmatrix} \begin{bmatrix} b \\ \lambda \end{bmatrix} = \begin{bmatrix} 0 \\ \mathbf{y} \end{bmatrix} \tag{2.6}$$

Where, $\mathbf{1} = (1, 1, ..., 1)^T$. $\mathbf{I}$ is the identity matrix. $\mathbf{y} = (y_1, y_2, ..., y_N)^T$. $K = (k(\mathbf{x_i}, \mathbf{x_j}))_{i,j=1}^{N}$ is called the kernel or Gram matrix defined by the inner product of the feature basis function $k(\mathbf{x_i}, \mathbf{x_j}) = \phi^T(\mathbf{x_i})\phi(\mathbf{x_j})$. The length of the vector $\phi^T(\mathbf{x_i})$ is M and the dimensions of the square kernel matrix $\mathbf{K}$ are $N \times N$.

It follows that using the LS-SVM regression model, the physical quantity that needs to be predicted as a function of a new feature $\mathbf{x}$ can be expressed in the form:

$$y_f(\mathbf{x}) = \sum_{i=1}^{N} \lambda_i k(\mathbf{x}, \mathbf{x_i}) + b \tag{2.7}$$

From (2.6) and (2.7), it can be seen that neither the basis function $\phi_j(\mathbf{x})$ nor their number M need to be specified explicitly. All LS-SVM requires is the inner product of $\phi_j(\mathbf{x})$, i.e., the kernel function $k(\mathbf{x_i}, \mathbf{x_j})$. This property is known as the "kernel

trick" and is a key attribute of the SVM regression algorithm.

Some widely used kernels are the linear, polynomial and Gaussian functions.

$$\text{Gaussian kernel:} \quad k(\mathbf{x}, \mathbf{z}) = exp(-\|\mathbf{x} - \mathbf{z}\|^2/\sigma^2) \tag{2.8}$$

$$\text{Linear kernel:} \quad k(\mathbf{x}, \mathbf{z}) = \mathbf{x}^T\mathbf{z} \tag{2.9}$$

$$\text{Polynomial kernel:} \quad k(\mathbf{x}, \mathbf{z}) = (\mathbf{x}^T\mathbf{z} + t)^d \tag{2.10}$$

In (2.8), $\|\cdot\|$ denotes the Euclidean norm. σ is the "scale" that determines the width or variance of the Gaussian kernel. In (2.10), d is the degree of the polynomial kernel and t is its bias term. More generally, the value of d may be positive or negative, it does not need to be an integer, but its value and that of the bias must be such that the kernel (2.10) is positive definite [18].

Expression (2.7) provides an explicit nonlinear model for the dependent quantity. The summation in (2.7) is over the number of samples N used to train the SVM algorithm with the values of the sample features which appear in the second argument of the kernel. The Lagrange multipliers are obtained from the solution of the linear system (2.6) and are known in the SVM literature as the "support vectors".

The regularization and kernel parameters are calibrated to optimal values during the training and validation stages of the SVM nonlinear regression using a sufficiently large number of samples. Then the nonlinear model (2.6)-(2.7) can be solved and used either to generate time-series forecasts or to represent complex physical quantities dependent on the selected set of features.

2.3 Optimization of hyperparameters

As expressed in (2.2), (2.6) and (2.8)-(2.10), to solve the LS-SVM regression problem, one needs to determine the regularization parameter γ and the kernel parameters (e.g. σ for the Gaussian kernel, or (t,d) for the polynomial kernel), which are referred as hyperparameters. The selections of hyperparameters would reflect the trade-off of the flexibility of the model [34]. One can determine the hyperparameters a priori based

on specific domain knowledge or statistical assumptions. However, the most common way to optimize the hyperparameters is via cross-validation.

Cross-validation is a very common way for general model assessment and selection. The basic idea is to test the model's ability to predict new data that was not used in estimating it and to give an insight on how the model will generalize to an independent data set.

Ideally, if we had enough data, we would set aside a validation set and it to assess the performance of the prediction model. However, in practice, this is usually not possible. So the feasible way is to partition the data into complementary subsets, perform the analysis on one subset (the training set) and validate the analysis on the other subset (the validation set or testing set). Based on different ways of partitioning and selecting the training and validation set, the cross-validation can be categorized into different types, for example, leave-p-out cross-validation, K-fold validation, holdout method, etc [15].

In this study, we have used K-fold cross validation for hyperparameter optimization. The K-fold cross validation algorithm splits the data into K roughly equal-sized parts. And for each of the kth part, the model is fitted using the data in all the other K-1 partitions and the prediction error of the fitted model is tested using the kth part of the data. This process is then repeated K times and the overall performance is estimated by combining the K estimates of prediction error[33]. The most common choice of K is 5 or 10.

In detail, the K-fold cross validation can be summarized as following. Let $\kappa : \{1, ..., N\} \mapsto \{1, ..., K\}$ be the function that split a data set with N samples into K partitions which observation i is allocated by the randomization. Denote $\hat{f}^{-k}(x)$ as the fitted model using the data without the kth partition. Then the cross-validation estimate of the prediction error is:

$$CV(\hat{f}) = \frac{1}{N} \sum_{i=1}^{N} L(y_i, \hat{f}^{-\kappa(i)}(x_i)) \tag{2.11}$$

Take the hyperparameters that need to be optimized into consideration, let $f(x, \alpha)$

refers to the a set of models with tuning parameters α. Then we can revise (2.11) to represent the cross-validation estimate with regard to the hyperparameters:

$$CV(\hat{f}, \alpha) = \frac{1}{N} \sum_{i=1}^{N} L(y_i, \hat{f}^{-\kappa(i)}(x_i, \alpha)) \tag{2.12}$$

The function (2.12) provides an estimate of the test error, and the objective is to tune the hyperparameters α to get the optimal values $\hat{\alpha}$ that minimizes (2.12). After having selected the optimal hyperparameters, the model $f(x, \hat{\alpha})$ would be used to fit all the data set (i.e., the overall K partitions).

As stated in (2.12), in order to solve for the optimal value of α, one has to solve an optimization problem as:

$$\hat{\alpha} = \arg\min_{\alpha} CV(\hat{f}, \alpha) = \frac{1}{N} \sum_{i=1}^{N} L(y_i, \hat{f}^{-\kappa(i)}(x_i, \alpha)) \tag{2.13}$$

The objective function $L(\cdot)$ can take various forms depending on the specific problems. The most commonly used cost functions include mean squared error (MSE) or mean absolute error (MAE).

To solve the optimization problem (2.13), there exists various types of numerical approaches, including different search algorithms, gradient-based optimization methods, etc. In this study, to optimize the hyperparameters both robustly and efficiently, a two step optimization approach is implemented [10]. The coupled simulated annealing (CSA) [20] method is used to determine a suitable set of initial parameter values. Then these initially optimized parameters are given to a second optimization procedure to perform a fine-tuning step, which uses the simplex method [61].

2.4 Further discussion on general kernel selection

The selection of the Gaussian kernel appears at first to be somewhat arbitrary. Moreover its connection to the set of basis functions has not yet been made explicit.

Assume that the physical quantity under study has a well-defined mean and that is otherwise oscillatory around its mean, a common occurrence in ocean applications dealing with signals that are deterministic or quasi-stationary and stochastic. In such cases appropriate basis functions would be a set of orthonormal functions in a multi-dimensional space with dimensions equal to the number of features.

The connection between the kernel and the basis functions in the SVM algorithm is established by Mercer's theorem [18] which states that for a positive definite kernel:

$$\begin{aligned} \iint_X k(\mathbf{x},\mathbf{z})\phi_j(\mathbf{z})d(\mathbf{z}) &= \mu_j\phi_j(\mathbf{x}) \\ k(\mathbf{x},\mathbf{z}) &= \sum_{j=1}^{\infty}\mu_j\phi_j(\mathbf{x})\phi_j(\mathbf{z}) \end{aligned} \tag{2.14}$$

The solution of the first kind integral equation (2.14) is in principle not available in closed form nor is the a priori selection of the kernel evident. A reasonable selection of the basis functions capable to accurately describe the physical quantity under study according to (2.1) would a reasonable starting point. For such a basis function set the kernel would be the generating function as indicated by the second equation in (2.14). This would also require knowledge of the eigenvalues. Moreover the robust performance of the LS-SVM algorithm is a consequence of the positive definite kernel which guarantees a unique solution of the optimization problem (2.2). Within the LS-SVM algorithm the positive definitiveness of the kernel matrix in (2.6) makes available robust algorithms for the inversion problems of large linear systems that arise when a large number of training samples is necessary.

For the Gaussian kernel the solution of (2.14) is available in closed form in any number of dimensions. The basis functions are the generalized Hermit functions which are orthogonal over the entire real axis and are known to be a robust basis set for the representation of the wide range of sufficiently smooth functions. This is the case for the ocean applications considered in the present study.

Consider the multi-dimensional Gaussian kernel assuming K un-correlated

features. The explicit solution of (2.14) takes the form:

$$\begin{aligned} k(\mathbf{x},\mathbf{z}) &= exp[-\epsilon_1^2(x_1-z_1)^2-\epsilon_2^2(x_2-z_2)^2,...,-\epsilon_K^2(x_K-z_K)^2] \\ &= \sum_{k\in N^K} \mu_k \phi_k(\mathbf{x})\phi_k(\mathbf{z}) \end{aligned} \tag{2.15}$$

Where, $\epsilon_k^2 = 1/\sigma_k^2$ and σ_k refers to the constant determining the scale or variance of the k-th feature of Gaussian kernel (as in (2.8)). The cross-correlation of the features is assumed to vanish following a Principal Components Analysis or singular value decomposition of the covariance matrix of input feature dataset.

The eigenvalues and eigenfunctions in (2.15) are available in closed form:

$$\mu_k = \prod_{j=1}^{K} \mu_{k_j} = \prod_{j=1}^{K} \sqrt{\frac{\alpha_j^2}{\alpha_j^2+\delta_j^2+\epsilon_j^2}} \left(\frac{\epsilon_j^2}{\alpha_j^2+\delta_j^2+\epsilon_j^2}\right)^{k_j-1} \tag{2.16}$$

$$\phi_k(\mathbf{x}) = \prod_{j=1}^{K} \phi_{k_j}(x_j) = \prod_{j=1}^{K} \gamma_{k_j} exp(-\delta_j^2 x_j^2) H_{k_j-1}(\alpha_j\beta_j x_j) \tag{2.17}$$

Where, $H_n(\cdot)$ is the classical Hermite polynomial of degree n. α_j are the integral weights which are related to the global scale of the problem. ϵ_j are the scale parameters which are related to the local scale of the problem. $\delta_j, \beta_j, \gamma_j$ are auxiliary parameters defined in terms of α_j, ϵ_j. Refer to [27] for details on the derivation of (2.16) & (2.17).

This formulation of (2.16) and (2.17) allows us to select different shape parameters ϵ_j and different integral weights α_j for different space dimensions (i.e., K may be an anisotropic kernel), or we may assume that they are all equal (i.e., K is spherically isotropic).

The eigenvalues of the Gaussian kernel are seen in equation (2.16) to be positive therefore the matrix of the linear system (2.6) is positive definite. The basis functions $\phi_k(\mathbf{x})$ in (2.17) are the product of an exponential term and Hermite functions where both are dependent on the auxiliary parameters α_k which must be properly selected. While these parameters do not appear explicitly in the definition of the kernel they affect the condition number of the matrix in equation (2.6). They must be properly

selected to determine the rank of the matrix and in order to develop a robust inversion algorithm for the inversion of large linear systems (2.6) that may be ill-conditioned. More details on the robust inversion of (2.6) are presented in [27].

The set of equations (2.15)-(2.17) underscore the popularity of the Gaussian kernel in LS-SVM applications. The reason is that the orthonormal Hermite functions are known to be a robust basis set for the approximation of a wide range functions on the entire real axis. These properties of the Gaussian kernel have led to the use of the LS-SVM algorithms in wide range of problems and underscore its popularity.

In a number of LS-SVM applications a polynomial kernel is used instead of the Gaussian. In the context of the ocean applications this is equivalent to replacing the Gaussian in the right-hand side of (2.7) by a polynomial of $(\mathbf{x}, \mathbf{x_i})$ which may involve linear, quadratic, cubic and higher order terms. On closer inspection of (2.15) this is equivalent to expanding the Gaussian kernel into Taylor series for small values of the inverse scales ϵ_k^2.

A polynomial representation of the physical quantity $y(\mathbf{x})$ would for example be justified when developing an LS-SVM model for a viscous load in terms of the ambient flow kinematics, the Morison drag formula being an example. Another example involves the representation of the hydrodynamic derivatives in the ship maneuvering problem by a high-order polynomial of the ship kinematics. It follows from the Taylor series expansion of (2.15) that the polynomial kernel with an integer power d is related to the Gaussian kernel for small values of ϵ_k^2 for some or all of the K features. Therefore the use of the polynomial kernel may be unnecessary and emphasis must instead be placed upon the proper calibration of the parameters ϵ_k^2 for each of the K features depending of the physics of the flows under study. In a number of applications the same value of ϵ^2 for all features is selected simplifying the calibration process often with very satisfactory results. In marine ocean applications the selection of small values of ϵ_k^2 for some features may be appropriate but not for others, leading to a kernel that is a mixture of polynomial like factors for some features and exponential factors for others. These choices will be determined by the cross-validation procedure during the training of the LS-SVM algorithm.

Chapter 3

Short-term wave and wave force prediction

3.1 Introduction

Offshore floating structures are exposed to continuous stochastic wave excitations, which might be a source of energy that we want to harvest or a disturbance that we want to mitigate the influence for better safety design. And whether we want to mitigate the influence or to take advantage of the ocean waves, we have to gain knowledge of it in priori. And this is especially true for the designing of control strategies of offshore renewable energy systems. Different researchers from both the offshore wind and wave energy industry have proved that model predictive control can have better performance than the general feedback controllers if the disturbance term can be predicted with good accuracy [64] [90]. And clearly, the wave excitations are a dominating factor of the system dynamics, i.e. the targeted disturbance term in the context of controller design.

The short-term wave prediction problem can be approached from different methodology, exploring the characteristics of the wave elevation signal from different aspects. From one perspective, ocean waves in deep water can be categorized as a Gaussian random process in the stochastic process approach [62]. The auto-correlation structure of the narrow-banded wave signal is well defined (see Figure

3-1 as an example) and is the basis of forecasting future values based on the past records via the concept of auto-regressive models. Instead of using the traditional auto-regressive models which assumes a linear basis function, the dependence of the future values on the past records would be determined through the kernel-based methodology, i.e., the SVM regression method. In this way, a more generalized nonlinear mapping relation is determined by training and validation which leads to better accuracy and forecast capability.

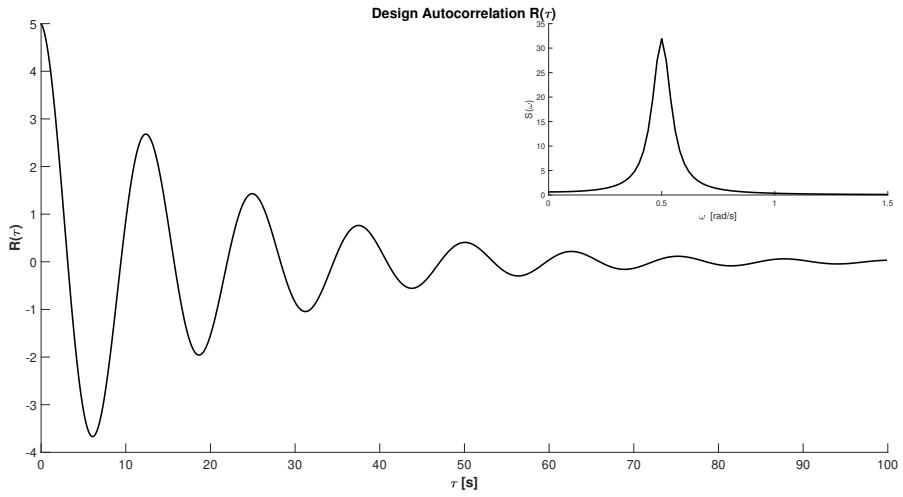

Figure 3-1: An example of the auto-correlation function of wave elevations

On the other hand, unidirectional ocean waves in deep water can be considered as a superposition of linear sinusoidal waves with different amplitudes and phases [50]:

$$\eta(t) = \sum_{j=-\infty}^{\infty} A_j e^{i\omega_j t + i\phi_j} + e_j \tag{3.1}$$

Where, $\eta(t)$ is the real-time wave elevations and e_j is the noise. ω_j is the jth wave frequency, A_j and ϕ_j are the corresponding amplitude and phase. If the measured or simulated signal with noise can be represented by a finite number of frequency components, the representation can be extended to derive forecast wave elevations in future times. And this type of estimation problems of signal parameters is the primary objective for many subspace-based methods of signal processing [30], among which

the approximate Prony-type method is one of the most commonly used algorithms [65].

Therefore, in this chapter, two different forecast algorithms have been proposed and validated using measured wave elevations from a tank test, which are the SVM regression method and approximate Prony method based on ESPRIT. The performance of the two algorithms are compared and discussed in detail.

3.2 LS-SVM regression model

The general mathematical formulation of LS-SVM regression algorithm has been described in the previous section (see Chapter 2). In the context of the prediction of wave elevations or wave excitation forces, consider a one-step ahead prediction for a time series using the autoregressive model first:

$$\eta_{t+1} = f(\eta_t, \eta_{t-1}, ..., \eta_{t-d+1}) \tag{3.2}$$

Where, η_t denotes the sampled time series. d is the order of autoregressive model.

In the context of the LS-SVM, the training data $\{\mathbf{x_i}, y_i\}_{i=1}^{N_{training}}$ would be formatted as:

$$\begin{aligned} \mathbf{x_i} &= [\eta_{t_i}, \eta_{t_i-1}, ..., \eta_{t_i-d+1}] \\ y_i &= \eta_{t_i+1} \end{aligned} \tag{3.3}$$

Where, $N_{training}$ is the number of the data sets used in the training procedure.

After training, (2.6) is solved. Denote the current time as t_c, then for one-step ahead prediction, the input and output in (2.7) is:

$$\begin{aligned} \mathbf{x} &= [\eta_{t_c}, \eta_{t_c-1}, ..., \eta_{t_c-d+1}] \\ y_f &= \eta_{t_c+1} \end{aligned} \tag{3.4}$$

To achieve multi-step ahead prediction, one only needs to repeat the one-step ahead prediction multiple times, substituting the output y_i in (3.3) as η_{t_k+k} in the training step and similarly y_f in (3.4) as η_{t_c+k} in the forecast (k=1,2,...,$N_{forecast}$).

3.3 Approximate Prony Method based on ESPRIT

The approximate Prony method based on ESPRIT [67] is a method that identifies signals composed of complex exponentials, which is essentially based on the Singular Value Decomposition (SVD) of a specially constructed Hankel matrix. This signal processing technique has been widely used in speech enhancement and recognition, direction of arrival estimation of sensor arrays, time series analysis and forecasting, etc.

In principle, the Prony-type method or polynomial methods identify the exponents from the roots of a characteristic polynomial. The variants of this method differ in the way the coefficients of the polynomial are defined, which would extend the Prony method for extracting exponential signals from uniformly sampled time series data when there is no noise to the case when the signal is embedded in noise. The algorithm introduced in this study uses a truncated singular value decomposition of a Hankel matrix defined by the noisy signal to solve for the polynomial coefficients, which allows one to determine the number of representative exponential terms of the signal that is appropriate for the noise level [65].

Consider a sampled signal h_k which can be expressed as:

$$h_k = \sum_{j=1}^{M} \rho_j z_j^k, \quad k = 1, 2, ..., N \tag{3.5}$$

Where, N is the number of samples. M is the order of the exponentials, which is unknown.

Based on the theory of Prony-like methods, z_j are eigenvalues of the matrix pencil:

$$zH_{N-L,L}(0) - H_{N-L,L}(1) \tag{3.6}$$

Where, the Hankel matrix H is $H_{N-L,L}(s) := (h(s + r + m))_{m,r=0}^{N-L-1,L-1}(s = 0, 1)$. $L \geq M$ is a parameter representing the upper bound of the exponential order M.

To solve the eigenvalue problem described in (3.6), the algorithm is formed as follows:

a. Form the rectangular Hankel matrix:

$$H := (h_{k+l})_{k,l=0}^{N-L-1,L} \tag{3.7}$$

b. Carry out a singular value decomposition of H:

$$H = U\Sigma V^* \tag{3.8}$$

c. Form the matrices:

$$V_1 := V(1:L, 1:L) \tag{3.9}$$

$$V_2 := V(2:L+1, 1:L) \tag{3.10}$$

$$F := V_1^+ V_2 \tag{3.11}$$

Where, $V_1^+ := (V_1^* V_1)^{-1} V_1^*$ is the Moore-Penrose pseudoinverse of V_1.

d. Compute the eigenvalues z_j, j=1,2,. . . ,L, of the matrix F

e. Compute ρ_J as the least squares solution of the overdetermined linear Vandermonde-type system:

$$h_k = \sum_{j=1}^{L} \rho_j z_j^k, \quad k = 1, 2, ..., N \tag{3.12}$$

f. Set a tolerance bound ϵ, delete all the pairs (z_j, ρ_j) with $|\rho_j| \leq \epsilon$ and denote the remaining exponential set by $\{z_j : j = 1, ..., M\}$ with M $\leq$ L.

g. Repeat step e and solve the new overdetermined linear Vandermonde-type system with order M again:

$$h_k = \sum_{j=1}^{M} \rho_j z_j^k, \quad k = 1, 2, ..., N \tag{3.13}$$

Output: $\rho_j, z_j, j = 1, ..., M$

Clearly, the simulated or measured wave elevations expressed as (3.1) based on linear wave theory, can be expressed in a form similar to (3.5) with a sampling rate Δt:

$$\eta_l = \sum_{j=1}^{M} \rho_j z_j^k \tag{3.14}$$

Where, η_k is the sampled wave record, k=1,2...,N.

The complex amplitudes $A_j e^{i\phi_J}$ in (3.1) are represented by ρ_j. The complex exponentials $e^{i\omega_j t}$ are represented by z_j^k by converting $t = k\Delta t, z_j = e^{i\omega_j \Delta t}$.

Using the algorithm described by (3.7)-(3.13), the wave records over a certain length of time can be fitted by complex frequencies and amplitudes (ρ_j, z_j) . Correspondingly, the forecasted wave elevations can be expressed as:

$$\eta_k = \sum_{j=1}^{M} \rho_j z_j^k, \quad k = N+1, ..., N+N_{forecast} \tag{3.15}$$

Where, $N_{forecast}$ is the forecast horizon.

3.4 Validation and comparison of forecast algorithms

As mentioned in the previous sections, the purpose of the short-term forecast of wave elevations and wave excitation forces is to design better behaved control algorithms for offshore floating wind turbines and wave energy converters. In the context of the optimal controls, the physical quantity that needs to be evaluated and forecasted is indeed the wave excitation force.

In real-time implementation, two approaches may be used to obtain the wave excitation force. One is to use real-time wave elevation measurements such as on-board wave probes or remote wave sensing techniques [55]. Then the wave loads can be simulated by priori derived frequency domain transfer functions. Such transfer functions can be computed using penal method codes based on linear and second-order wave potential theory such as WAMIT [45]. Following this, the wave excitation

force essentially can be expressed in the same form (3.16) with that of wave elevations (3.1):

$$\begin{aligned} F_e(t) &= \sum_{j=-\infty}^{\infty} H_j e^{i\Delta\phi_j} A_j e^{i\omega_j t + i\phi_j} \\ &= \sum_{j=-\infty}^{\infty} F_j e^{i\omega_j t + i\psi_j} + \epsilon_j \end{aligned} \tag{3.16}$$

Where, $F_e(t)$ is the real-time wave excitation force. $H_j e^{i\Delta\phi_j}$ is the transfer function derived from panel method codes. F_j and ψ_j are the eventual corresponding amplitudes and phases of the excitation force. ϵ_j is the noise contained in the measurements or modeling.

Another approach is to use on-board measurements of motion and structural responses to inversely evaluate the wave excitation forces based on pre-simulated system dynamics. Either way, the derivation of wave excitation forces would contain noise terms due to inaccurate measurements or modeling errors.

Ideally, due to the physical essence of wave excitation forces and platform motions, the floating structure itself can be treated as a natural low-pass filter. Therefore, the wave excitation forces contain lower frequency components and less noise than ambient wave elevations. Taking account of the additional noise due to inaccurate measurements or modeling errors, as stated in (3.1) and (3.16), the time series of wave elevation records and wave excitation forces essentially have the same characteristics. Therefore, to better validate the forecast algorithms under real-world noise, records of wave elevations measured in tank tests are considered as a good representation of real-time input signal for the evaluation of wave excitation forces. The two forecast algorithms, approximate Prony method based on ESPRIT and LS-SVM regression method, are implemented and compared.

For the approximate Prony method based on ESPRIT described in (3.6)-(3.13), there are three parameters affecting the accuracy of the forecast. One parameter is the number of the training samples N, one is the upper bound of the number of the complex exponentials L and one is the bound ϵ to determine the actual number

of complex exponentials eliminating the components regarded as noise. The choice of these three parameters can be specified for each record since the noise level and dominant frequency components can vary as time marches for different sea states. In this study, we have done multiple sensitivity studies to get the most consistent and robust results as time marching for one wave record as well as for multiple wave records using fixed parameters. Based on these sensitivity studies, reasonable values for ϵ are $10^{-10} \sim 10^{-8}$. The number of training samples N in time scale are in the range of $3 \sim 6$ wave typical periods, and the upper bound of frequency terms L needs to be set close to N (approximately N-10).

For the LS-SVM regression method, there are two parameters in the training process that need to be specified based on the characteristics of the signal, namely the order of the autoregressive model d in (3.2) and the number of training samples $N_{training}$ in (3.3). Besides, there are two hyperparameters of the model itself, the regulation parameter γ in (2.2) and the kernel width parameter σ in (2.8), that needs to be optimized. Similar to the approximate Prony method based on ESPRIT, the order of the autoregressive model d and the number of training samples $N_{training}$ are determined based on sensitivity studies to get the most consistent and robust results as well. The order of the autoregressive model is around $1 \sim 2$ typical wave periods and the number of training samples in time scale is about $50 \sim 60$ typical wave periods. The two hyperparameters are tuned automatically using 10-fold cross-validation [22] for each forecast (see section 2.3 for detailed reference).

Two different sea states are tested to validate and compare the two forecast algorithms. One is a mild operational sea state with significant wave height (Hs) 1.7 meters and typical wave period (Tp) 8.7 seconds, while the other one is a more severe sea state with Hs 4.5 meters and Tp 11.8 seconds.

The tank test was conducted in MARIN's Offshore Basin. The measured wave records are 2.5-hours long. The sampling rate of the original tank wave records is 0.0707 seconds, and resampled with sampling rate 0.495 seconds. The forecast horizon is 5 seconds. Three 300-second segments are tested here as examples to show the performance of the algorithm, which are located at 6000s $\sim$ 6300s, 9000s $\sim$ 9300s

and 11000s $\sim$ 11300s of the records.

The RMS error of the forecasted signal is defined as:

$$\text{RMS error} = \sqrt{\frac{1}{N}\sum_{k=1}^{N}|\hat{\eta_k} - \eta_k|^2} \tag{3.17}$$

Where, $\hat{\eta_k}$ is the forecasted wave elevation. η_k is the original wave elevation. To better evaluate the forecast performance, the RMS error is normalized using the significant wave height Hs.

The statistical results of the forecast error and algorithm parameters are listed in Table 3.1 and Table 3.2. The overall RMS error of the entire forecasted signal of the three segments is summarized. Besides, the maximum RMS error occurred of each five-second forecast horizon is listed as a measure of worst-case performance. The number of training samples used in the two methods as well as the order of the autoregressive model for LS-SVM regression are listed here as a measure of the computational cost. Comparisons of the original and forecasted wave elevations of one segment are shown here to give a sketch of the forecast performance (Figure 3-2, Figure 3-3, Figure 3-4, Figure 3-5).

Table 3.1: Sea state 1: Hs=1.7m, Tp=8.7s

Algorithms	Overall RMS Error/Hs (%)	Maximum 5-second RMS Error/Hs(%)	Training Intervals (s)
Approximate Prony method based on ESPRIT	17.36	59.57	$\sim$ 6Tp=52s
LS-SVM regression	13.16	32.33	AR model $\sim$ 2Tp=17s, Training $\sim$ 60Tp=522s

Table 3.2: Sea state 2: Hs=4.5m, Tp=11.8s

Algorithms	Overall RMS Error/Hs (%)	Maximum 5-second RMS Error/Hs(%)	Training Intervals (s)
Approximate Prony method based on ESPRIT	14.74	36.63	$\sim$ 6Tp=71s
LS-SVM regression	12.74	32	AR model $\sim$ 2Tp=24s, Training $\sim$ 60Tp=708s

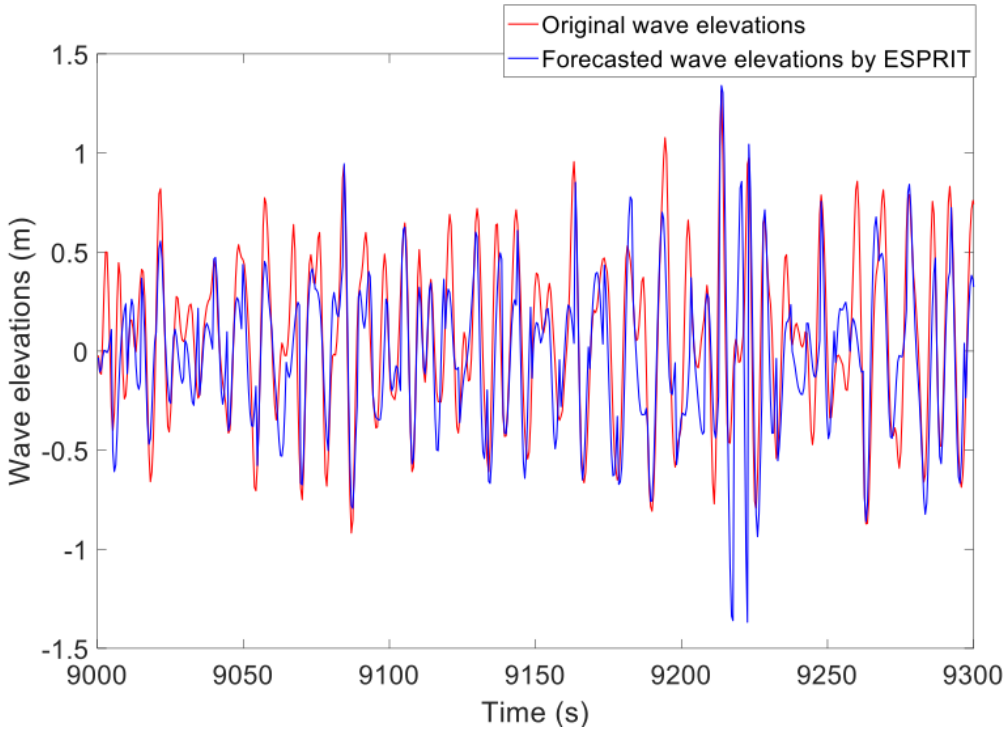

Figure 3-2: Sea state 1: Approximate Prony method based on ESPRIT, RMS error = 18.47% Hs

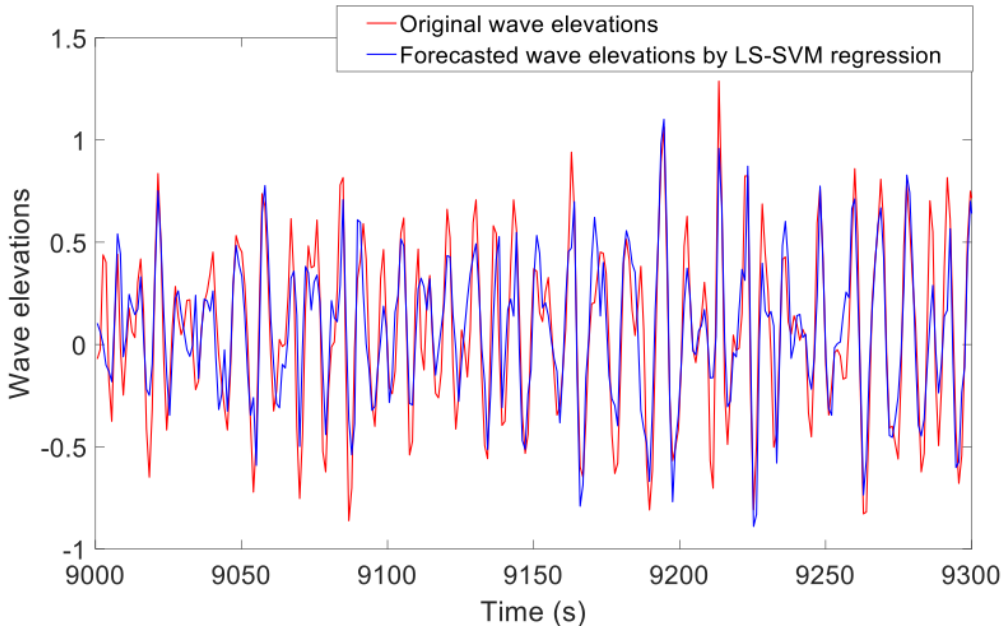

Figure 3-3: Sea state 1: LS-SVM regression method, RMS error = 12.8% Hs

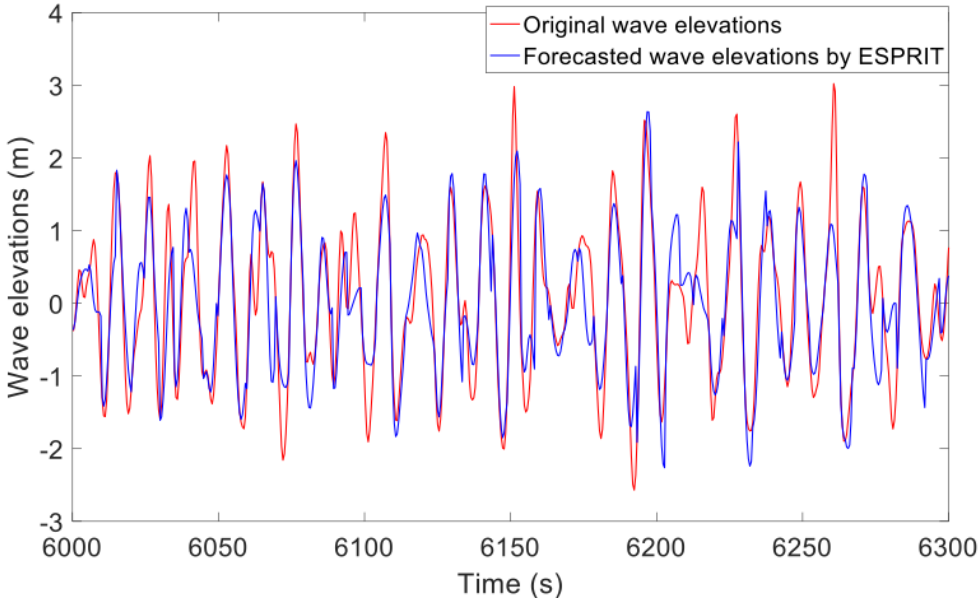

Figure 3-4: Sea state 2: Approximate Prony method based on ESPRIT, RMS error=12.73% Hs

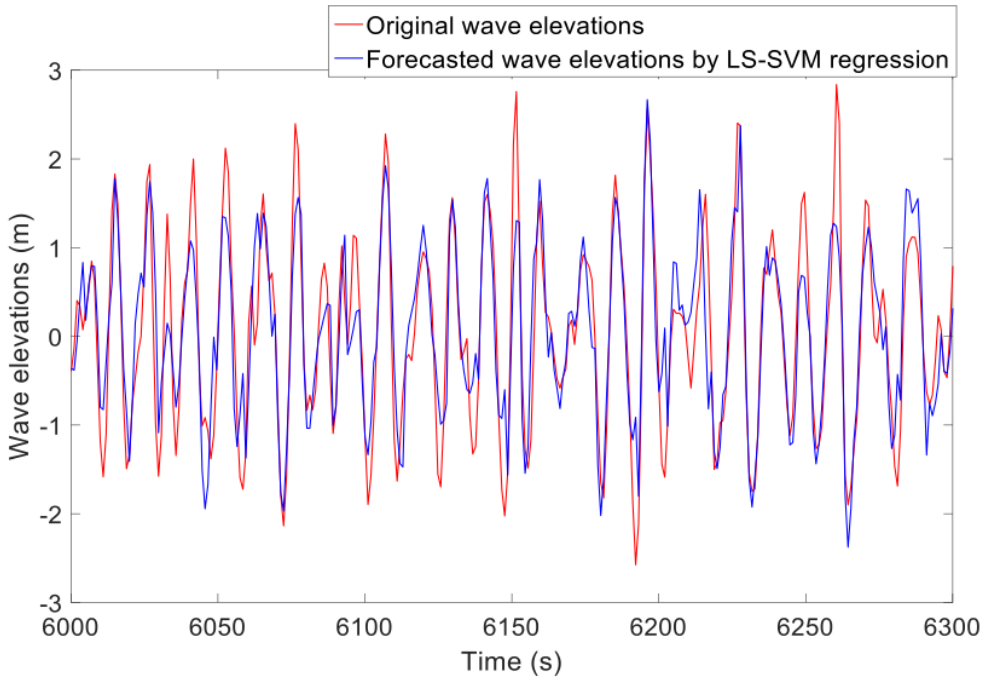

Figure 3-5: Sea state 2: LS-SVM regression method, RMS error=12% Hs

All the tested records above are the original measured wave records without any filtering. As mentioned before, the real-time measured wave elevations contain unknown noise. To forecast a time series, a challenge is to learn higher frequency components of the signal itself and to cancel noise simultaneously. This can be interpreted as a trade-off between underfitting and overfitting. If the algorithm treats the noise as components of the signals, identifying noise would lead to overfitting, whereas, forgetting higher frequency components would cause underfitting. Furthermore, the real-time measured wave elevations or wave excitation forces are actually non-stationary signals. The frequency components that a finite length of wave elevation and wave force records contain are changing over time, so as is the signal to noise ratio.

From the results shown in Table 3.1, Table 3.2 and Figure 3-2 $\sim$ Figure 3-5, the LS-SVM regression method has an overall better performance, for both the overall RMS error and worst-case RMS error, than the approximate Prony method based on ESPRIT. Moreover, the LS-SVM regression methods performs significantly better for the milder sea state (sea state 1). Figure 3-6 is a comparison of the normalized

wave spectrum of the two sea states. From the spectra, sea state 1 contains relatively more higher frequency components which makes it more difficult to forecast. LS-SVM regression method inherently prohibits over-fitting the signal and thus is more capable of distinguishing high frequency components from noise without causing too much overfitting, while the approximate Prony method based on ESPRIT performs better for signals with relatively lower frequency components and clean signals. In terms of the computational cost, the approximate Prony method needs fewer training samples than the LS-SVM regression leading to less computational time.

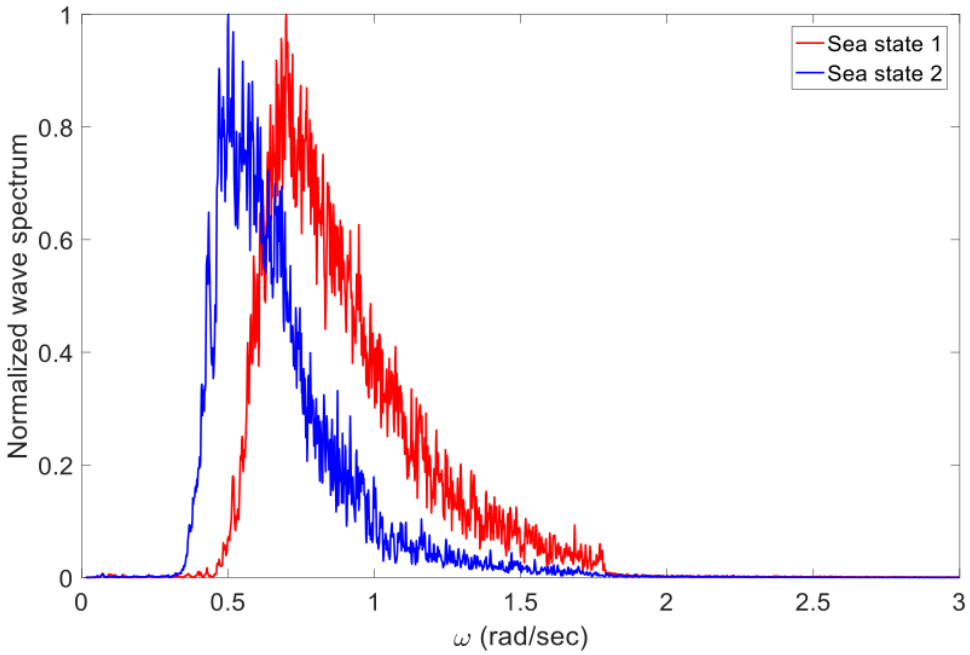

Figure 3-6: Comparison of the normalized wave spectrum of the two sea states

3.5 Conclusions and discussions

In this study, successful wave elevation and exciting force forecast algorithms have been developed for further use in optimal control of offshore wind and wave energy systems. Two forecast algorithms, the approximate Prony method based on ESPRIT and the LS-SVM regression method, are developed and validated using real-time measurements.

The general predictability of a sea state is a difficult question to answer in principle since real sea states are nonstationary and multi-directional. Therefore, we rely on the performance of the forecast algorithms in our study and do not address the more fundamental question of how forecastable real seastate elevations are. The error in the forecasts generated by the algorithms consist of three components a) algorithm bias b) algorithm variance c) noise. Alternative algorithms introduce different bias vs variance tradeoffs, which is a topic that we do not address in this thesis as well. Ambient noise is unforecastable by any algorithm. The relative magnitude of these three sources of error is only possible after a systematic study among alternative algorithms and parameters within each algorithm. This topic is beyond the scope of the present thesis and will be addressed in the future work.

Therefore, considering the forecast algorithm itself, the performance would degenerate significantly as the forecast horizon gets larger. The trade-off between the forecast accuracy and required forecast horizon should be balanced depending on specific problems and objectives. In the context of this thesis, the forecast accuracy of the wave elevations up to a 5-second horizon is considered by the ESPRIT and LS-SVM regression algorithm and found to be good. Meanwhile, this time scale is also considered as sufficient for controller design purposes which would be described in more detail in the following sections.

Chapter 4

Model Predictive Control for Offshore Floating Wind Turbines

4.1 Introduction

Due to the energy crisis and increasing concern on environmental issues, the study and commercialization of renewable energy have been attracting more and more attention. Among a variety of the potential resources of energy production, wind energy is currently the fastest-growing sources of electricity in the world [42]. Figure 4-1 shows the fast growing of the wind energy over the past decades. A recent trend of the wind industry is to go further offshore to overcome limited land availability and avoid visual and acoustic pollution. Besides, the ocean wind tends to blow more strongly and consistently, allowing the utilization of larger wind turbines that enjoy better economics per rated megawatt (MW). Meanwhile, using floating support structures in offshore wind farms adds more complexity to the system and leads to more technical and economic challenges [12].

The prototype used in this study is a tension-leg platform (TLP) supported floating wind turbine. TLPs have been widely used in the oil and gas industry and adapted for offshore floating wind turbines as well. TLPs are constrained with vertical tethers which are balanced by an excessive buoyancy force. The advantage of TLPs is that they usually have extremely small heave, pitch and roll motions compared to

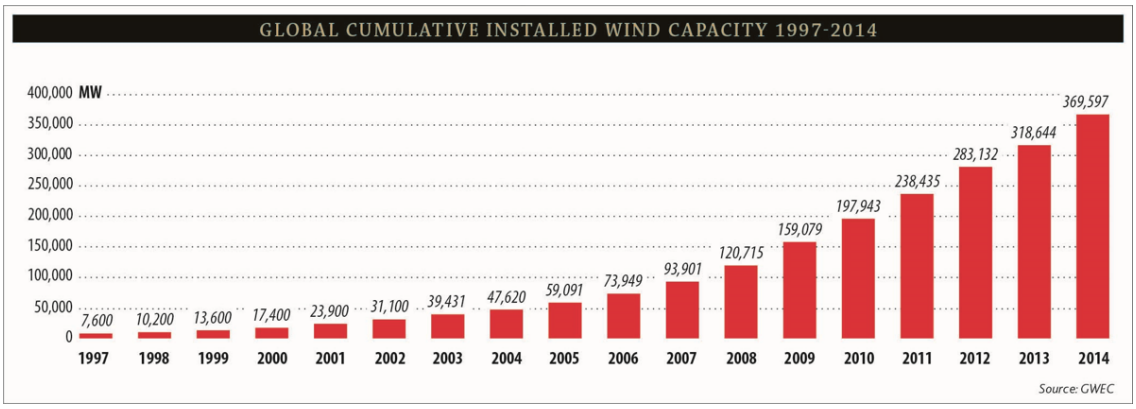

Figure 4-1: Growing trend of wind energy [4]

other floating platforms and the potential to offer significantly reduced fabrication costs due to the reduced steel weight compared to fixed offshore wind turbines [63]. Meanwhile, they usually have large compliance to tranlational modes of motion.

Therefore, the offshore wind turbine is an integrated aero-hydro-elastic-servo system, which is compliant to both external aerodynamic and hydrodynamic loads. In the meantime, as modern turbine size increases and factors of weight/cost are considered, the flexibility of turbine structures tends to increase. Thus it is critical to consider coupling between different structural modes and mitigate the damaging loads at the blade roots and the tower base [42]. And the means to address these issues is to develop advanced control systems to achieve load mitigation while maintaining the optimal power output.

For offshore floating wind turbines, the baseline controller usually operates in two power generation zones, below rated wind speed and above rated speed. And depending on the different operation region, the basic control strategy is either optimizing the power capture by variational rotor speed or maintaining the rated power by collective blade pitch control [35]. To address additional load mitigation issues, optimal controls need to be designed and overlaid with these baseline controllers.

Among the existing control algorithms developed to mitigate structural loads, model predictive control is considered very promising. Most of the current developments have been targeting wind induced loads which utilized recent

improvements in LIDAR (Light Detection and Ranging) techniques [85]. However, researches have shown that wave-excited loads are a significant source for structural fatigue as well [19], and little work has done to accommodate wave-excited disturbances. In the previous chapter, we have established that real-time implementation of short-term predictions of wave elevations and wave excitation forces is feasible and with good accuracy. On the basis of the wave forecast capability, similar model predictive control approaches can be developed targeting wave-excited loads as well.

To summarize, in this chapter, the proposed model predictive control is designed for the above rated speed region and overlaid with the original baseline PI control, which aims to mitigate the fore-aft tower base bending moment that is largely excited by ocean waves. The controllers are integrated and validated against a TLP type floating wind turbine.

4.2 Modeling of the TLP supported floating wind turbine

4.2.1 Introduction of the prototype

The prototype studied in this thesis is Glosten's PelaStar TLP coupled with the GE Haliade turbine. The Glosten Pelastar platform is a five-arm tension leg platform with synthetic tendons. A more detailed introduction of the prototype can be found in the following references [83] [82]. A sketch of the coordinate system associated with the floating wind turbine is shown in Figure 4-2.

The overall system dynamics of the floating turbine is simulated using FAST (Fatigue, Aerodynamics, Structures, and Turbulence) code, which is a comprehensive aero-hydro-servo-elastic simulator for wind turbines [37]. The linearized state space model around an operation point for control design purpose is also generated using FAST [36]. The hydrodynamic coefficients required in the simulations are calculated using potential flow panel methods as WAMIT [45].

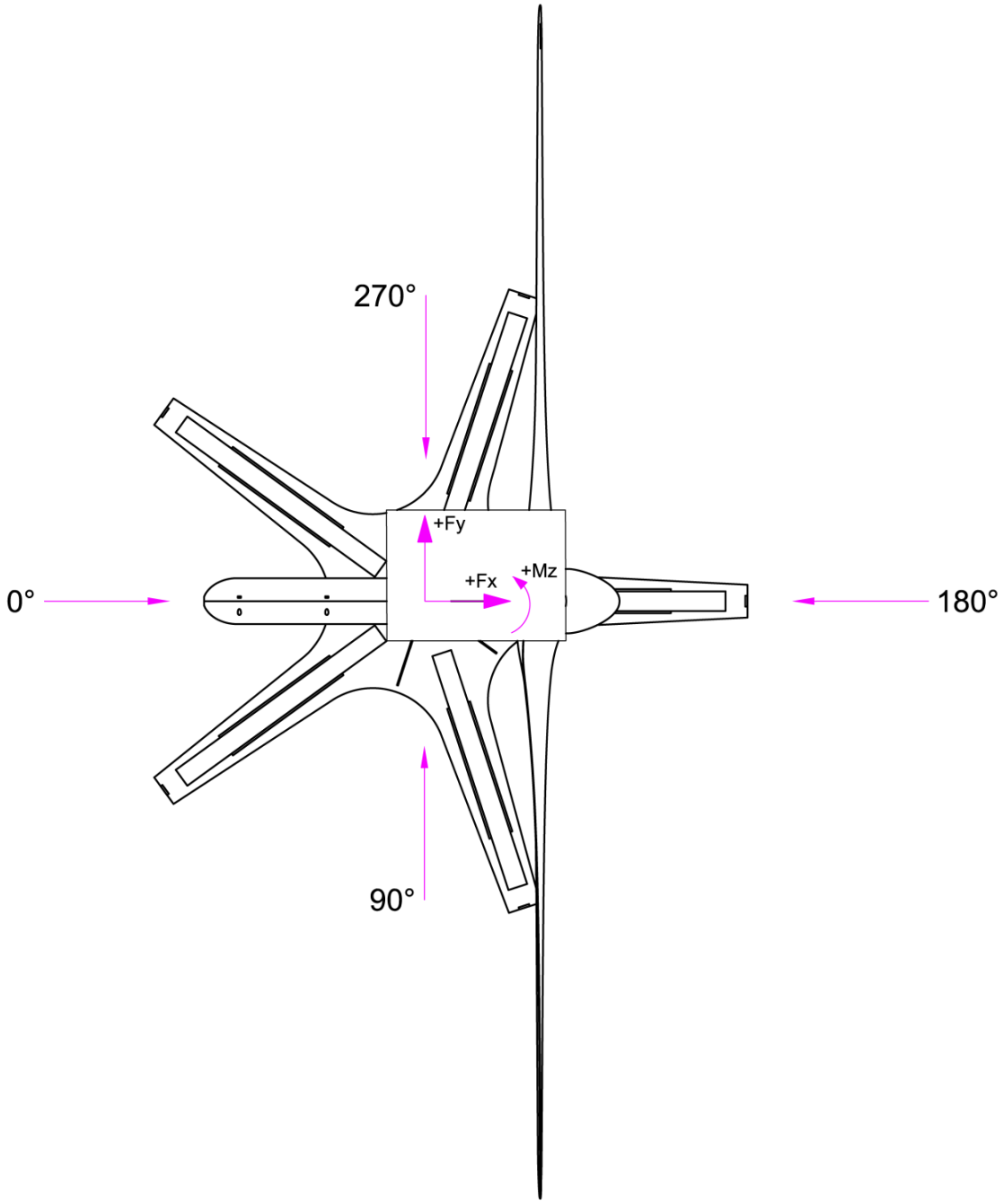

Figure 4-2: A sketch of the coordinate system

4.2.2 Modeling and validation of the linear state space model

The focus of this study is to reduce structural loads when operating above rated wind speed, which would be achieved by adjusting the blade pitch angle collectively.

Therefore, to better design and validate the control system, the system dynamics of the offshore floating wind turbines is firstly linearized around an operational point above the rated speed.

Using FAST, the open-loop system dynamics above rated wind speed under calm water condition can be linearized as:

$$\begin{cases} \Delta\dot{x} &= A\Delta x + B\Delta\beta + B_d\Delta v \\ \Delta y &= C\Delta x + D\Delta\beta + D_d\Delta v \end{cases} \tag{4.1}$$

Where, Δx is the states deviating from steady values under the operation condition. In this study, Δx has totally 23 states describing the kinematic and structural characteristics of the floating wind turbine system. The states of the linearized turbine model (x) include:

$$x = \begin{bmatrix} \text{Row 1 = Platform horizontal surge translation DOF} \\ \text{Row 2 = Platform horizontal sway translation DOF} \\ \text{Row 3 = Platform vertical heave translation DOF} \\ \text{Row 4 = Platform roll tilt rotation DOF} \\ \text{Row 5 = Platform pitch tilt rotation DOF} \\ \text{Row 6 = Platform yaw rotation DOF} \\ \text{Row 7 = 1st tower fore-aft bending mode DOF} \\ \text{Row 8 = 1st tower side-to-side bending mode DOF} \\ \text{Row 9 = 2nd tower fore-aft bending mode DOF} \\ \text{Row 10 = 2nd tower side-to-side bending mode DOF} \\ \text{Row 11 = Drivetrain rotational-flexibility DOF} \\ \text{Row 12 to 21 = First derivatives of row 1 to 10} \\ \text{Row 22 = First derivatives of Variable speed generator DOF} \\ \text{Row 23 = First derivatives of row 11} \end{bmatrix} \tag{4.2}$$

Δy is the output variables deviating from the corresponding steady values, in this study, Δy includes two tower base bending moments (side-side and fore-aft). $\Delta\beta$ is

the blade pitch angle apart from the operation point. Δv is the incoming wind speed apart from the operation point. A, B, B_d, C, D, D_d are the corresponding state space matrices representing aero-elastic behavior of the 6 MW offshore wind turbine.

Since this study aims to apply an optimal control for reducing structural loads excited by wave excitation forces, the incoming wind is assumed to be known. In practice, the optimal control would be overlaid with the baseline rotor speed regulator, thus the linear model needs to be modified by adding a PI controller into the loop. The design of this baseline controller has taken the instability issue due to "negative damping" into consideration and a more detailed investigation is beyond the scope of this study. Detailed information of the baseline controller can be found in reference [28].

The baseline PI controller regulating the rotor speed is added to (4.1) to form a revised linear model, with gains k_p and k_i. Then, the linear model is modified to:

$$\begin{cases} \Delta\dot{x} &= A\Delta x + B\Delta\beta_{PI} + B_d\Delta v \\ \Delta y &= C\Delta x + D\Delta\beta_{PI} + D_d\Delta v \end{cases} \tag{4.3}$$

Where,

$$\beta_{PI}(t) = k_p e(t) + k_i \int_0^t e(\tau)d\tau \tag{4.4}$$

$$e(t) = x_{22}(t) - r = \Delta x_{22}(t) \tag{4.5}$$

Where, $x_{22}(t)$ is the actual rotor speed. r is the reference value. $\Delta x_{22}(t)$ is the 22nd state of Δx in (4.3).

The PI controller (4.4)-(4.5) can be expressed in state space form by introducing an additional state:

$$\begin{cases} \Delta\dot{z} = e = \Delta x_{22} \\ \beta_{PI} = k_i z + k_p e = k_i z + k_p \Delta x_{22} \end{cases} \tag{4.6}$$

Plugging (4.6) into (4.3), the modified linear model becomes:

$$\begin{aligned} \begin{bmatrix} \Delta\dot{x} \\ \dot{z} \end{bmatrix} &= \begin{bmatrix} A + BK_p & k_i B \\ [0, 0, ..., 1, 0] & 0 \end{bmatrix} \begin{bmatrix} \Delta x \\ z \end{bmatrix} + \begin{bmatrix} B_d \\ 0 \end{bmatrix} \Delta v \\ \Delta y &= [C + DK_p \quad k_i D] \begin{bmatrix} \Delta x \\ z \end{bmatrix} + D_d \Delta v \end{aligned} \tag{4.7}$$

Where, $K_p = [0, 0, ..., k_p, 0]$.

To validate the linear model, (4.7) is solved numerically in the time domain. The model is validated under the calm water condition. The same wind velocity is input to the linear model as in FAST nonlinear simulations. The mean wind velocity is 16m/s and the turbulence intensity is about 0.0564, which is above rated-speed and temporally coherent. Under the calm water condition, there is no incident wave excitation force and the effects of wave radiation force have already been included in the state space model. Therefore, under such wind-only conditions, model (4.7) should ideally capture all the system dynamics. The comparisons of output variables (fore-aft tower base bending moment TwrBsMy and side-side tower base bending moment TwrBsMx), control variable (blade pitch angle) and concerned states (rotor speed) between the linear model and the FAST nonlinear simulations are shown in Figure 4-3 $\sim$ Figure 4-6.

All the concerned physical quantities in this section are normalized to [-1, 1] and the non-dimensional results should not affect the discussions and conclusions drawn from this study.

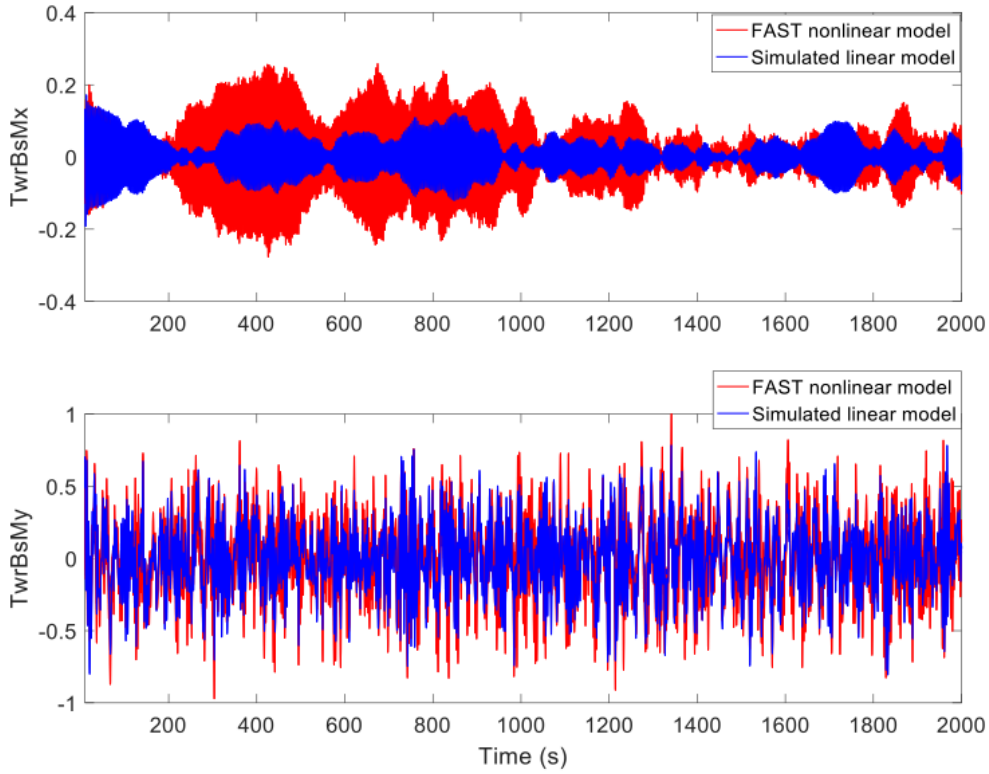

Figure 4-3: Comparison of the linearized model and FAST nonlinear simulation under calm water: tower bending moments in time domain

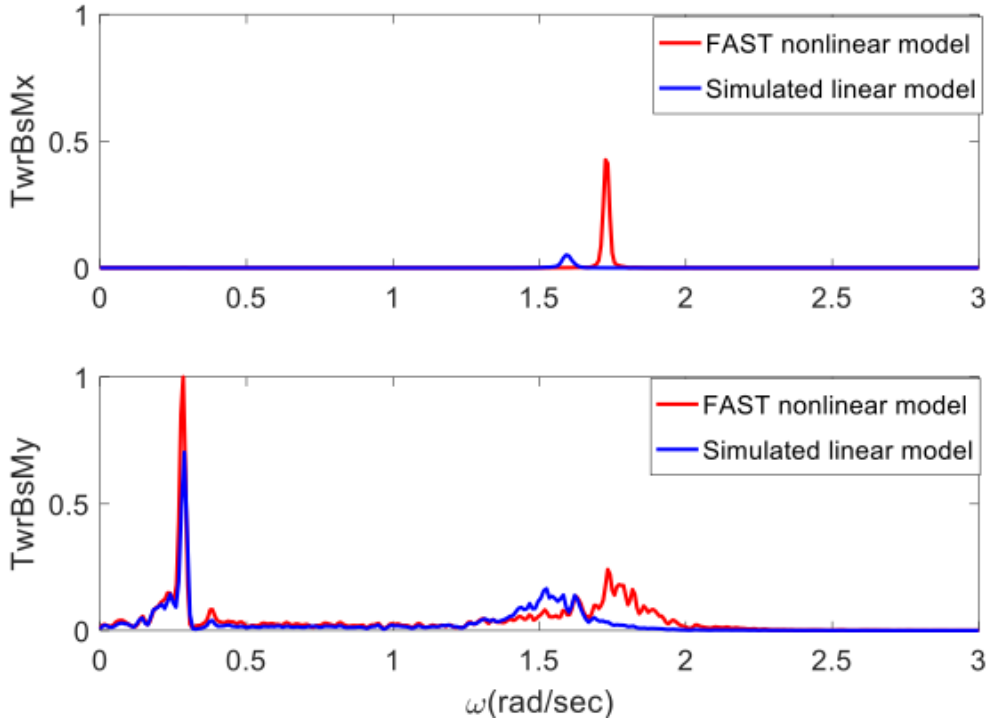

Figure 4-4: Comparison of the linearized model and FAST nonlinear simulation under calm water: tower bending moments in frequency domain

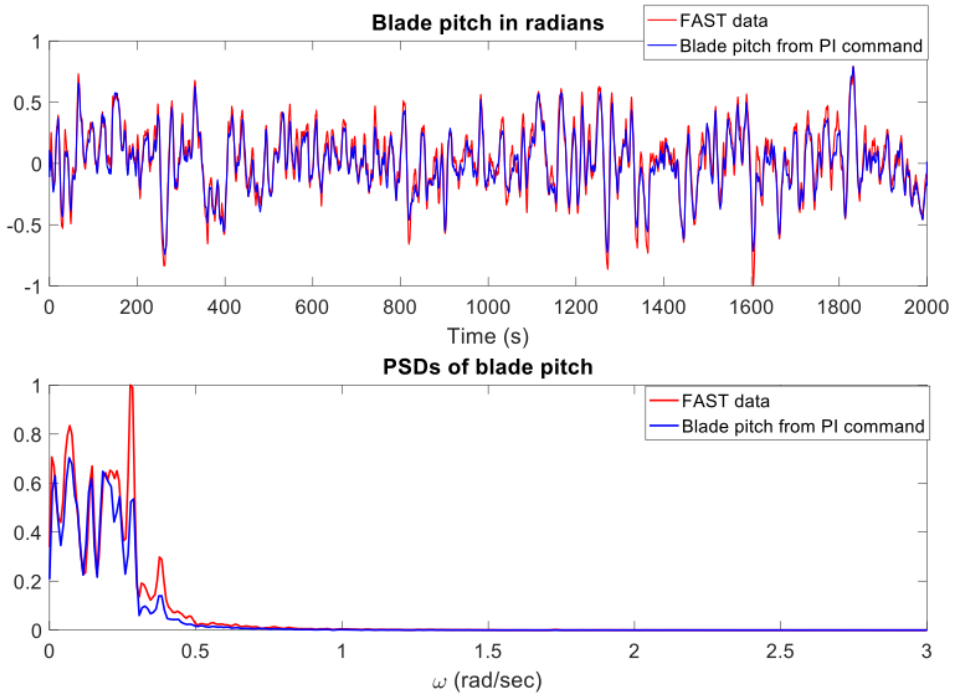

Figure 4-5: Comparison of the linearized model and FAST nonlinear simulation under calm water: blade pitch angle

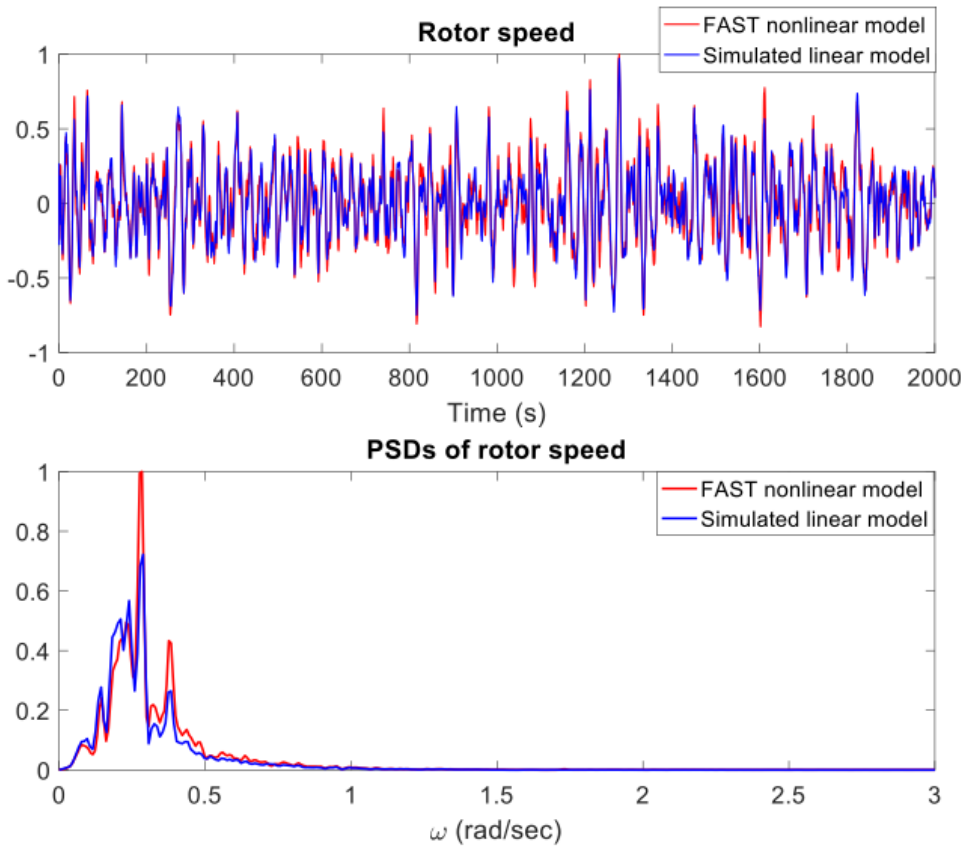

Figure 4-6: Comparison of the linearized model and FAST nonlinear simulation under calm water: rotor speed

From Figure 4-3 $\sim$ Figure 4-6, it can be seen that the linear model (4.7) captures most of the system dynamics affecting the fore-aft tower base moment under the calm water condition, while it has a significant gap for the side-side tower base moment. Figure 4-7 shows a frequency domain result of the tower bending moments under the same wind condition but also with an irregular wave sea state (Hs=2.75m, Tp=8s) by nonlinear FAST simulations. From Figure 4-7, it can be shown that the side-side tower base bending moment (TwrBsMx) is mostly dominated by the first tower bending mode (around 1.5 $\sim$ 2 rad/sec). In the other hand, the fore-aft bending moment (TwrBsMy) has multiple peaks corresponding to platform surge resonance frequency (around 0.25 rad/sec), wave excitation frequencies (around 0.5 $\sim$ 1.5 rad/sec) and the first tower bending mode (around 1.5 $\sim$ 2 rad/sec). Clearly, wave excited loads have a major impact on the fore-aft bending moment (TwrBsMy). Since the major

objective of this study is to reduce the wave excited fore-aft tower base moment, the linear model (4.7) is considered reasonable enough to proceed with the implementation of optimal control.

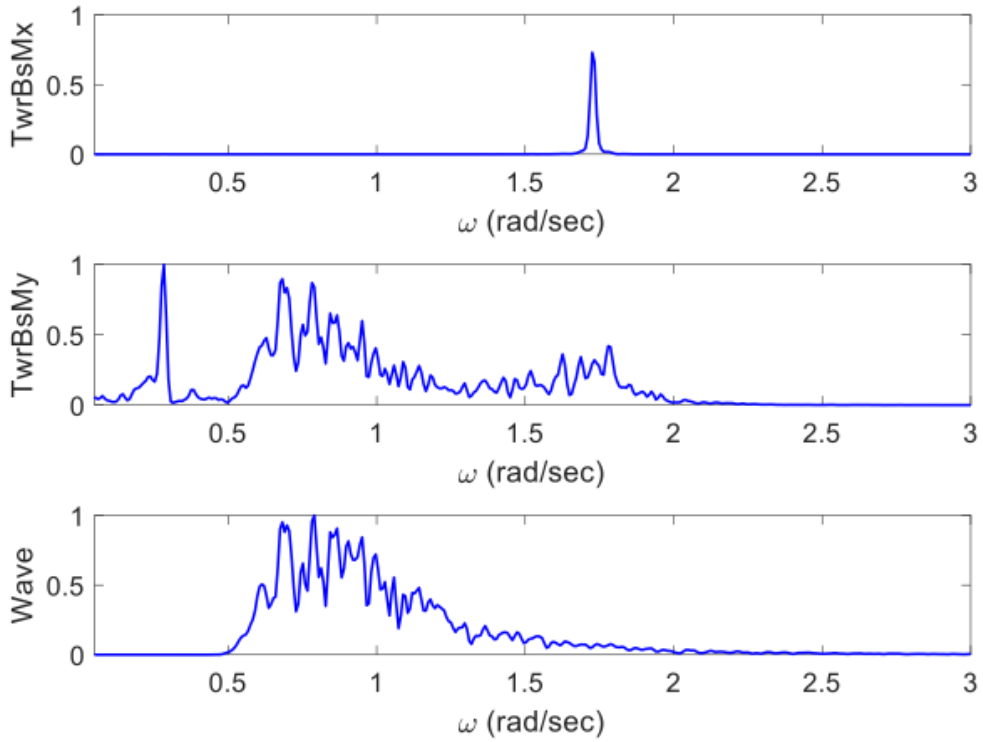

Figure 4-7: Power spectrum of irregular wave (Hs=2.75m, Tp=8s) and corresponding tower bending moments simulated by FAST

4.3 Optimal control formulation

The offshore floating wind turbines are compliant to both wind and wave induced loads. As mentioned previously, the baseline controller of the wind turbine system at above rated wind speed is mainly designed to regulate the rotor speed to reduce power fluctuation using a PI control. In this study, the focus is to propose an overlaid optimal control aiming to additionally mitigate the fore-aft tower base bending moment, which is largely excited by ocean waves. To achieve such an objective, the wave excitation forces are modelled as persistent external disturbances that need to be evaluated and

forecasted.

Consider the general form first, the linearized system dynamics above the rated wind speed with the wave excitations can be represented as a state space model:

$$\begin{aligned} \dot{x}(t) &= Ax(t) + Bu(t) + f_e(t) \\ y(t) &= Cx(t) + Du(t) \end{aligned} \tag{4.8}$$

Where, $f_e(t)$ represents the external disturbance, i.e. wave induced loads in this study. x(t), u(t), y(t) are the system states, input and output perturbations around an operation point. A, B, C, D are the associated state, input and output matrices.

The objective is to find an optimal control law u_{opt} such that:

$$u_{opt}(t) = \arg\min_u J(u) = \frac{1}{2}\int_{t_0}^{t_0+T} (x^T Q x + u^T R u + 2u^T S x)dt + \frac{1}{2}x(t_0+T)^T G x(t_0+T) \tag{4.9}$$

Where, t_0 is the present time. T is the optimization horizon. Q, R, S, G are the weighting matrices penalizing the states, control efforts, cross term of states and control efforts and the final time states, respectively.

Thus, the optimization problem is to find an optimal solution of (4.9) subject to the linear constraints (4.8). The optimal control law u_{opt} under such a problem takes a generalized state feedback form [88]:

$$u_{opt} = -R^{-1}[(B^T P(t) + S)\bar{x}(t) + B^T \phi(t)], \quad t \in [t_0, t_0 + T] \tag{4.10}$$

$P(t), \phi(t), \bar{x}(t)$ are solutions of the following ordinary differential equations (ODEs):

$$\begin{cases} \dot{P}(t) & = P(t)BR^{-1}B^T P(t) - Q + S^T R^{-1} S - P(t)(A - BR^{-1}S) - (A - BR^{-1}S)^T P(t), \\ & t \in [t_0, t_0 + T] \\ P(t_0 + T) & = G \end{cases} \tag{4.11}$$

$$\begin{cases} \dot{\phi}(t) = [P(t)BR^{-1}B^T - (A - BR^{-1}S)^T]\phi(t) - P(t)f_e(t), \quad t \in [t_0, t_0 + T] \\ \phi(t_0 + T) = 0 \end{cases} \tag{4.12}$$

$$\begin{cases} \dot{\bar{x}}(t) = \{A - BR^{-1}[B^T P(t) + S]\}\bar{x}(t) - BR^{-1}B^T\phi(t) + f_e(t), \quad t \in [t_0, t_0 + T] \\ \bar{x}(t_0) = x(t_0) \end{cases} \tag{4.13}$$

The ODEs (4.11) and (4.12) have a known final value and thus need to be solved backwards in time. Making a change of variable $t' = t_0 + T - t$, (4.11)-(4.12) can be transformed into initial value problems as:

$$\begin{cases} \dot{P}(t') &= -P(t_0 + T - t')BR^{-1}B^T P(t_0 + T - t') + Q - S^T R^{-1} S \\ &\quad + P(t_0 + T - t')(A - BR^{-1}S) + (A - BR^{-1}S)^T P(t_0 + T - t'), \quad t' \in [0, T] \\ P(0) &= G \end{cases} \tag{4.14}$$

$$\begin{cases} \dot{\phi}(t) = [P(t)BR^{-1}B^T - (A - BR^{-1}S)^T]\phi(t) - P(t)f_e(t) \quad t' \in [0, T] \\ \phi(0) = 0 \end{cases} \tag{4.15}$$

(4.13)-(4.15) are initial value ODE problems, which can be solved by numerical methods such as ABM4 (Adams-Bashforth-Moulton 4th order predictor-corrector) method. Once the optimal control law u_{opt} is solved, the system dynamics would be updated as:

$$\begin{aligned} \dot{x}(t) &= Ax(t) + Bu_{opt}(t) + f_e(t) \\ y(t) &= Cx(t) + Du_{opt}(t) \end{aligned} \tag{4.16}$$

Following the general formulation of the optimal controller described in (4.9)-(4.16), the actual system dynamics described in (4.7) can be modified as follows to

take account the irregular wave excitations:

$$\begin{aligned}\begin{bmatrix}\Delta\dot{x}\\ \dot{z}\end{bmatrix} &= \begin{bmatrix}A+BK_p & k_iB\\ [0,0,...,1,0] & 0\end{bmatrix}\begin{bmatrix}\Delta x\\ z\end{bmatrix} + \begin{bmatrix}B_d\\ 0\end{bmatrix}\Delta v + f_e\\ \Delta y &= [C+DK_p \quad k_iD]\begin{bmatrix}\Delta x\\ z\end{bmatrix} + D_d\Delta v\end{aligned} \tag{4.17}$$

Where, f_e is the wave excitation force vector.

Evaluate f_e as follows assuming knowledge of the system states:

$$f_e = \begin{bmatrix}\Delta\dot{x}\\ \dot{z}\end{bmatrix} - \begin{bmatrix}A+BK_p & k_iB\\ [0,0,...,1,0] & 0\end{bmatrix}\begin{bmatrix}\Delta x\\ z\end{bmatrix} - \begin{bmatrix}B_d\\ 0\end{bmatrix}\Delta v \tag{4.18}$$

Where, $\Delta x, z, \Delta v$ are real-time measurements of the system states and wind speeds when evaluating the force vector f_e.

If the linear model matches the system dynamics exactly, f_e would be the incident wave excitation force. However, from results shown in Figure 4-3 $\sim$ Figure 4-6, there is a large gap for the side-side tower bending moment. This indicates that f_e evaluated from (4.18) would include components introduced by this modeling error. We consider f_e derived from (4.18) as an equivalent forcing vector that can be measured online in terms of the system states and predict it using the approximate Prony method based ESPRIT or LS-SVM regression.

With the knowledge of predicted equivalent wave disturbance terms f_e, the finite-horizon LQR problem (4.10)-(4.15) can be solved. And the system dynamics with the optimal control effort u_{opt} can be derived in time domain (4.16).

4.4 Simulation results of the optimal control for load reduction

To validate the finite-horizon LQR with the prediction of equivalent wave force vector, three different scenarios are tested and compared with the baseline controller. The

FAST simulations with baseline controller are 2000-second long. The finite-horizon LQR problem subject to the modified linear state space model (4.17) is solved in the time domain using FAST simulation data as initializations. The LQR controller is turned on at t=200s.

The time step of the numerical solver for the optimization problem and system dynamics are set to be 0.025 seconds based on convergence tests. The optimal controller update rate is 1 second and the optimization horizon T in (4.9) is 1 second, which is also the forecast horizon of the equivalent forcing vector f_e. The average value of blade pitch angle solved from (4.10) is applied until the next controller update.

The controller with the predictor is tested under three different scenarios. The mean value of wind velocity is 16 m/s as the linearization point. In addition, a coherent turbulence model is used to generate the actual wind time series. Two unidirectional wave conditions with different significant wave heights and typical wave periods are tested in the simulations, which both have zero degree wave headings. Furthermore, the controller and the predictor are also tested under spread sea conditions. The main wave heading is zero degrees and a Cosine-2s spreading model is used. The combination of wind and wave conditions for the three tested cases are listed in Table 4.1.

Table 4.1: Wind and wave conditions for the three tested cases

Case No.	Wind	Wave		
		Hs	Tp	Heading
Case 1	Coherent turbulent wind, mean speed 16 m/s, turbulence intensity 0.0564	2.75	8	Zero degree
Case 2	Coherent turbulent wind, mean speed 16 m/s, turbulence intensity 0.0564	3.5	11	Zero degree
Case 3	Coherent turbulent wind, mean speed 16 m/s, turbulence intensity 0.0564	2.75	8	Spread sea, main wave heading is zero degree

The performance of the overlaid optimal controller is measured by the percentage

of changes for variables of concern:

$$\frac{Var(Y_{optimal}) - Var(Y_{baseline})}{Var(Y_{baseline})}\% \tag{4.19}$$

Where, Y could be the fore-aft tower bending moment TwrBsMy, side-side tower bending moment TwrBsMx and rotor speed. $Var(\cdot)$ denotes the variance of the concerning variables. The variance of tower bending moments is treated as an indirect measure of fatigue loading.

Taking account of the actuator limits, the maximum blade pitch rate is normally up to 7 degrees/second. The trade-off between the performance and control efforts are adjusted through the penalty matrix Q and R in (4.9). The weighting matrices S and G in (4.9) are set to be zero.

The performance of the finite-horizon LQR controller with the prediction of the equivalent forcing vector is summarized in Table 4.2 and Figure 4-8 $\sim$ 4-10. From the results, the finite-horizon LQR controller with prediction of the equivalent wave force vector significantly reduces the fore-aft tower base bending moment. Meanwhile, the side-side tower bending moment and rotor speed variation are slightly increased as a cost, which is acceptable since the side-side tower bending moment is far lower than that in the fore-aft direction thus not leading to increased structural requirements. In addition, depending on different concerns of structural safety or power stabilization, the effects of the optimal controller on different quantities can be adjusted via the penalty matrix in the optimization process.

As for the optimal controller itself, the performance is influenced by the optimization horizon, accuracy of the predictor, trade-off of the elements in LQR weighting matrices, etc. Furthermore, the input wind and wave conditions and accuracy of the linearization process would also have significant effects on the overall performance for the load reduction. From the results, the proposed LQR controller as well as the predictor is robust performing consistently under different wave conditions and is capable of tolerating non-negligible modeling residues in the linearization process.

Table 4.2: Performance of the finite-horizon LQR with predictor

Case No.	TwrBsMx (side-side) (%)	TwrBsMy (fore-aft) (%)	Rotor speed variation (%)	Maximum blade pitch (deg/sec)
Case 1	+19.87	-69.86	+28.94	6.8
Case 2	+17.65	-55.74	+14.32	6.84
Case 3	-0.58	-67.34	+17.80	6.76

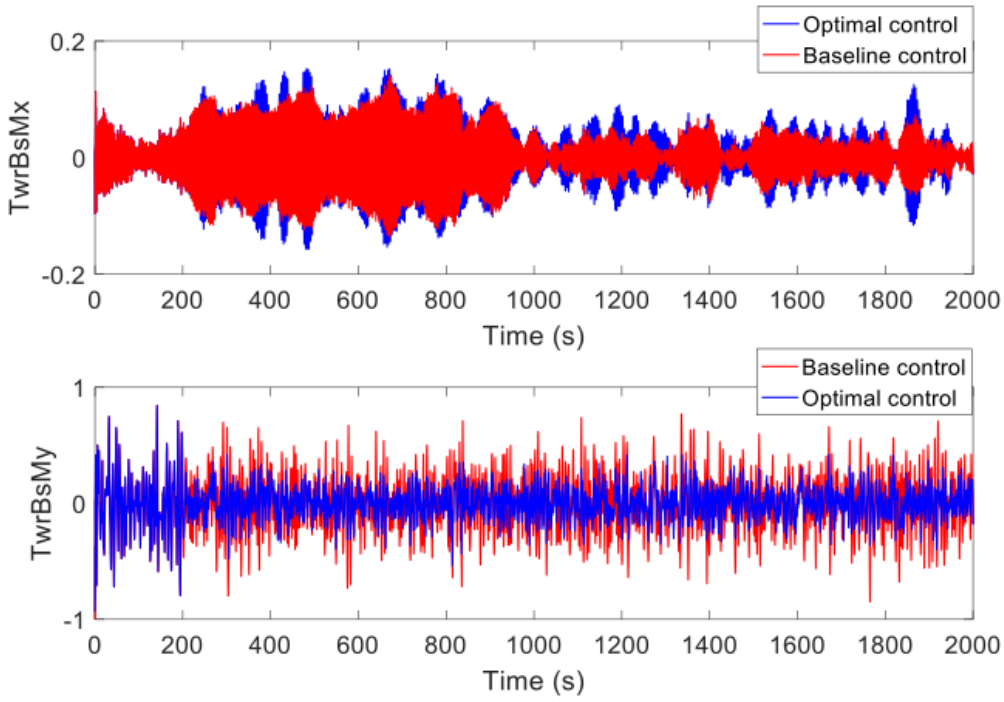

(a) Tower bending moments in time domain

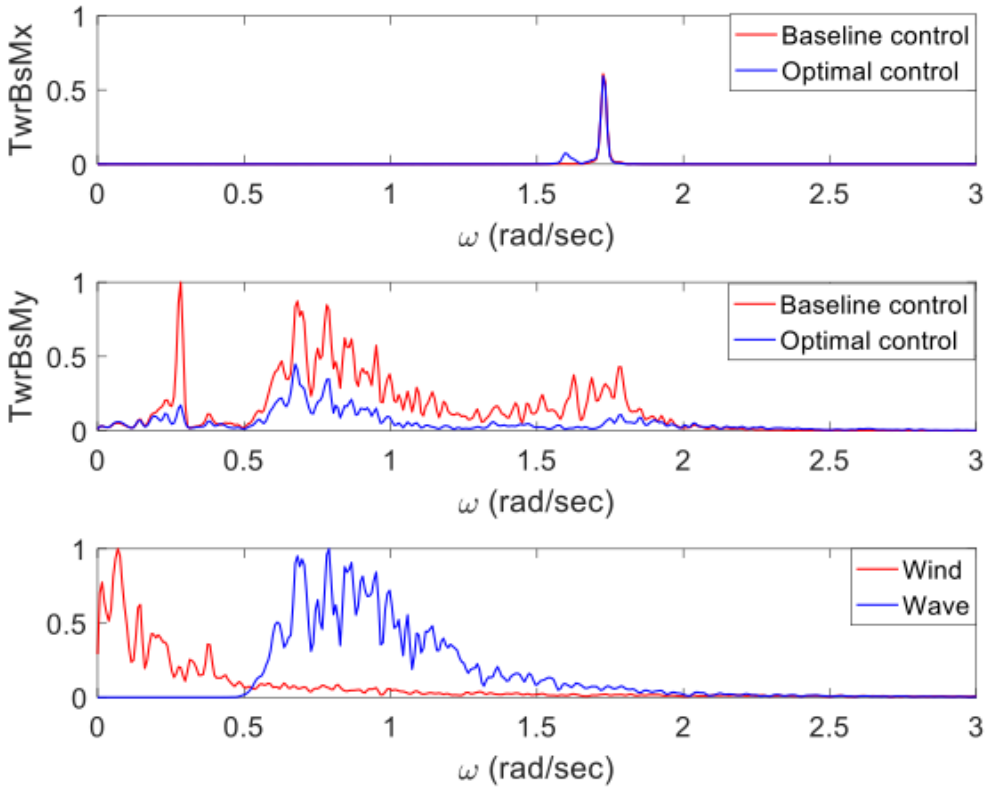

(b) Tower bending moments in frequency domain

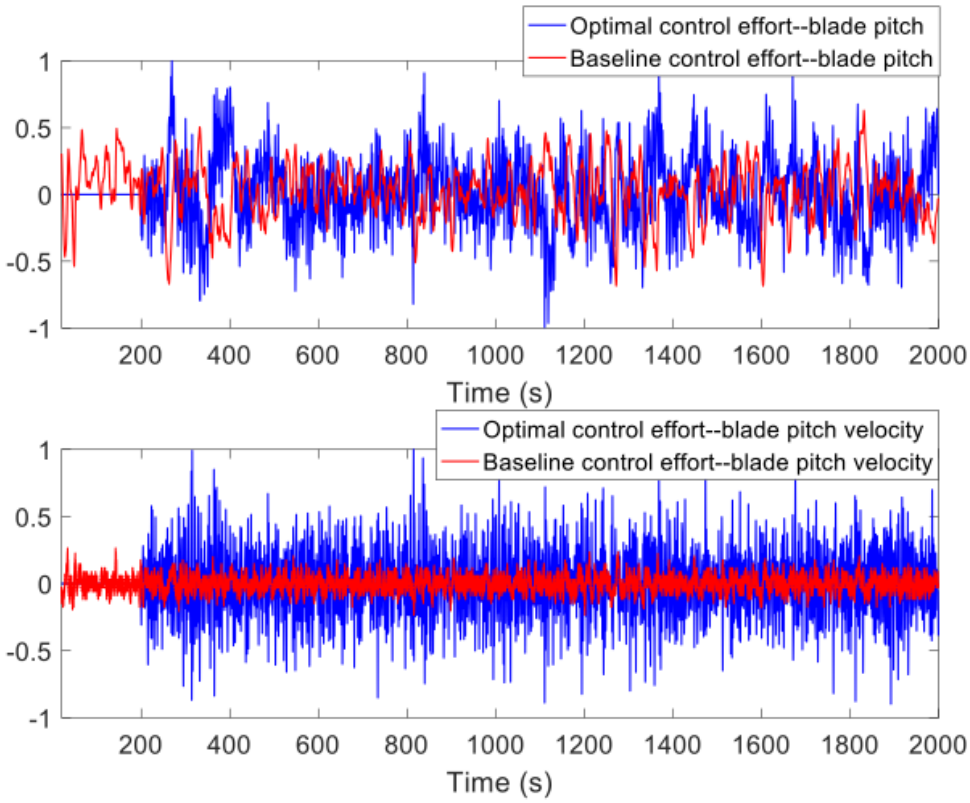

(c) Control efforts: blade pitch angle and blade pitch velocity

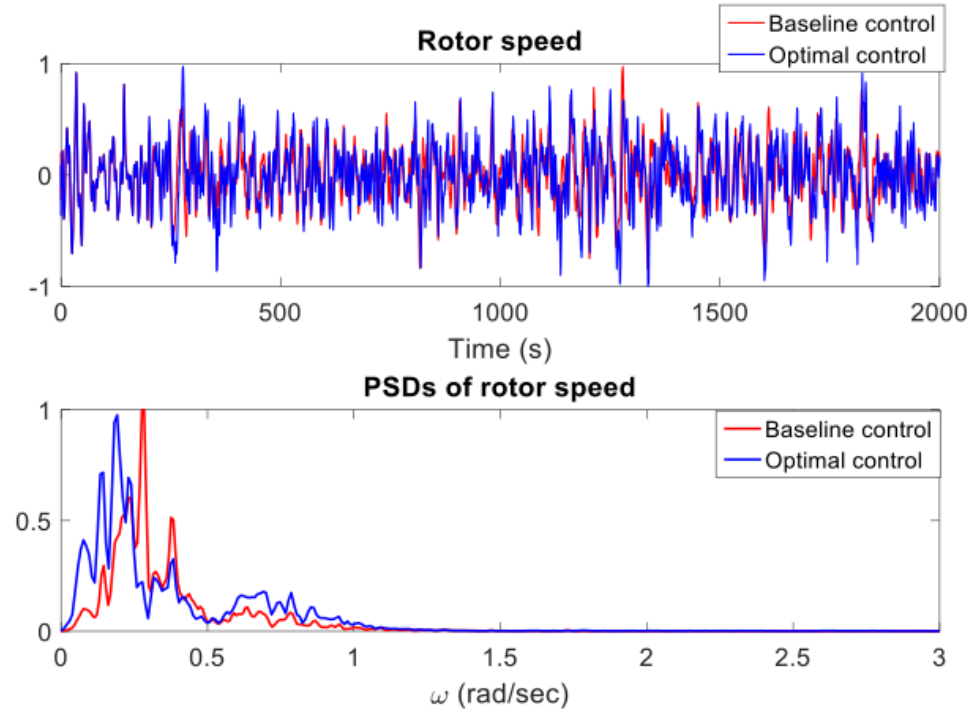

(d) Rotor speed

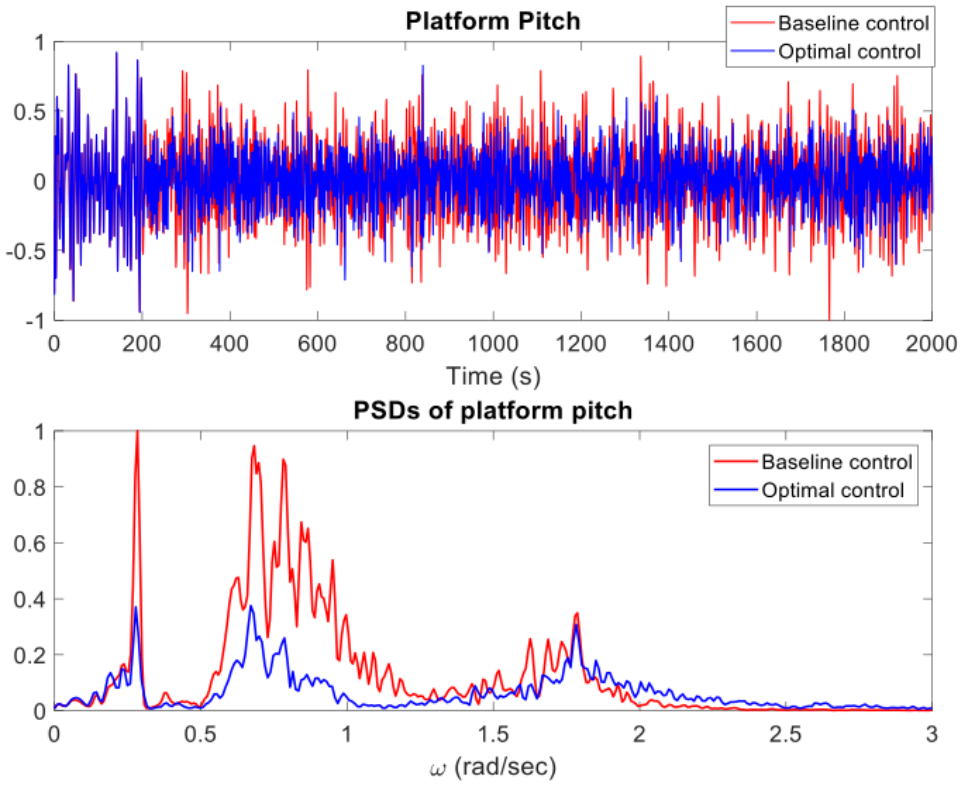

(e) Platform pitch motion

Figure 4-8: Case 1: Comparison of the optimal control and baseline controller

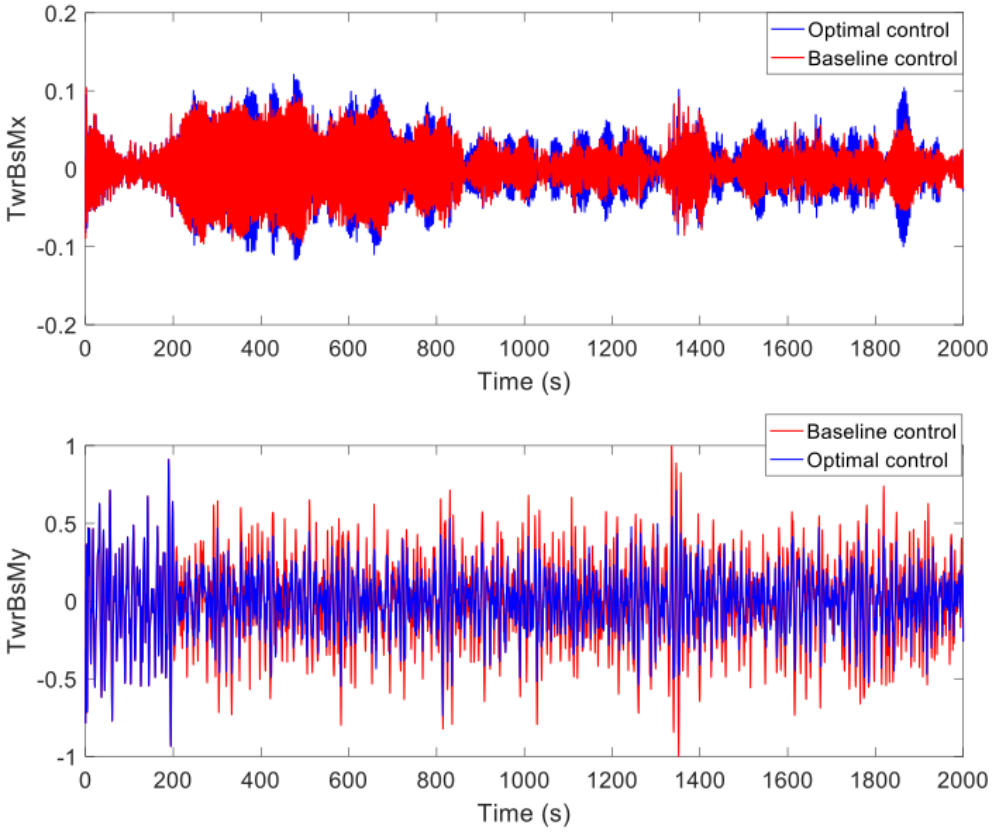

(a) Tower bending moments in time domain

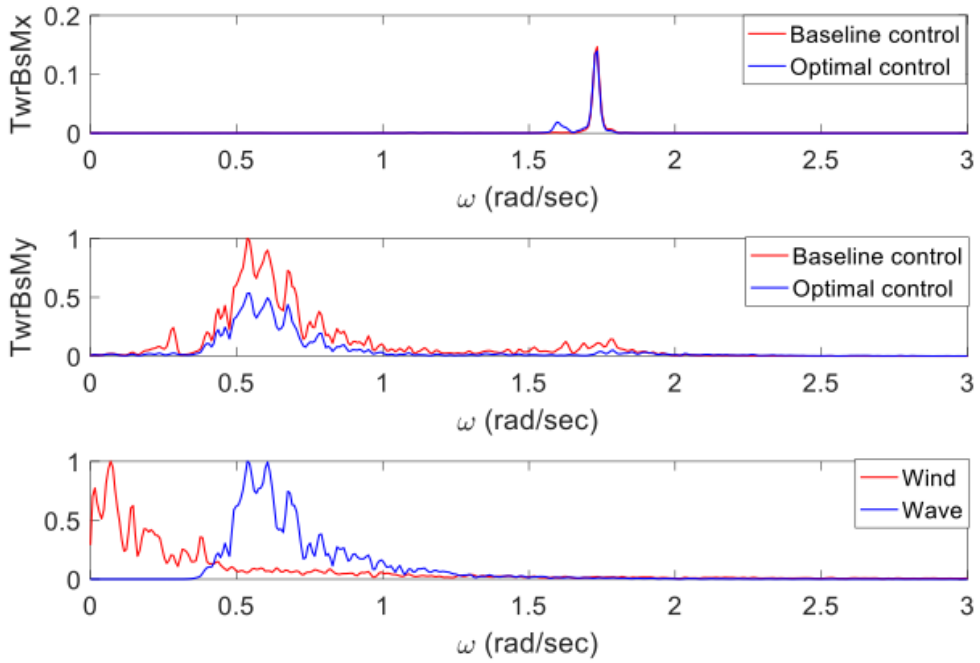

(b) Tower bending moments in frequency domain

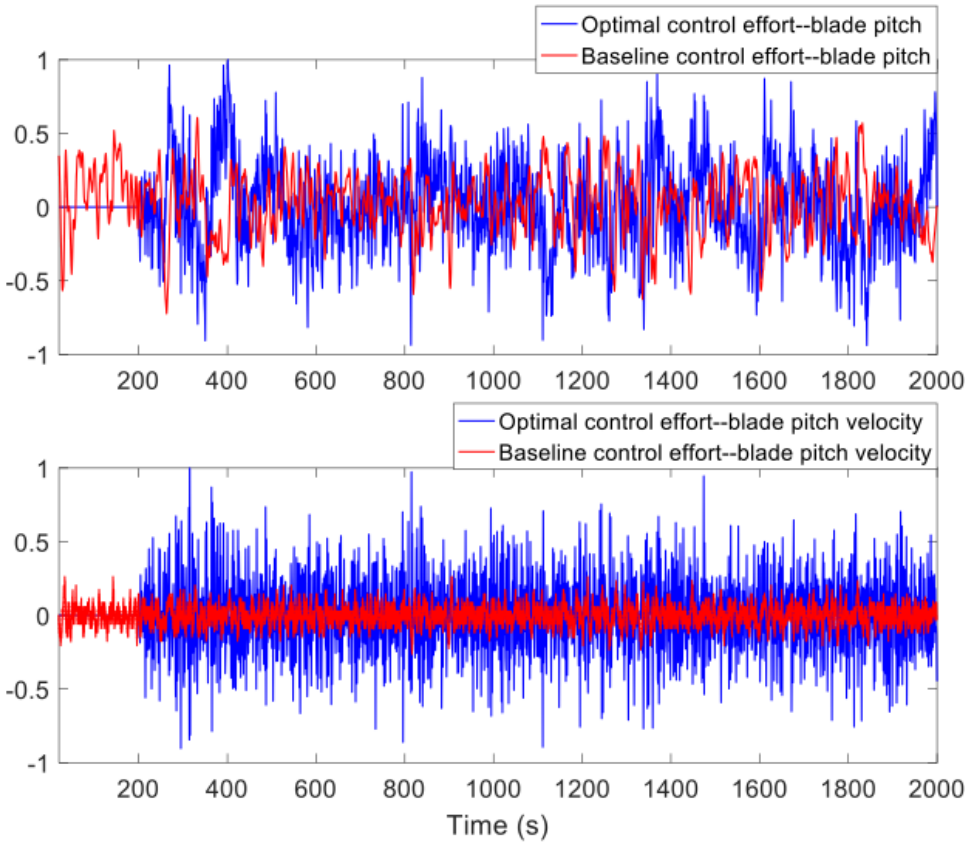

(c) Control efforts: blade pitch angle and blade pitch velocity

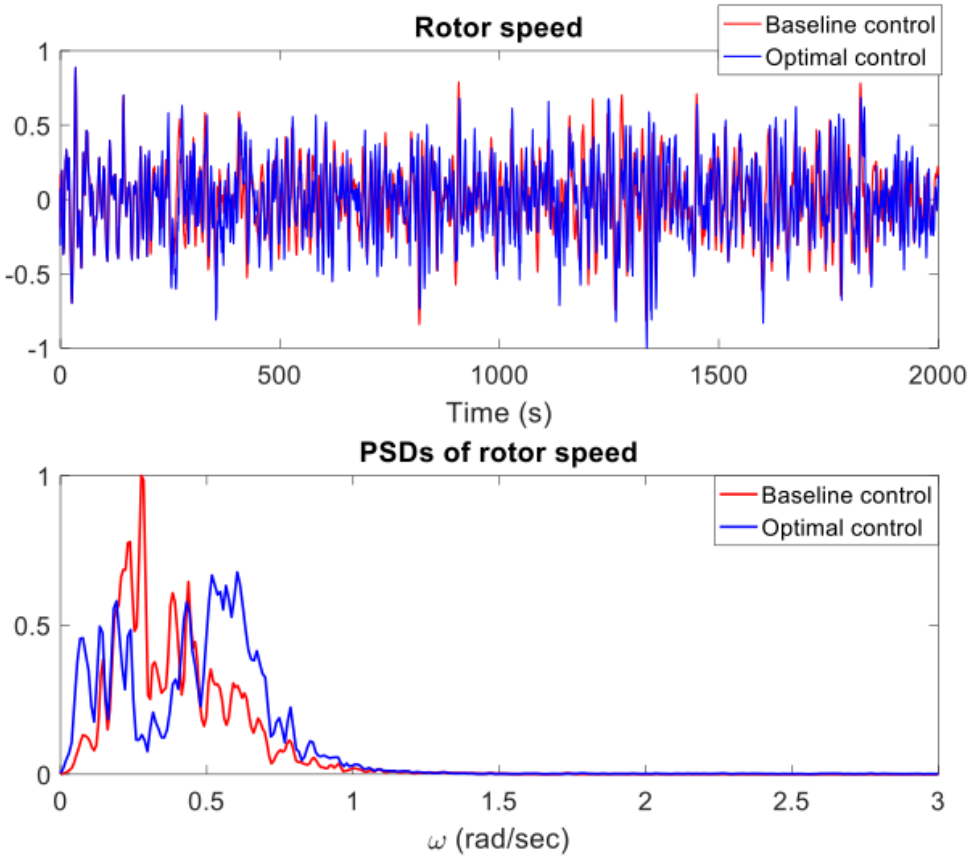

(d) Rotor speed

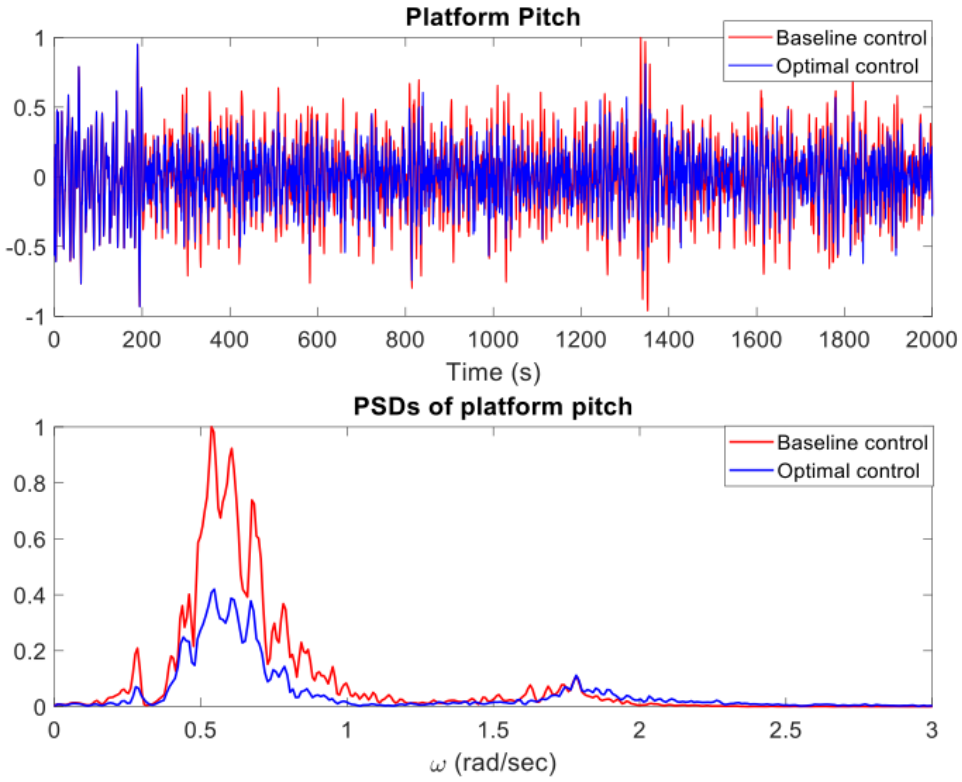

(e) Platform pitch motion

Figure 4-9: Case 2: Comparison of the optimal control and baseline controller

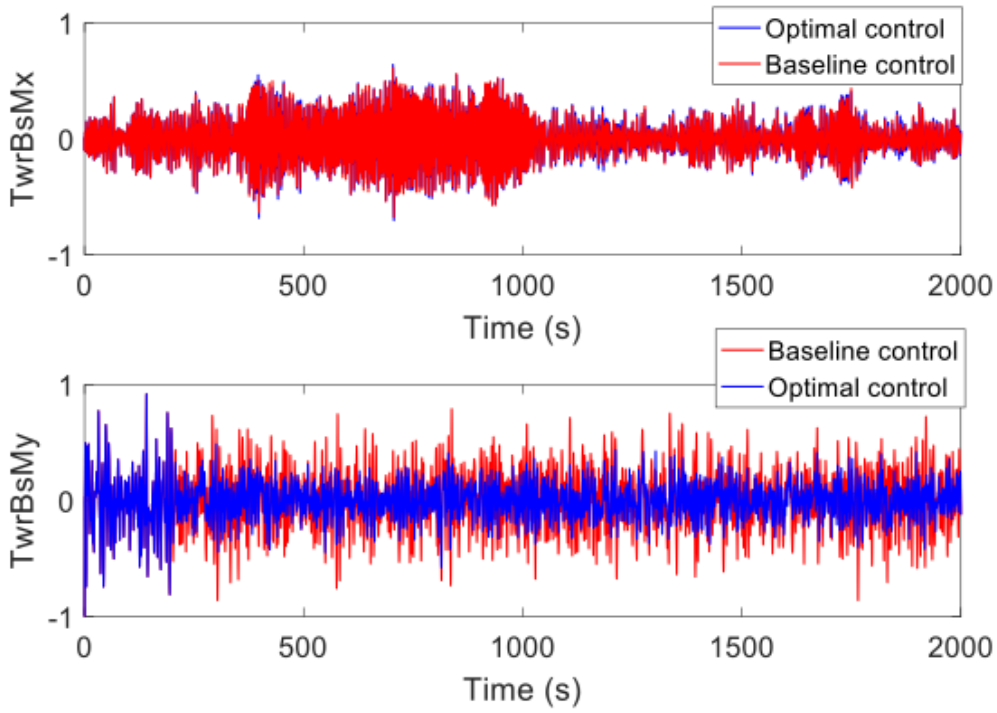

(a) Tower bending moments in time domain

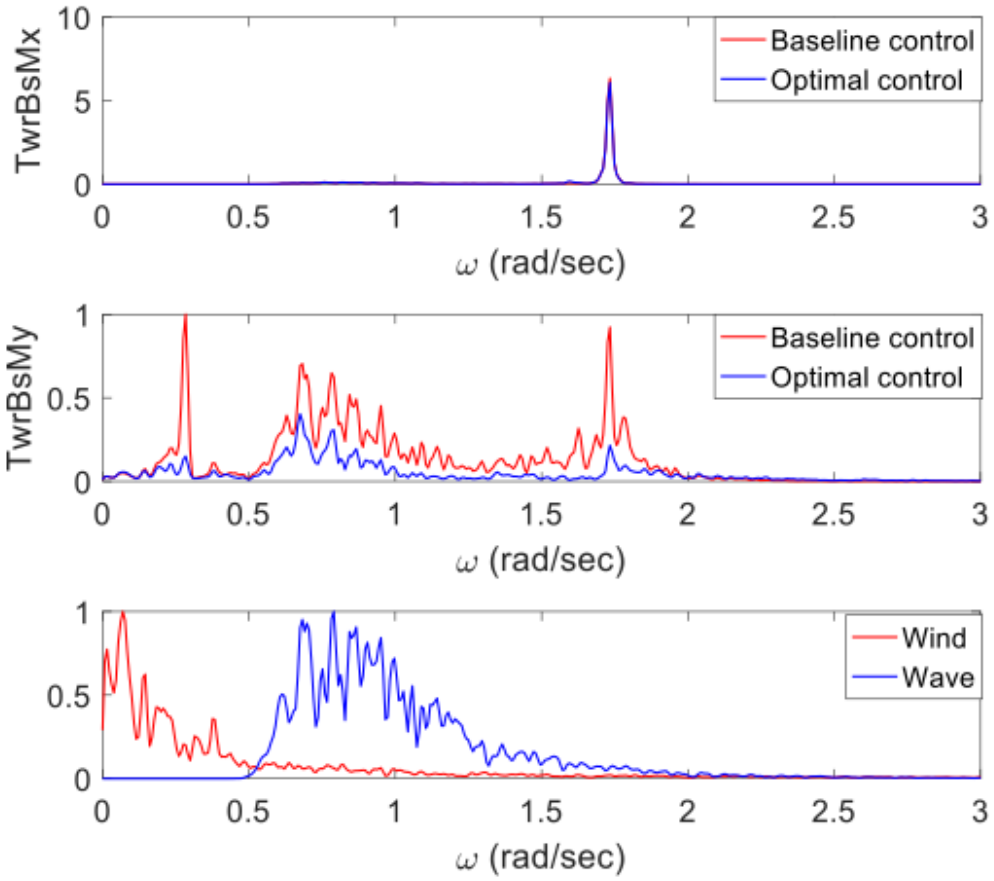

(b) Tower bending moments in frequency domain

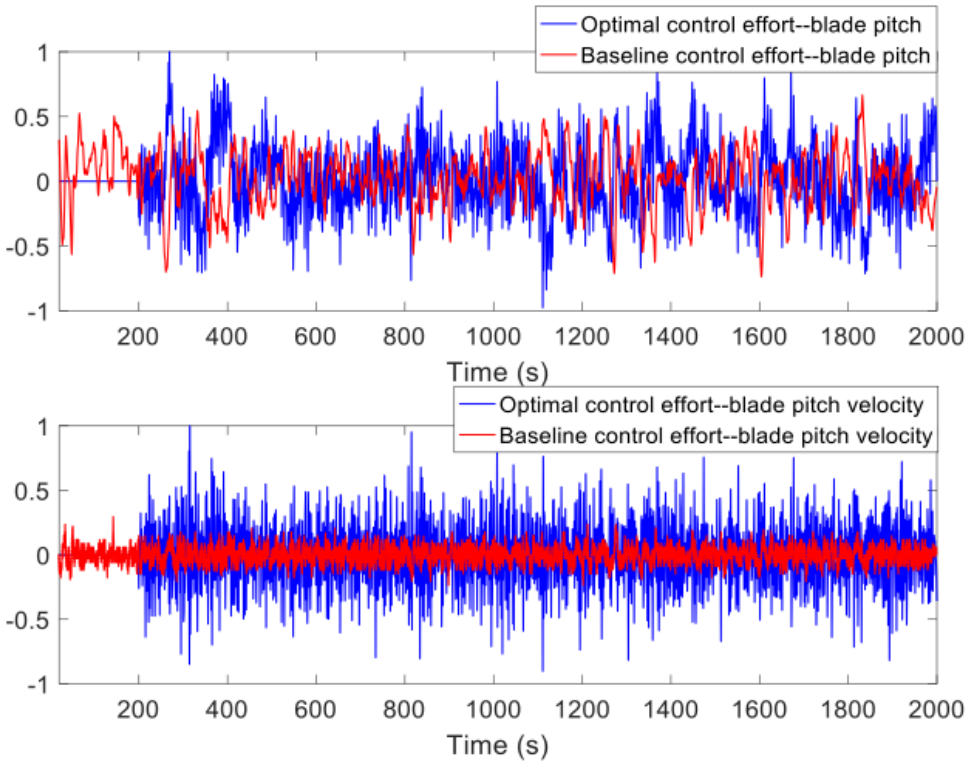

(c) Control efforts: blade pitch angle and blade pitch velocity

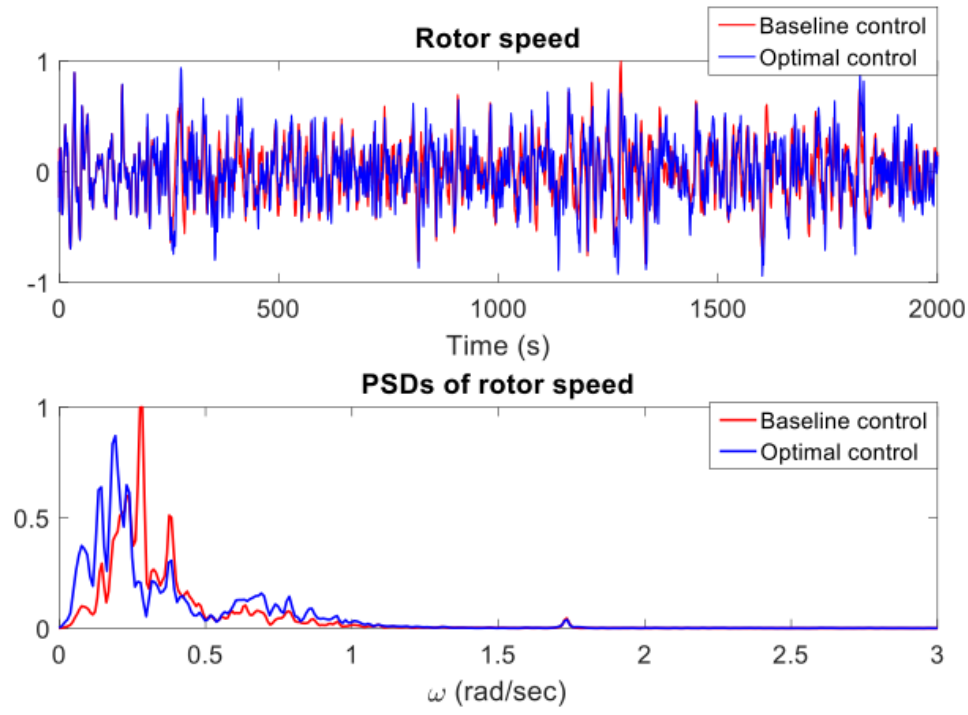

(d) Rotor speed

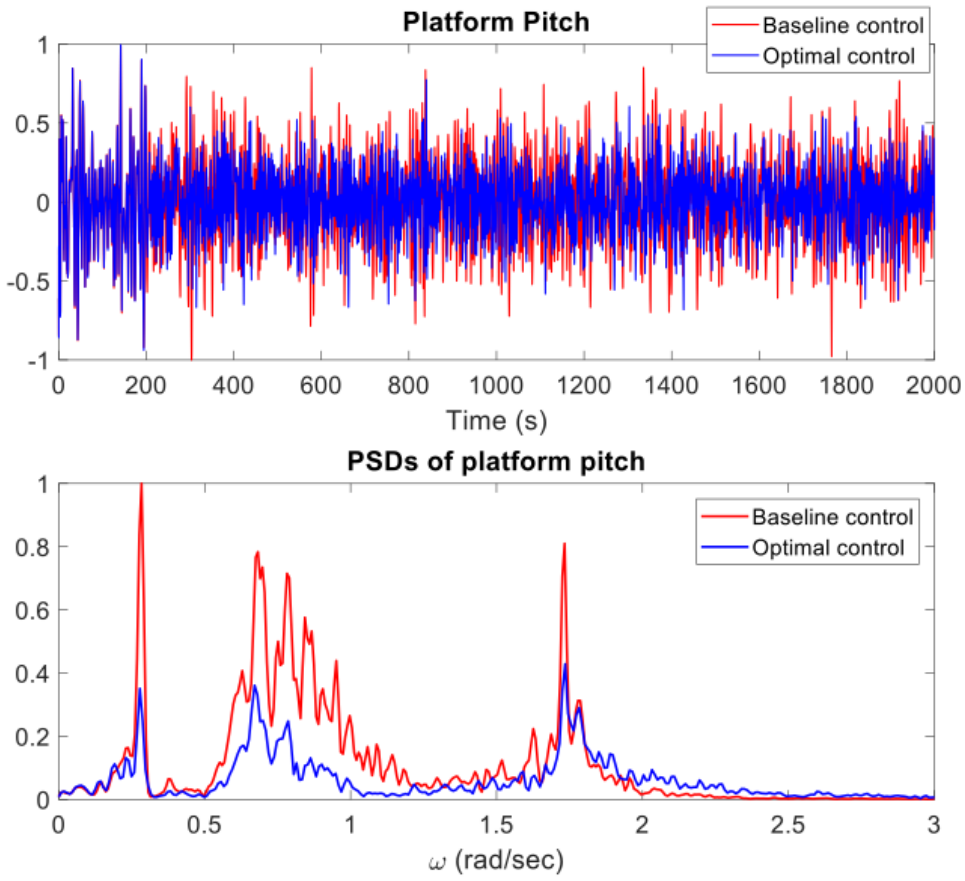

(e) Platform pitch motion

Figure 4-10: Case 3: Comparison of the optimal control and baseline controller

4.5 Conclusions and discussions

On the basis of the ability to forecast the wave force over a finite horizon into the future, a deterministic finite-horizon LQR controller is designed to reduce the fore-aft tower base bending moment, especially the components excited by the wave force. The performance of the optimal control is effective and robust for the aimed load reduction comparing to the baseline speed regulator.

In future work, more detailed sensitivity studies will be conducted in terms of the effects of the optimization horizon, controller update rate and predictor accuracy. Furthermore, on-line linearization and optimization techniques would be considered for better real-time implementations. The computational effort necessary to generate

the forecasted signals needs to be addressed so that the on-line implementation can be achieved efficiently for sequential controller updates.

The control algorithm developed in this chapter for a stiff TLP floating wind turbine may be also implemented with minor modifications for "softer" floating wind turbine concepts like Spars and Semisubmersibles. For example, the effectiveness of blade-pitch controllers has been already demonstrated for the Hywind concept for the mitigation of responses at frequencies well below the peak of the wave spectrum. Meanwhile, this approach is also promising for different control targets combined with the ability to forecast wind speed.

Chapter 5

Model Predictive Control for Offshore Wave Energy Converters

5.1 Introduction

Wave energy is another important resource of renewable energy that ocean provides and be of great potential. In order to extract energy from waves and convert it to mechanical and electrical energy that we can utilize, various types of wave energy converters (WEC) have been proposed [60]. Examples of initiated commercial wave energy converter projects with different buoy and power take-off concepts include Oscillating-Water-Column (OWC) plants like the Pelamis WEC [3], overtopping WEC types like the Wave Dragon [2] and point absorber approaches like the Wavestar device [1].

Due to the stochastic nature of ocean waves, an optimal control design is critical for harvesting energy and reducing cost. Many control strategies have been proposed and validated throughout past decades, including resistive control, approximate complex-conjugate control, latching control, etc. Falnes [25] pointed out that the maximum useful absorbed energy for a body oscillating in one mode is achieved by providing an optimum load impedance that is equal to the complex conjugate of instrinsic impedance of the WEC. He also described two alternative strategies for achieving this [24], which are complex conjugate control and phase and amplitude control.

The complex conjugate control involves anticausal transfer functions from velocity to machinery force, in which the optimal machinery force depends on future values of the buoy velocity [32]. It is impossible to implement the ideal complex conjugate control since future velocities would depend on the choice of machinary force, which leads to different realizable and sub-optimal approximations of this approach [80]. The phase and amplitude control expresses the optimal velocity in terms of the excitation force to provide a reference signal, which is noncausal as well. People can overcome the issue of non-causality by either predicting the wave excitation force or approximate the transfer function into a causal one [60].

In recent years, model predictive controls are introduced into optimizing wave energy conversion as well. Different from feedback type controllers that are optimized off-line, model predictive control solves a constrained optimization problem on-line based on the current state of the plant, which can better take account the state changes and reject disturbances [90]. Hals et al. [32] has shown that the model predictive control can yield power absorption close to optimum in irregular wave waves with perfect prediction. In the same study, they also compared the performance of MPC with a simple predictor and concluded that an accurate and robust forecast of the wave excitation force is necessary.

Therefore, based on the forecast capability we have developed, in this chapter, the model predictive control is developed and validated against a point obsorber oscillating in the heave direction. The floater is a vertical cylinder with radius 5 m and draft 8 m. The performance of the model predictive control is evaluated under irregular wave sea states.

5.2 WEC Equation of motion

Assuming linear potential flow, the equation of motion of a single degree of freedom WEC in heave in the time domain is governed by the Cummins equation:

$$(m + A_\infty)\ddot{\xi}(t) + \int_{-\infty}^{t} K_r(t-\tau)\dot{\xi}(\tau)d\tau + C\xi(t) = f_e(t) + f_m(t) \tag{5.1}$$

Where, m is the mass of the structure, A_∞ is the added mass at infinite frequency, K_r is the impulse response function of the wave radiation force, C is the restoring coefficient, f_e is the incident wave excitation force and f_m is the PTO machinery force [24].

The radiation and diffraction impulse response functions are obtained from the Fourier transform of the frequency domain transfer functions computed by WAMIT [45]. For the purpose of implementing the control algorithm, the impulse response functions are cast in state-space form. Nonlinear free surface and viscous effects may affect the WEC hydrodynamic loads for large amplitude motions and may be learned online by a machine learning algorithm analogous to that used to forecast the exciting force.

The PTO force $f_m(t)$ is a signal regulated by the feedforward controller in order to maximize the wave energy captured under constraints on the heave displacement, force, active and reactive power of the PTO. The proper settings for these constraints are PTO specific and can be adjusted accordingly. The PTO force is a function of the current values of the system states, which include the WEC kinematics, the states of the radiation impulse response functions and the exciting force.

Because of the non-causality of the diffraction impulse response function, the ambient wave elevation or the exciting force need to be forecasted over a sufficiently large time window into the future. These forecasts require knowledge of either the ambient free-surface elevation which is often hard to measure or of the exciting force which may be estimated by sensors on the WEC. The latter approach is adopted in this note. Accurate forecasts of the exciting force are obtained by using the SVM regression model developed in Chapter 3.

5.3 State space model of impulse response functions

The governing equation (5.1) includes a convolution integral $\int_{-\infty}^{t} K_r(t-\tau)\dot{\xi}(\tau)d\tau$, which represents the wave radiation force. Denoting the convolution term as $F_r(t)$,

it can be approximated by a state-space model [66]:

$$\begin{aligned} \dot{x_r}(t) &= A_r x_r(t) + B_r \dot{\xi}(t) \\ F_r(t) &= C_r x_r(t) + D_r \dot{\xi}(t) \end{aligned} \tag{5.2}$$

Where, $x_r(t)$ are the introduced states, A_r, B_r, C_r, D_r are obtained via the parametric identification methodology [66].

Figure 5-1 shows a very good agreement of the original kernel function and its state-space approximation.

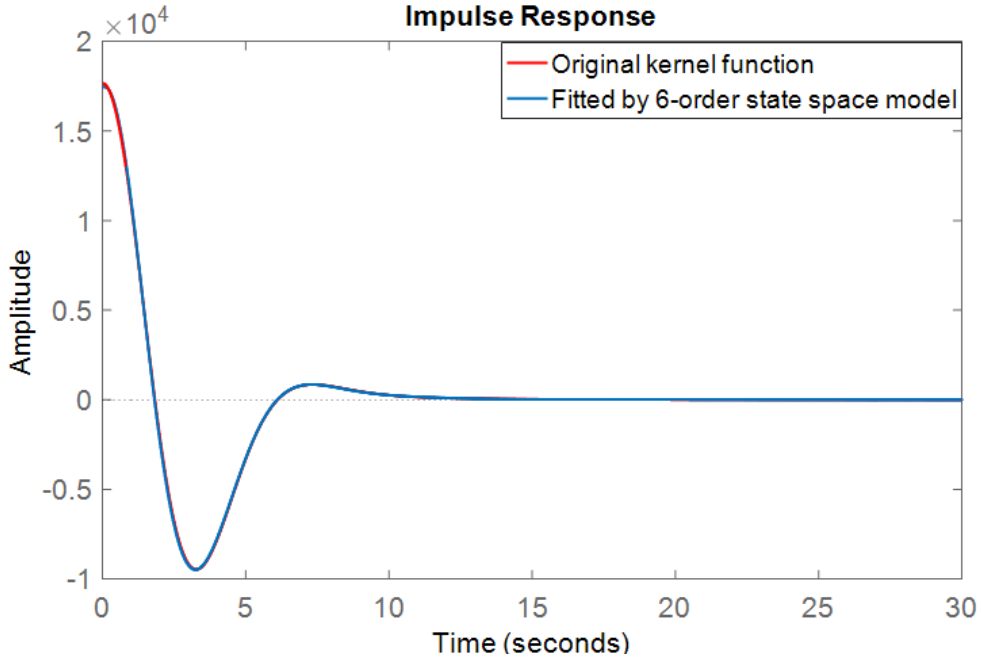

Figure 5-1: Fitted radiation kernel function

The state space model of the dynamical system (5.1) is thus cast in the standard form:

$$\begin{aligned} \dot{\mathbf{x}} &= A_s \mathbf{x} + B_s(u + w) \\ y &= C_s \mathbf{x} \\ z &= C_z \mathbf{x} \end{aligned} \tag{5.3}$$

Where, $\mathbf{x} = [\xi, \dot{\xi}, \mathbf{x_r}]^T$, $u = f_m$, $w = f_e$, $y = \dot{\xi}$, $z = \xi$.

$$
\begin{aligned}
As &= \begin{bmatrix} 0 & 1 & 0 \\ -C/(m+A_\infty) & -D_r/(m+A_\infty) & -C_r/(m+A_\infty) \\ 0 & B_r & A_r \end{bmatrix} \\
B_s &= [0, \quad 1/(m+A_\infty), \quad \mathbf{0}]^T \\
C_s &= [0, \quad 1, \quad \mathbf{0}] \\
C_z &= [1, \quad 0, \quad \mathbf{0}]
\end{aligned}
\tag{5.4}
$$

5.4 Forecasts of the exciting force via LS-SVM regression

From the governing equation (5.1) or (5.3), the wave excitation force f_e is the driving force of the system. To better optimize the wave energy capture by optimally adjusting the PTO mechanical force f_m, the forecast of wave force f_e is necessary. In Chapter 3, we have developed and validated the LS-SVM regression method for the forecast of wave elevations, in which we have also demonstrated that the forecast of wave excitation force can be applied in the same way. Moreover, due to the fact that the floating structure itself is a natural low-pass filter, the wave excitation forces contain lower frequency components and less noise than ambient wave elevations if the wave excitation force is provided with accurate measurement or estimation.

Figure 5-2 shows the performance of the LS-SVM regression model in predicting the heave excitation force which is simulated by convolving the impulse response function output by WAMIT with the wave elevations measured in a tank test. The forecast horizon is 5 seconds and the root-mean-square(RMS) error of the signal is 9.6% of ($4\sigma_{F_{ex}}$). $\sigma_{F_{ex}}$ is the standard deviation of the exciting force. Using $4\sigma_{F_{ex}}$ as the non-dimensionalization factor is analogous to using the significant wave height for the wave elevations since $Hs = 4\sigma_\eta$.

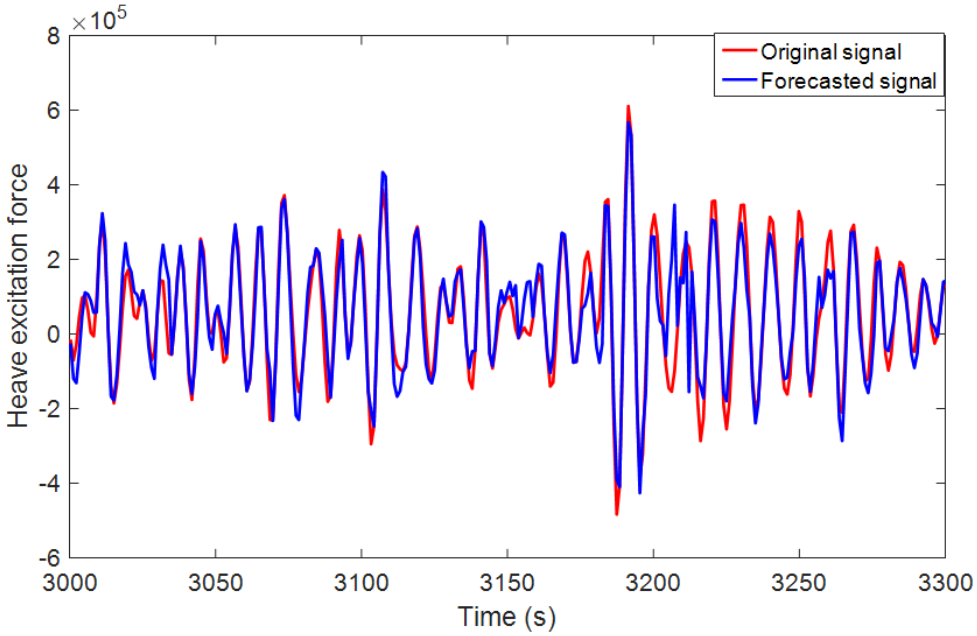

Figure 5-2: Comparison of the original and forecasted wave exciting force

5.5 Formulation of the model predictive control

The objective is to maximize the energy E extracted by the PTO system over a predicted time horizon T_h:

$$E = \int_0^{T_h} P(t)dt = \int_0^{T_h} -f_m(t)\dot{\xi}(t)dt \tag{5.5}$$

Therefore, the optimization problem will be foumulated as:

$$\max E = \min(-E) = \min \int_0^{T_h} u(t)y(t)dt \tag{5.6}$$

with constraints on both the heave motion and PTO machinery force:

$$|z| < \xi_{max} \tag{5.7}$$

$$|u| < f_{m,max} \tag{5.8}$$

The objective function (5.6) subject to an equality constraint (the system

dynamics (5.3)) and two inequality constraints (the heave motion and machinery force constraints (5.7)-(5.8)) forms a non-convex quadratic programming (QP) problem [46]. However, for non-convex QP problems, the global optimal solution cannot be guaranteed. Different kinds of modifications of the objective function have been proposed to take account the problem of convexity [46], [90], [32]. In this study, a similar approach is used as [90] proposed:

$$\min(-E) = \min \int_0^{T_h} u(t)y(t) + r(\Delta u)^2 dt \tag{5.9}$$

Where, $\Delta u = u(t) - u(t-1)$ denotes the change rate of the control effort. r is the penalty weight which can be adjusted.

To numerically solve the optimization problem defined by (5.9) subject to constraints (5.3), (5.7), (5.8), the system dynamics (5.3) is discretized using zero-order hold [32] with a sample time Δt:

$$\begin{aligned} x_{k+1} &= A_d x_k + B_d(u_k + w_k) \\ y_k &= C_d x_k \\ z_k &= C_{zd} x_k \end{aligned} \tag{5.10}$$

Where,

$$\begin{aligned} A_d &= e^{A_s \Delta t} \\ B_d &= A_s^{-1}(A_d - I)B_s \\ C_d &= C_s \\ C_{zd} &= C_z \end{aligned} \tag{5.11}$$

Correspondingly, the objective function and constraints would be expressed as:

$$J = \Delta t \sum_{k=0}^{N-1} u_k y_k + r|\Delta u_k|^2 \tag{5.12}$$

$$|z_k| < \xi_{max} \tag{5.13}$$

$$|u_k| < f_{m,max} \tag{5.14}$$

Where, $\Delta u_k = u_k - u_{k-1}$.

Denote the control effort (i.e., the PTO machinery force) and disturbance term (i.e., the wave excitation term) during the optimized horizon as:

$$\begin{aligned} U &:= [u_0, u_1, ..., u_{N-1}] \\ W &:= [w_0, w_1, ..., w_{N-1}] \end{aligned} \tag{5.15}$$

for which, U is the control actions that need to be optimized.

The state equation (5.10) can be propagated from the current state to the whole optimization horizon to obtain:

$$\begin{aligned} \hat{y}(k+i|k) = CA^i x_k + \sum_{j=0}^{i-1} CA^{i-j-1} B(\hat{u}(k+j|k) + \hat{w}(k+j|k)), \\ i = 0, 1, ..., N-1 \end{aligned} \tag{5.16}$$

Where, $\hat{y}(k+i|k)$ denotes the state y_{k+i} estimated at time k, and the same holds for $\hat{u}(k+j|k)$ and $\hat{w}(k+j|k)$. Clearly, $\hat{u}(k+j|k)$ would be the optimized control effort that need to be solved. And $\hat{w}(k+j|k)$ is the predicted wave excitation force described in Section 5.4, which is assumed known in the optimization process.

Denote $Y = [\hat{y}(k|k), \hat{y}(k+1|k), ..., \hat{y}(k+N-1|k)]$, we can express (5.16) in a matrix form as:

$$Y = S_x x_k + S_u(U + W) \tag{5.17}$$

where,

$$S_x = \begin{bmatrix} C \\ CA \\ CA^2 \\ \vdots \\ CA^{N-1} \end{bmatrix}, \quad S_u = \begin{bmatrix} 0 & & & & \\ CB & 0 & & & \\ CAB & CB & \ddots & & \\ \vdots & \vdots & \ddots & 0 & \\ CA^{N-2}B & CA^{N-3}B & \dots & CB & 0 \end{bmatrix} \tag{5.18}$$

Similarly, we can express the vector of states $Z = [\hat{z}(k|k), \hat{z}(k+1|k), ..., \hat{z}(k+N-$

$1|k)]$ as:

$$Z = S_{x,z}x_k + S_{u,z}(U + W) \tag{5.19}$$

where, $S_{x,z}, S_{u,z}$ can be derived by substituting C_z for C in (5.18).

Also, rewrite the slope of control effort $\Delta U := [\Delta u_0, \Delta u_1, ..., \Delta u_{N-1}]$ as:

$$\Delta U = T_\Delta U - g_u \tag{5.20}$$

where,

$$T_\Delta = \begin{bmatrix} 1 & & & & \\ -1 & 1 & & & \\ & -1 & \ddots & & \\ & & \ddots & 1 & \\ & & & -1 & 1 \end{bmatrix}_{N\times N}, \quad g_u = \begin{bmatrix} u_{-1} \\ 0 \\ \vdots \\ 0 \end{bmatrix}_{N\times 1} \tag{5.21}$$

where, u_{-1} is the control input applied to the system at current time and u_{-1}=0 at the intial point of simulation.

Then, the cost function J in (5.12) can be expressed as:

$$J = U^T Y + (T_\Delta U - g_u)^T R(T_\Delta U - g_u) \tag{5.22}$$

where, $R = r \times I_{N-1}$.

Substituting (5.17) into (5.22), the objective function J can be expressed in quadratic form:

$$J = \frac{1}{2}U^T HU + f_T U \tag{5.23}$$

where,

$$\begin{aligned} H &:= S_u + S_u^T + 2S_R \\ f &:= S_x x_k + S_u W - 2S_g \end{aligned} \tag{5.24}$$

with $S_R := T_\Delta^T R T_\Delta$, $S_g := T_\Delta^T R g_u$.

From (5.23)-(5.24), it can be seen that if the objective functions has not been modified with the extra penalty term $r\Delta u^2$, the Hessian matrix would be $S_u + S_u^T$

instead. Since the diagonal elements of S_u (see 5.18)) are zeros, the Hessian matrix would be indefinite and hence leads to a non-convex problem. Correspondingly, by adjusting the value of a positive r and checking the eigenvalues of H as expressed in (5.24), we can gurantee the convexity of the problem.

The inequality constraints (5.13)-(5.14) can be rewritten as:

$$A_u U \leq b_u \tag{5.25}$$

where,

$$A_u = \begin{bmatrix} I \\ -I \\ S_{u,z} \\ -S_{u,z} \end{bmatrix}, \quad b_u = \begin{bmatrix} U_{max} \\ U_{max} \\ Z_{max} - S_{x,z}x_k - S_{u,z}W \\ Z_{max} + S_{x,z}x_k - S_{u,z}W \end{bmatrix} \tag{5.26}$$

with $U_{max} = f_{m,max} \times [1, ..., 1]^T$ and $Z_{max} = \xi_{max} \times [1, ..., 1]^T$.

Combine (5.23)-(5.26), we now have a standard convex QP problem as:

$$\begin{aligned} U_{opt} = \arg\min_U J = \frac{1}{2}U^T H U + f_T U \\ \text{subject to} \quad A_u U \leq b_u \end{aligned} \tag{5.27}$$

which can be numerically solved by standard quadratic programming solvers [61].

5.6 Simulation results of the optimal control for maximum energy capture

The performance of the model predictive control is tested for a heaving cylinder which is neutrally buoyant with radius 5m and draft 8m. The performance of the WEC is simulated under two different sea states (Hs=1.7m, Tp=8.7s; Hs=4.5m, Tp=11.8s) with varying regularization factors r (1e-5, 1e-4, 1e-3) to illustrate its effect on the generated power and corresponding control force and heave motion.

The optimization horizon for the MPC is 5 seconds and the wave force is forecasted

by the LS-SVM regression shown in Section 5.4. Figure 5-3 shows the RAO of the heave motion and the two seastate spectra.

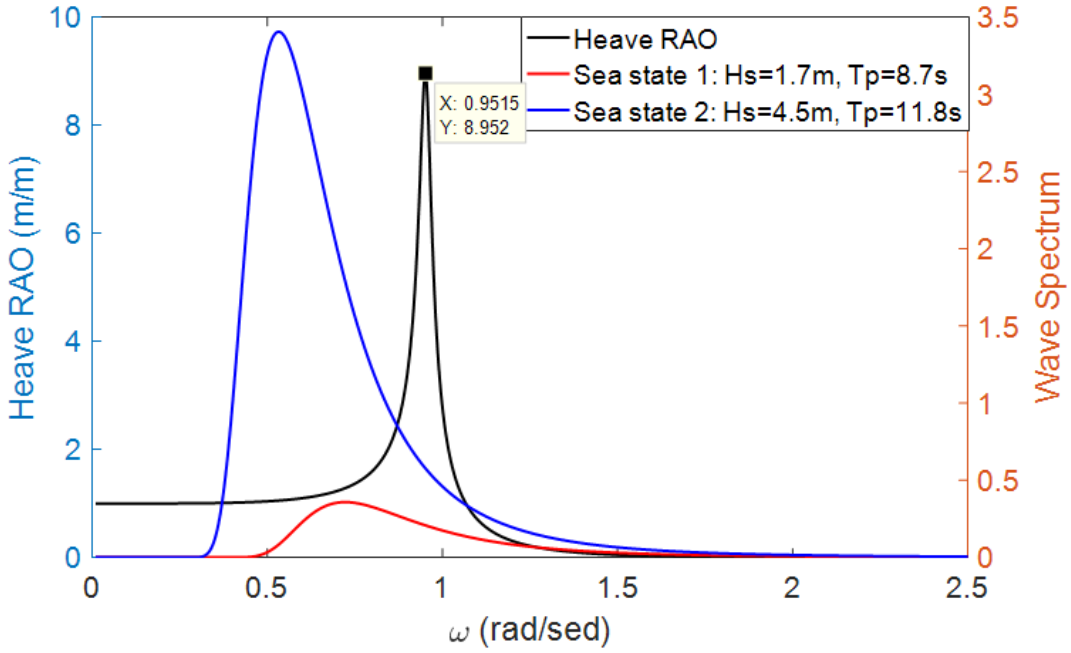

Figure 5-3: Heave RAO and wave spectra

The constraints $\xi_{max}, f_{m,max}$ are specified by the PTO machinery. Without specifying the PTO design in this study, the heave constraint is set to $\xi_{max} = H_s$ and the force constraint $f_{m,max}$ is set to a large value.

The statistical results are shown in Table 5.1, where $\bar{P}$ is the mean power over the simulation, $\sigma_{(\cdot)}$ is the standard derivation of the physical quantity. Figure 5-4 $\sim$ 5-5 shows the time records of cumulative power with different r under the two sea states. Clearly, with smaller r, the constraint on control effort is less thus more power is possible to achieve capturing.

To better illustrate the effects of the combined motion and machinery force constraints and the penalty term, Figure 5-6 $\sim$ 5-7 show time records of the heave displacement, heave velocity, wave force, control force and instantaneous power under different values of r under sea state 2. When r is small, the system tends to behave more resonantly with larger PTO machinery force and heave motion, which is the scenario that their own constraints start to come into play. From Figure 5-6 $\sim$ 5-7,

it also can be observed that under the model predictive control, the heave velocity is driven to match the phase of the wave excitation force, which makes the model predictive controller operated close to the theoretical optimal control law [60].

Table 5.1: Statistical results under different regularization factors r

Cases	$\bar{P}(KW)$	$\sigma_P(KW)$	$\sigma_{f_m}(N)$	$\sigma_\xi(m)$
Sea state 1, r=1e-5	89.2	265.6	4.94e5	1.16
Sea state 1, r=1e-4	61.7	212.7	3.5e5	0.96
Sea state 1, r=1e-3	41.8	86.4	1.6e5	0.58
Sea state 2, r=1e-5	720	2030	1.94e6	3.76
Sea state 2, r=1e-4	590	1780	1.26e6	3.02
Sea state 2, r=1e-3	280	615	5.1e5	1.52

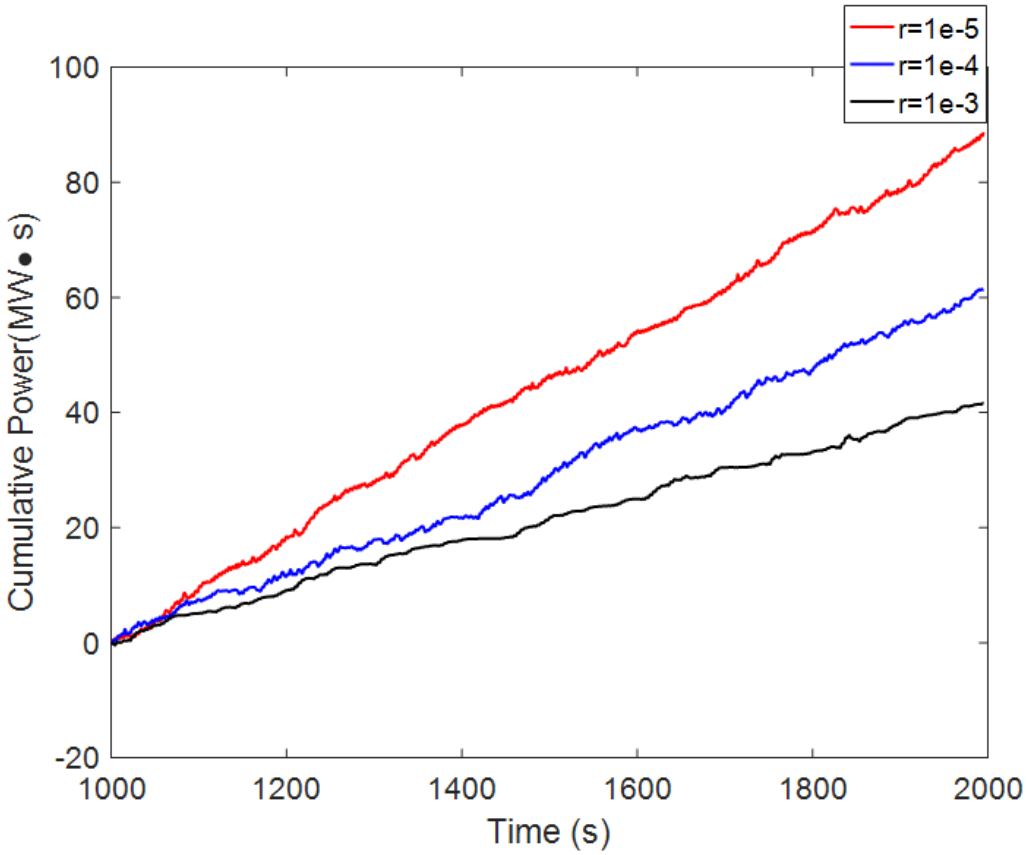

Figure 5-4: Cumulative power under sea state 1: Hs=1.7m, Tp=8.7s

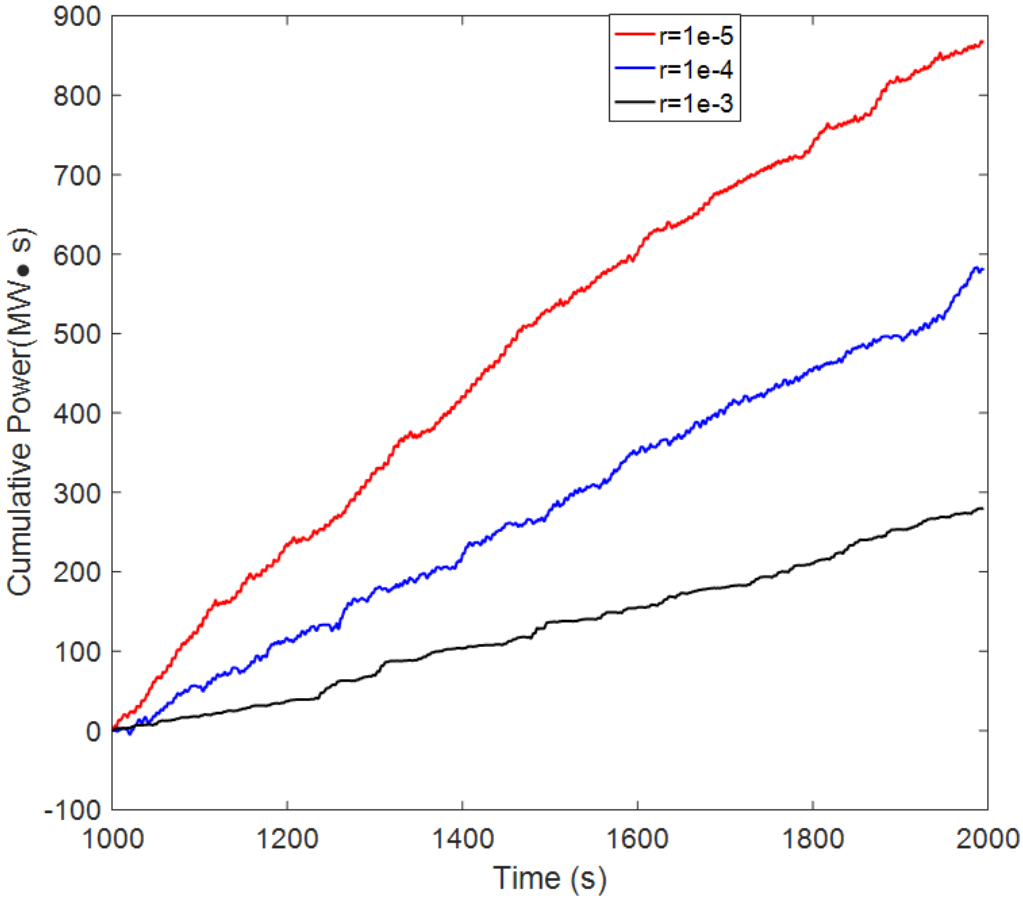

Figure 5-5: Cumulative power under sea state 2: Hs=4.5m, Tp=11.8s

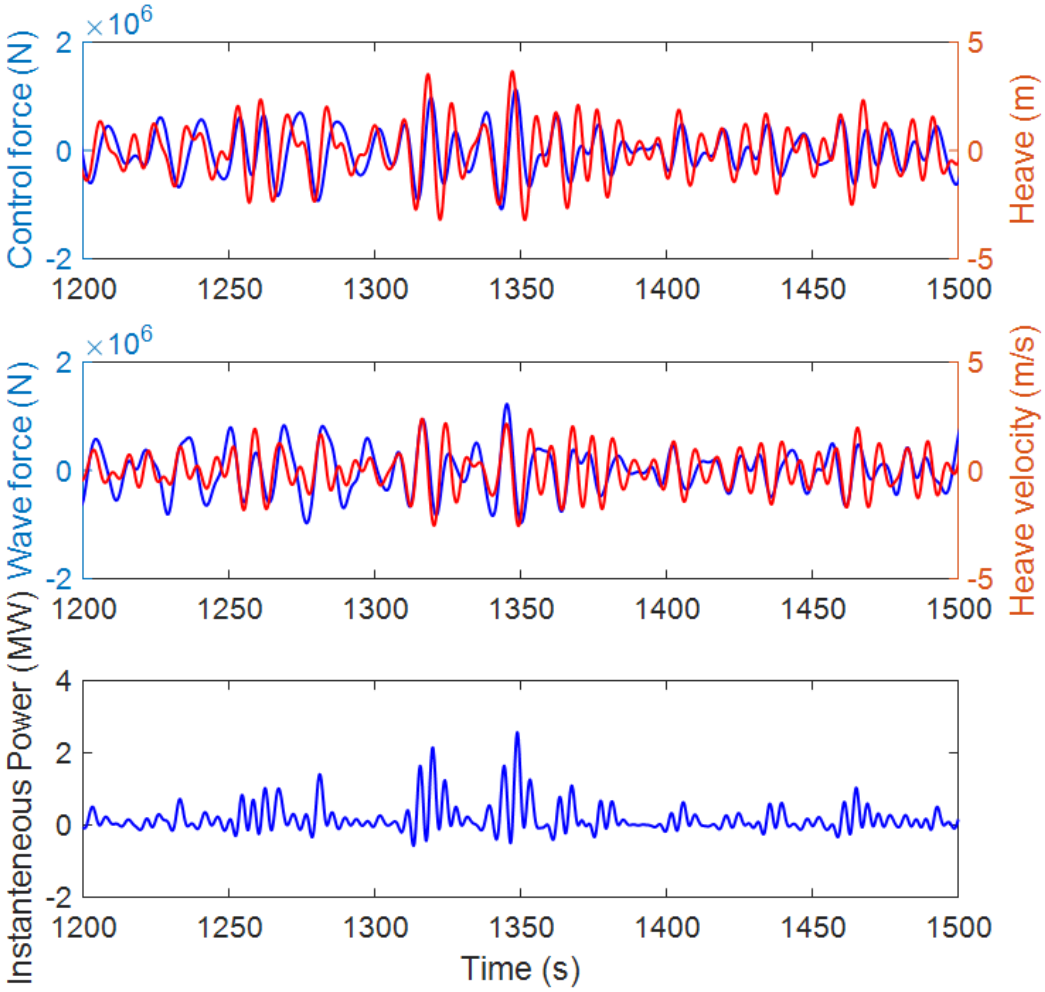

Figure 5-6: Time records of the WEC performance: sea state 2, r=1e-3

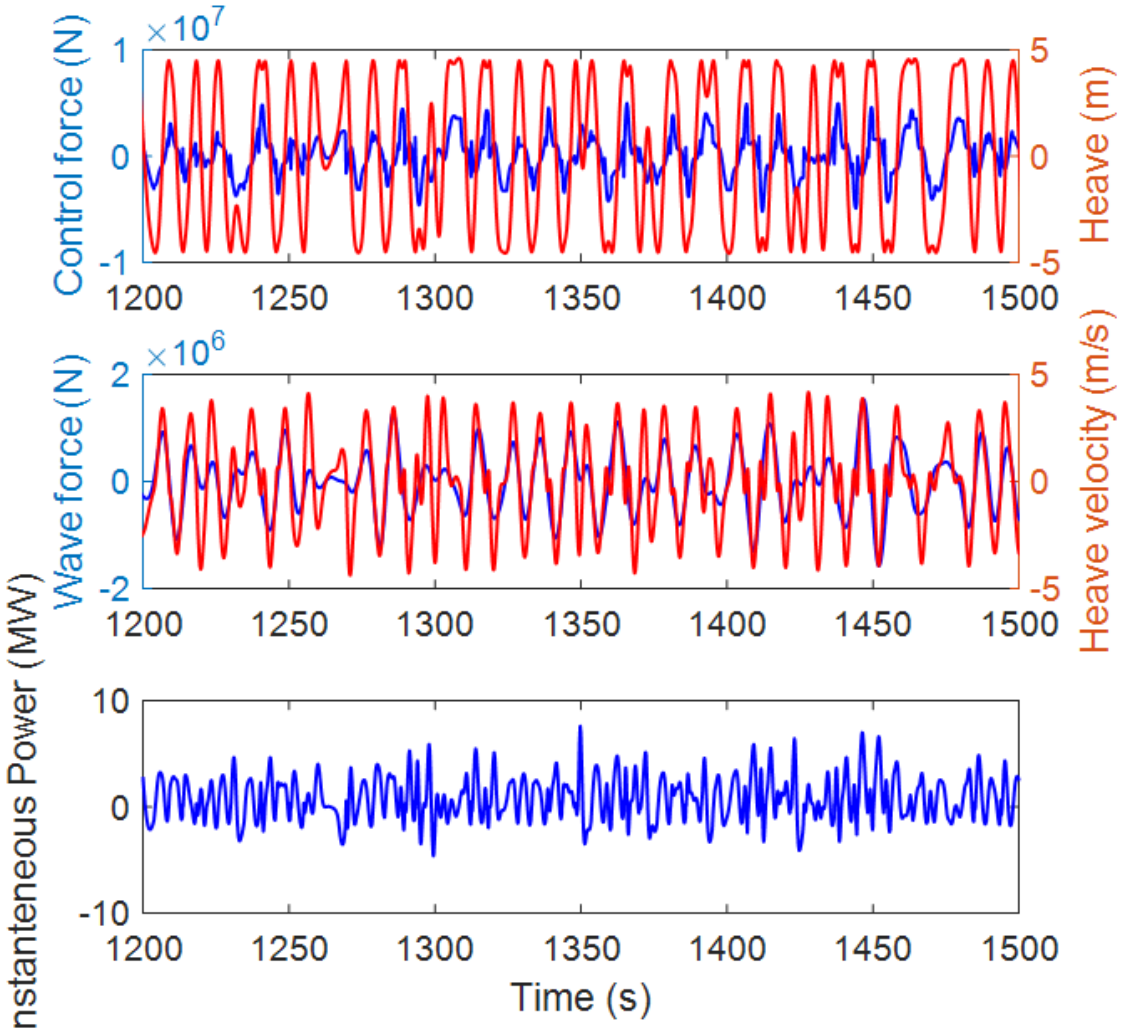

Figure 5-7: Time records of the WEC performance: sea state 2, r=1e-5

5.7 Conclusions and discussions

On the basis of the ability to forecast the wave force over a finite horizon into the future, a model predictive controller is designed to maximize the power capture with certain mechanical constraints. The performance of the optimal control is effective and robust for a heaving point absorber.

Similar to the model predictive control of the offshore floating wind turbines, there is a trade-off of the forecast accuracy and forecast horizon. Zhong and Yeung [90] in their study indicates that under regular wave conditions, increasing the optimization

horizon does not necessarily lead to a better performance of the MPC. Whether the same conclusion holds for irregular wave conditions still needs to be verified.

This study takes a simple form of a heaving cylinder as an example to illustrate the feasibility and effectiveness of such a model predictive controller with the ability of forecasting the wave excitation force without going deep into the study of specific PTO mechanisms. Future work could be done by applying the same principle of model predictive control to various types of floater designs with different PTO systems.

Chapter 6

Support Vector Regression Model of the Nonlinear Viscous Ship Roll Hydrodynamics

6.1 Introduction

Ships remain a primary means of modern transportation in the global economy. Thus it is important to ensure the safety and operational performance of ships since they would inevitably encounter harsh sea states during their lifetime. In the past decades, different numerical theories and experiments have been developed to understand and evaluate the global responses of ships. Among all the challenges remaining in the ship design and assessment process, ship roll motion is of particular interest, since it is highly nonlinear and subjected to significant viscous effects arising from eddies shed from the hull, lift effect in case of a ship advancing with a forward speed and bilge keel damping, etc. [26].

The most popular tool to evaluate the ship roll response is to combine semi-empirical models with experiments or CFD simulations for further design purposes and the prediction of motion responses [86] [38] [54] [53]. The existing semi-empirical models are usually based on polynomial approximations that connect the nonlinear

damping and restoring forces with the ship velocities and displacements.

However, as discussed by many researchers, the widely-used semi-empirical models with constant coefficents and linear or quadratic damping terms cannot fully capture the characteristics of ship roll hydrodynamics. Memory effects, the behavior under a large roll amplitude, the stochastic nature of irregular wave conditions, etc., need to be carefully taken into account. Towards this objective, Bassler [6] proposed a piece-wise damping model to better predict large amplitude roll damping. However, we still lack a more general model that takes into account all pertinent features of this problem.

In this chapter, the SVM model of the ship roll hydrodynamics problem proceeds along the following lines. A series of CFD simulations of a barge with bilge keels are counducted and validated. The results from these simulations serve as a database and are assumed to be an "exact" representation of the flow physics. An SVM regression model is established using the ship roll kinematics and wave elevations over a certain past time period as the features which account for memory effects as well as the stochastic nature of the ambient ocean wave. This study also compares and discusses the different feature and kernel selections used in the model.

6.2 CFD simulations

To establish the SVM regression model for the ship roll hydrodynamics problem, a baseline dataset is needed for the training and validation process. Due to the free surface nonlinearity and viscous flow separation physics that dominate the ship roll problem, it cannot be accurately modelled by potential flow theory. Therefore, besides model tests, numerical simulations of ship roll motion are conducted via a computational fluid dynamics (CFD) solver. In this study, a barge in model scale is modelled using the semi-2D CFD solver [14].

The prototype ship dimension in model scale has a width of 300 mm and depth of 200 mm with an overall length of 580 mm and a draft 120 mm, which was tested in a flume in the Department of Ocean Engineering, IIT Madras [54] [53]. The scale ratio

was 1/100. A series of CFD simulations are conducted and considered as the database used to train the SVM regression model. The inertia and hydrostatic properties of the ship model and bilge keel dimensions are summarized in Table 6.1. Figure 6-1 shows a sketch of the model test setup and the ship model [53].

Table 6.1: Properties of the ship model and bilge keels

Dimensions	Values
Draft	0.12m
Displacement	20.88 kg
Roll moment of inertia	0.2244 kg·m^2
Center of gravity (KG)	0.08 m
Bilge keel width	10 mm
Angle with horizontal	45 deg

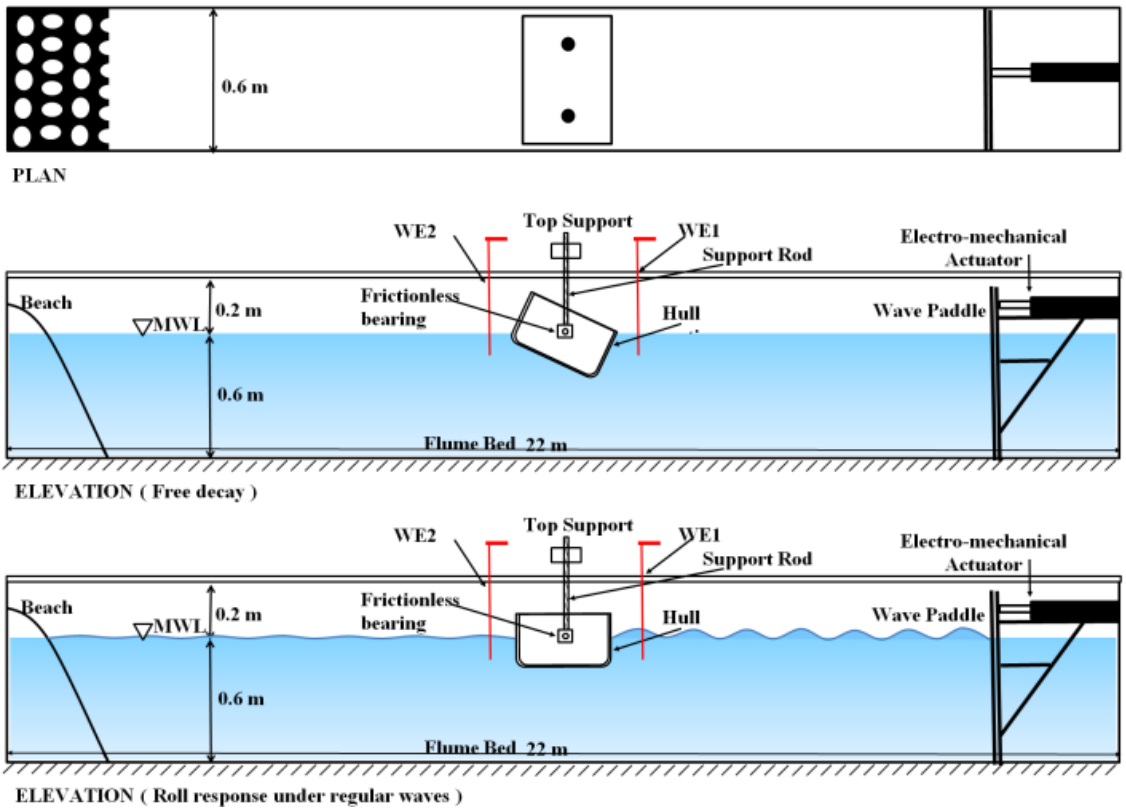

(a) Experimental setup in glass flume

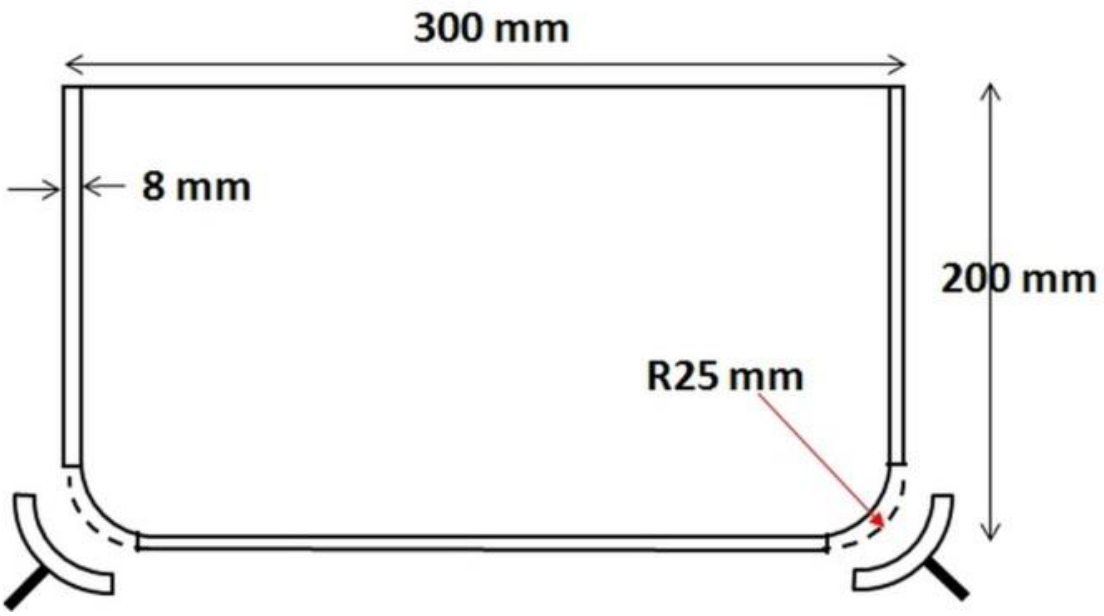

(b) Sectional view of the ship model

Figure 6-1: Sketch of the model test setup and ship model [53]

The CFD hull model is a 2D section with beam equal to 1/20 of the ship length where there is only one layer of mesh points in the longitudinal direction. Hexahedral meshes of varying resolution are used and mesh refinement is carefully carried out in the vicinity of the bilge keels as well as on the free surface. An Eulerian multi-phase volume of fluid (VOF) model is used to simulate and capture the free surface effects. The Reynolds stress is resolved using the $k-\omega$ SST turbulence model. The computational domain is modeled by the overset mesh technique. The sketch of the simulation domain and mesh visualization is shown in Figure 6-2.

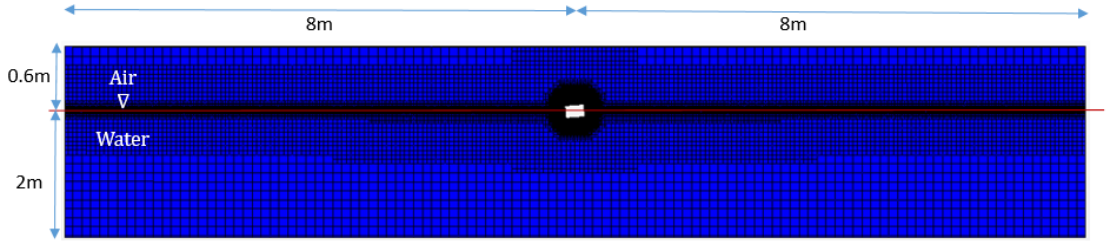

(a) Simulation domain

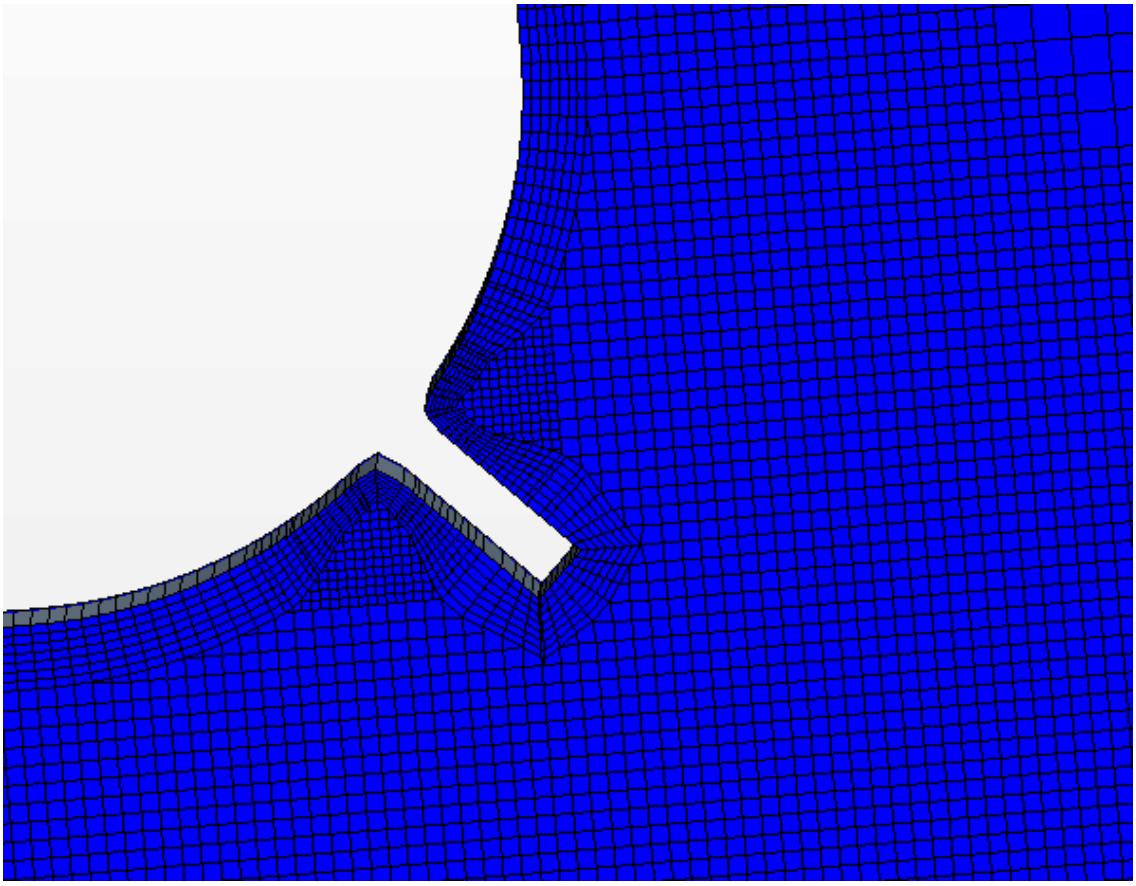

(b) Mesh refinement around the bilge keels

Figure 6-2: Sketch of mesh visualization

To validate the CFD simulations and further establish the SVM regression model, the single DOF ship roll motion is simulated under three different scenarios: free decay test under calm water condition, free ship roll motion excited by regular waves with different wave frequencies, and free ship roll motion under different irregular wave sea states.

Figure shows the comparison of results between the current CFD simulations and the experiments [54] [53] for the free decay test and the motion response under different regular wave conditions. The initial angle of the free decay test was set to 20 degrees. Five regular wave cases that covered the major excitation frequencies were simulated with the same wave height H=3cm in model scale. The five different regular wave periods were 0.75s, 1s, 1.125s, 1.25s, 1.5s.

The well matched results from the free decay test and motion responses (Figure

6-3) under regular wave conditions indicate that the refined mesh conditions around the ship hull and especially the bilge keels is accurate enough to capture the viscous flow physics.

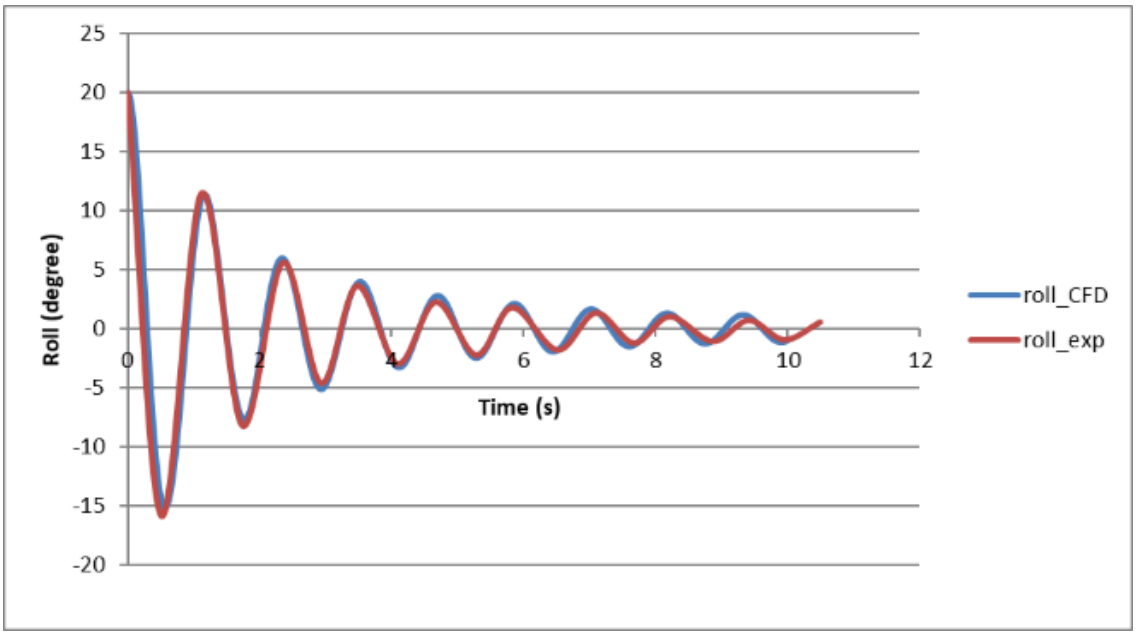

(a) Free decay test

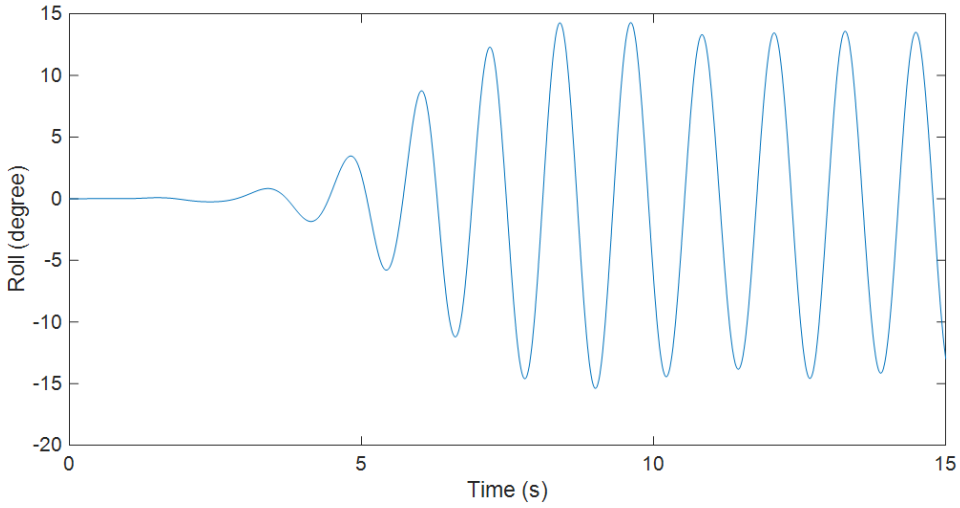

(b) Simulated ship roll response under regular wave with period 1.2s and wave height 3cm

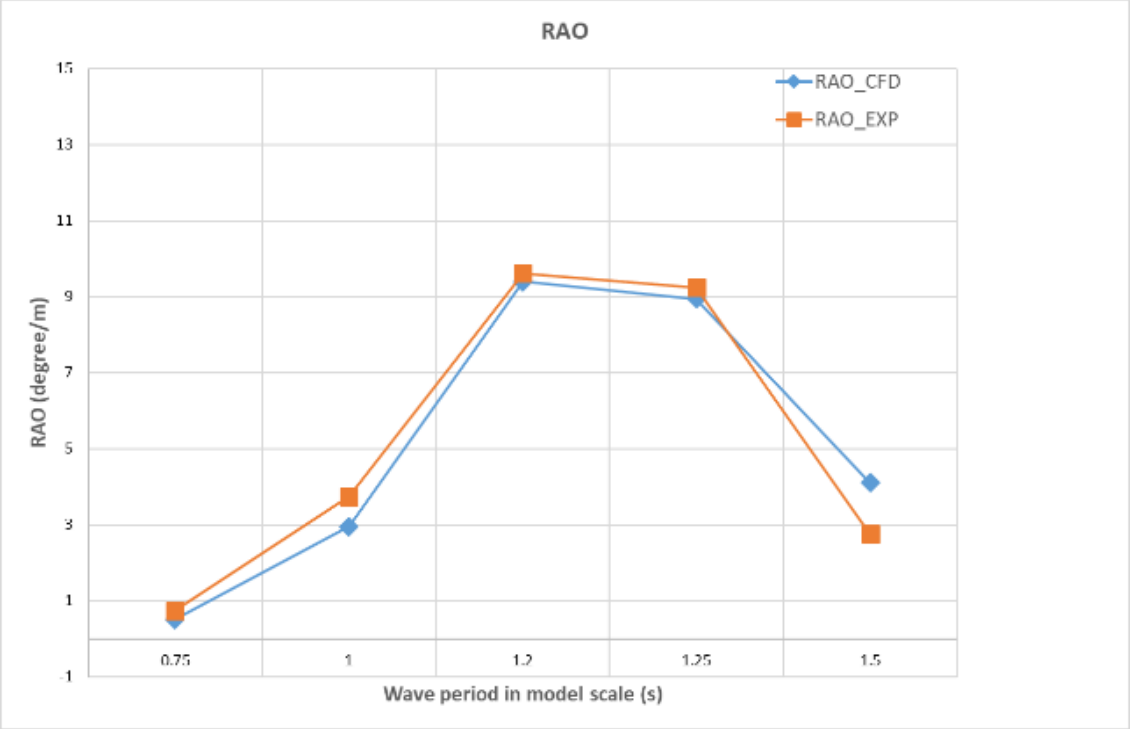

(c) Motion response under regular waves

Figure 6-3: Validation of the CFD simulations against wave tank tests

Furthermore, the single DOF ship roll motion was simulated under an irregular wave sea state as well. For clearer description, the data in the following sections would be converted to full scale with a scaling ratio 1/100. The JONSWAP spectrum is used in this study to simulate the irregular wave. The simulated sea state has siginificant wave height (Hs) 6m and modal wave period (Tp) 11.3s.

Although experimental results under irregular wave conditions are not available, Figure 6-4 shows the simulation of irregular waves in the absence of the ship. The simulated spectrum is well matched with the targeted one, which indicates that the refined mesh conditions around the free surface and the time step set in the simulations are sufficient to capture the free surface effects. Therefore, it is reasonable to assume that with the matched results from the free decay and regular wave cases, as well as the accurate modelling of the stochastic wave itself, the simulated ship roll hydrodynamics under the irregular wave condition is accurate enough to provide a database for the development of the SVM regression model. Figure 6-5 shows the simulated ship roll

motion under the irregular wave condition. The overall physical simulation time is 3600s (1hour) so that the results are statistically reliable.

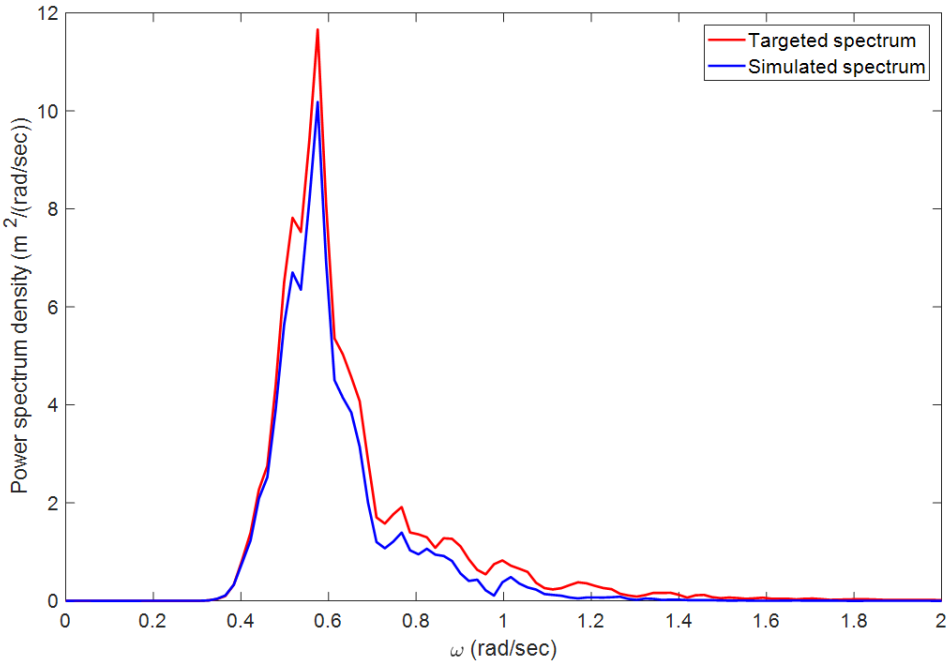

Figure 6-4: Validation of the irregular wave generation

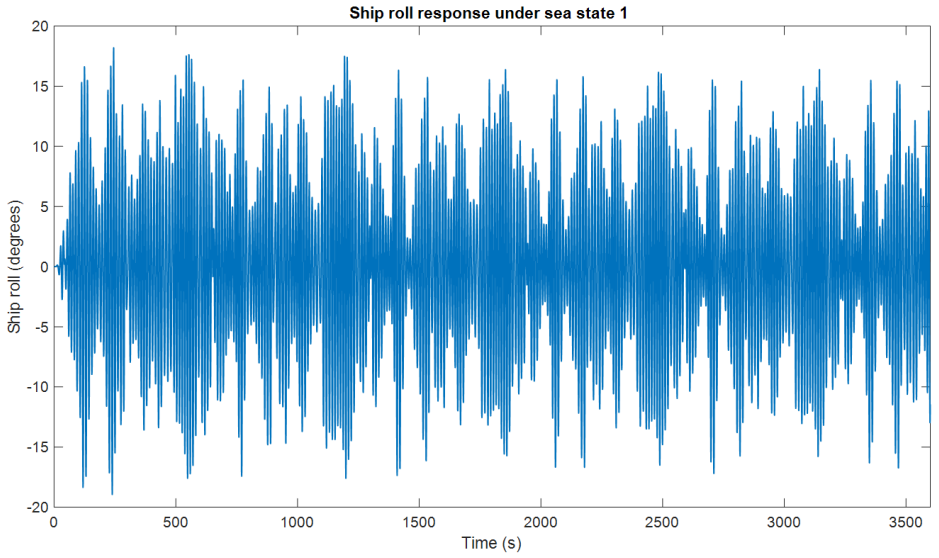

Figure 6-5: Simulated ship roll response under the irregular wave condition: Hs=6m, Tp=11.3s

6.3 Ship roll hydrodynamics modeling via SVM regression using free decay test data

For a free decay test, the 1DOF equation of the ship roll motion can be expressed as:

$$I\ddot{\xi}(t) = F_h(\xi(\tau), \dot{\xi}(\tau), \ddot{\xi}(\tau)) \tag{6.1}$$

Where, I is the moment of inertia of the ship hull structure. F_h denotes the overall hydrodynamic moment, which includes contributions from restoring, added mass and damping forces. $\xi(\tau), \dot{\xi}(\tau), \ddot{\xi}(\tau)$ are the past records of the ship roll displacement, velocity and acceleration, respectively, taking into account the memory effect. τ is a dummy variable representing the past time steps.

Conventionally, the overall hydrodynamic moment can be decomposed into several components:

$$F_h(t) = -A_\infty \ddot{\xi}(t) - C\xi(t) + F_{h,r}(t) \tag{6.2}$$

Where, A_∞ is the infinite frequency added mass and C is the linear hydrostatic restoring coefficient. The components contributed by the fluid inertia terms, nonlinear viscous damping and nonlinear restoring force are all included in the term $F_{h,r}(t)$.

Since $F_{h,r}(t)$ is the overall hydrodynamic moment derived from the integration of the pressure and stress from the CFD solver, and since the infinite added mass and hydrostatic restoring terms are easy to evaluate given the properties of ship hull, $F_{h,r}(t)$ can be thus expressed as:

$$F_{h,r}(t) = F_h(t) + A_\infty \ddot{\xi}(t) + C\xi(t) \tag{6.3}$$

The features that $F_{h,r}(t)$ depends upon are the past records of ship kinematics, which are output by the CFD simulations directly as well. Therefore, in the context of the LS-SVM model described in Chapter 2, the training and test data samples $\{\mathbf{x_i}, y_i\}$ are formatted as $\mathbf{x_i} = [\eta_{t_i}, \eta_{t_i-1}, ..., \eta_{t_i-d}, \xi_{t_i}, \xi_{t_i-1}, ..., \xi_{t_i-d}, \dot{\xi}_{t_i}, \dot{\xi}_{t_i-1}, ..., \dot{\xi}_{t_i-d}, \ddot{\xi}_{t_i}, \ddot{\xi}_{t_i-1}, ..., \ddot{\xi}_{t_i-d}]$, and $y_i = F_{h,r}(t_i)$. Where, d is the duration of

the past record that takes into account the memory effect.

The original sampling timestep of the CFD simulations is 0.01 seconds in full scale. The duration of the past record that takes into account the memory effect is set to 8 seconds. Therefore, to make the dimensions of the features reasonable, all of the CFD simulated data are resampled at a timestep 0.5s. The total number of samples generated in the free decay test is 1000 samples, and 500 random samples are used for training and the other 500 samples are used for testing. The hyper-pamaraters including the Gaussian kernel width and the regularization factor are optimized using 10-fold cross-validation during the SVM training process. The results of the training and testing are shown in Figure 6-6.

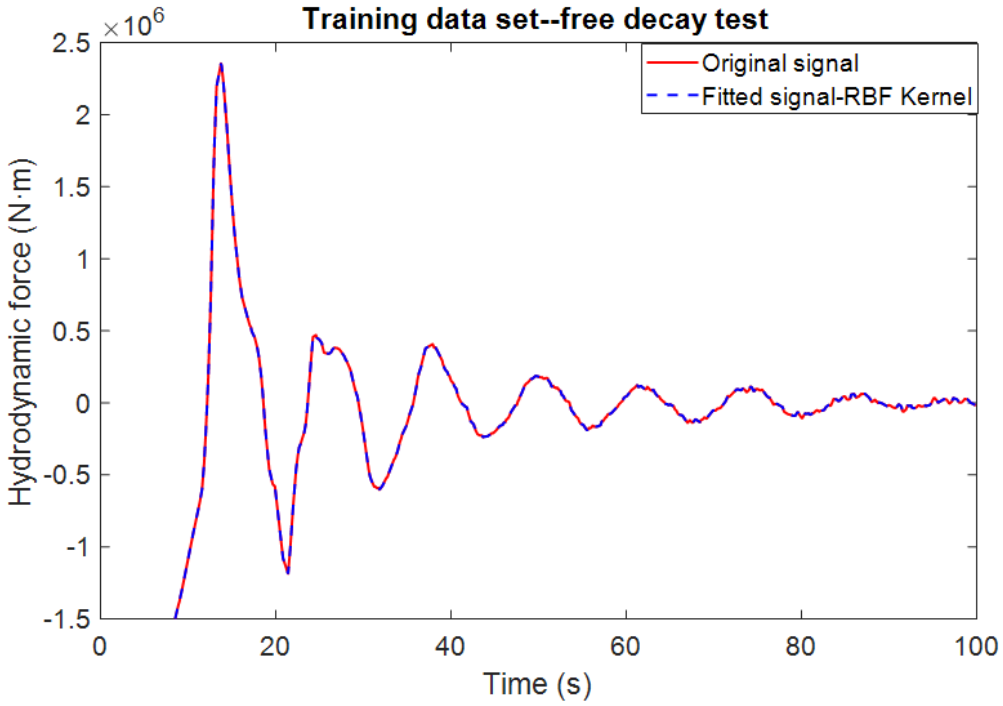

(a) Training results using data from free decay test

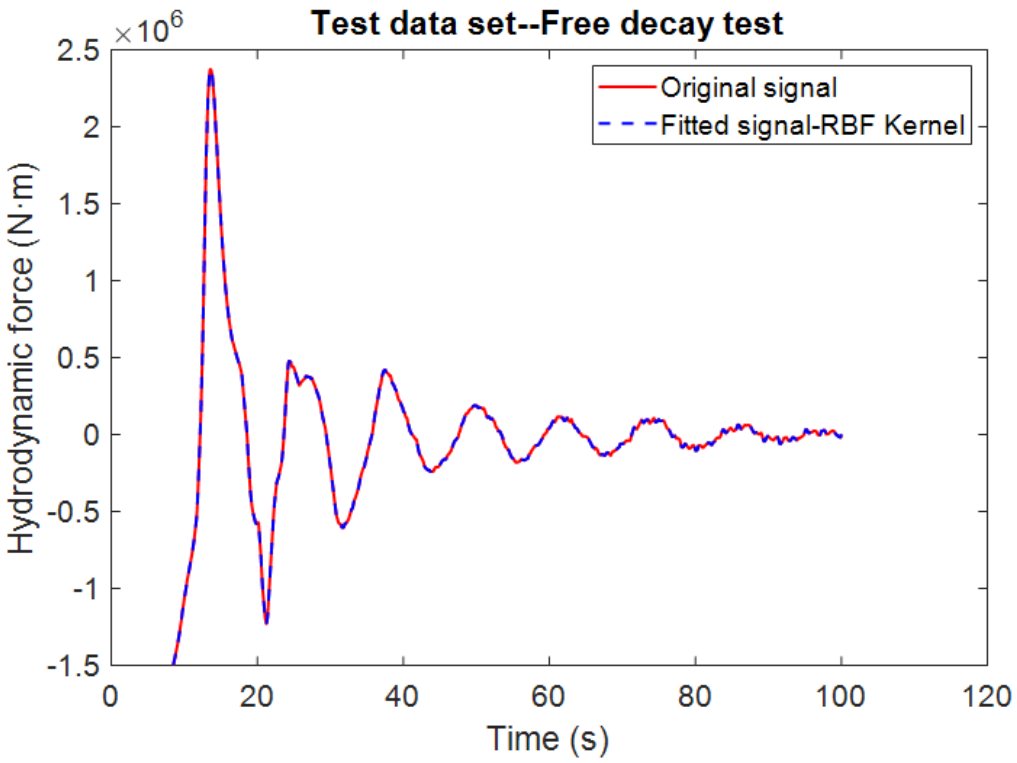

(b) Test results on free decay test

Figure 6-6: Training and test results of the SVM regression model using free decay test data

From these results, the SVM regression model is able to capture the nonlinear mapping between the ship roll kinematics and the corresponding hydrodynamic forces in calm water conditions.

6.4 Ship roll hydrodynamics modeling via SVM regression using irregular wave data

To better account for the stochastic effects of ship roll under irregular wave conditions, the data from the irregular wave case are used to establish the SVM model. In this case, the overall hydrodynamic moment in (6.1) would also include contributions from the incident wave. Correspondingly, the total wave force can be decomposed as

follows:

$$F_h(t) = -A_\infty \ddot{\xi}(t) - C\xi(t) - \int_{-\infty}^{0} K(t-\tau)\dot{\xi}(\tau)d\tau + F_{ex,l}(t) + F_{h,r}(t) \tag{6.4}$$

Where, A_∞ is the infinite frequency added mass, C is the hydrostatic restoring coefficient, K(t) is the radiation impulse kernel and $F_{ex,l}$ is the linear incident wave force. The radiation impulse kernel and linear incident wave force can be easily derived from linear potential theory. Therefore, the residual nonlinear force can be expressed as:

$$F_{h,r}(t) = F_h(t) + A_\infty \ddot{\xi}(t) + C\xi(t) + \int_{-\infty}^{0} K(t-\tau)\dot{\xi}(\tau)d\tau - F_{ex,l}(t) \tag{6.5}$$

The nonlinear residual force under stochastic wave conditions results from nonlinear wave-structure interactions and viscous effects. The features used in the model are records of wave elevations and ship roll velocities. Since the impulse function of the incident wave force is non-causal, the records of both past and future wave elevations are taken into account. In the context of the LS-SVM model described by equations (2.2)-(2.7), the training and test data samples $\{\mathbf{x_i}, y_i\}$ are formatted as $\mathbf{x_i} = [\eta_{t_i-d}, ..., \eta_{t_i-1}, \eta_{t_i}, \eta_{t_i+1}, ..., \eta_{t_i+d}, \dot{\xi}_{t_i}, \dot{\xi}_{t_i-1}, ..., \dot{\xi}_{t_i-d}]$, and $y_i = F_{h,r}(t_i)$. Where, d is the duration of the past and future record that takes into account the memory effect. In this case, d is set to be 8 seconds as well.

The wave elevations, ship kinematics, total hydrodynamic force output by the CFD simulation under the irregular wave condition as well as the linear potential terms output by the potential flow panel methods are used to train the model. In analogy to the previous section, part of the data is randomly selected as training samples and the rest are used for testing. The hyperparameters are optimized via cross-validation.

Two different kernels are considered in this section, the Gaussian kernel and the linear kernel. As stated in the previous Section 2.4, the linear kernel can be considered as the leading-order approximation of the more generalized Gaussian kernel model. Moreover, the linear kernel can be converted into a frequency-domain transfer

function, leading to a very efficient implementation in practice.

6.4.1 SVM regression model with linear kernel

Combining (6.1) and (6.4), the equation of motion under an irregular wave sea state can be expressed as:

$$(I + A_\infty)\ddot{\xi}(t) + C\xi(t) + \int_{-\infty}^{0} K(t-\tau)\xi(\tau)d\tau = F_{ex,l}(t) + F_{h,r}(t) \tag{6.6}$$

Where, $F_{h,r}(t)$ are estimated by the SVM regression model, and will be referred as $F_{SVM,lin-kernel}$ in what follows.

Since the linear kernel takes the form:

$$k(\mathbf{x}, \mathbf{z_i}) = \mathbf{x}^T\mathbf{z_i} + b \tag{6.7}$$

the estimated hydrodynamic force becomes:

$$F_{SVM,lin-kernel}(t) = \sum \lambda_i \mathbf{x}^T\mathbf{z_i} + b \tag{6.8}$$

where, $\mathbf{z_i} = [z_{i1}, z_{i2}, ..., z_{ip}]^T$ is the training sample with p features.

Expanding $\mathbf{x}^T\mathbf{z_i} = \sum x_j z_{ij}$, and plugging in (6.8) and re-organizing the terms, the SVM model with a linear kernel can be expressed in the form:

$$F_{SVM,lin-kernel}(t) = \sum_{i=1}^{p} c_i x_i + b \tag{6.9}$$

where, p is the number of features, x_i is the corresponding wave elevation $\eta(t+\tau), \tau = -T_c, ..., 0, ...T_c$ or ship roll velocity $\dot{\xi}(t-\tau), \tau = 0, ..., T_c$ defined as the features.

Converting (6.9) into the frequency domain via the Fourier transform, and invoking the time-convolution property of the transform:

$$\begin{aligned} x(t) &\rightarrow X(\omega) \\ x(t-\tau) &\rightarrow e^{-i\omega\tau}X(\omega) \end{aligned} \tag{6.10}$$

the estimated SVM force in the frequency domain becomes:

$$F_{SVM,lin-kernel}(\omega) = F_{SVM-\eta}(\omega)H(\omega) + i\omega F_{SVM-v}\Xi(\omega) \tag{6.11}$$

where, $H(\omega)$ is the Fourier transform of the wave elevation $\eta(t)$, and $\Xi(\omega)$ is the Fourier transform of the ship roll displacement $\xi(t)$.

Converting (6.6) into the frequency domain and plugging in (6.11), the equation of motion in frequency domain becomes:

$$\begin{aligned}&(-\omega^2(I + A_\infty) + i\omega K(\omega) + C)\Xi(\omega) \\ &= (F_{ex,l}(\omega) + F_{SVM-\eta}(\omega))H(\omega) + i\omega F_{SVM-v}(\omega)\Xi(\omega)\end{aligned} \tag{6.12}$$

Therefore, the transfer function of the roll displacement as a function of the incident wave elevations becomes:

$$\Xi(\omega) = \frac{F_{ex,l}(\omega) + F_{SVM-\eta}(\omega)}{-\omega^2(I + A_\infty) + i\omega K(\omega) + C - i\omega F_{SVM-v}(\omega)} \tag{6.13}$$

It is seen from equation (6.13) that the residual hydrodynamic force modeled by the linear SVM kernel induces an excitation residual force transfer function which appears in the numerator and a damping coefficient which appear in the denominator. These effects are additive to the corresponding contributions from conventional linear theory. Moreover they both are driven by nonlinear free surface and viscous separated flow physics contained in the CFD simulation record which is used to train the linear kernel SVM machine learning model (6.6)-(6.13).

Figure 6-7 shows the training and testing results of the linear-kernel-SVM model. Figure 6-8 shows the comparison of the transfer function derived using (6.13) and using purely linear potential theory. The comparison shown in Figure 6-8 clearly illustrates that the SVM force model introduces a significant damping effect.

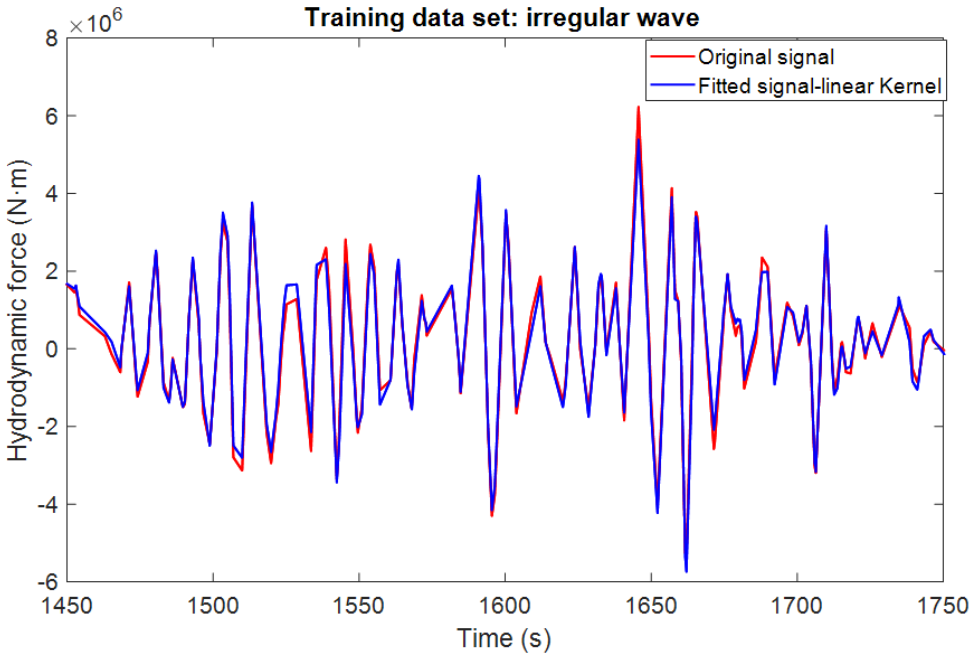

(a) Training results using data from irregular wave case

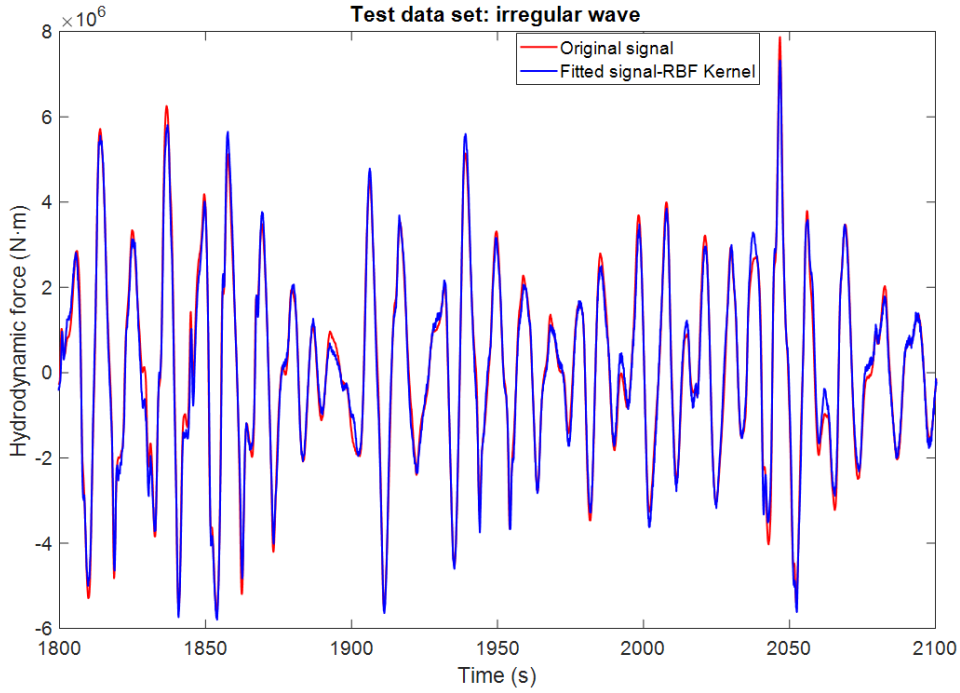

(b) Test results on the irregular wave condition

Figure 6-7: Training and test results with linear kernel under irregular wave conditions

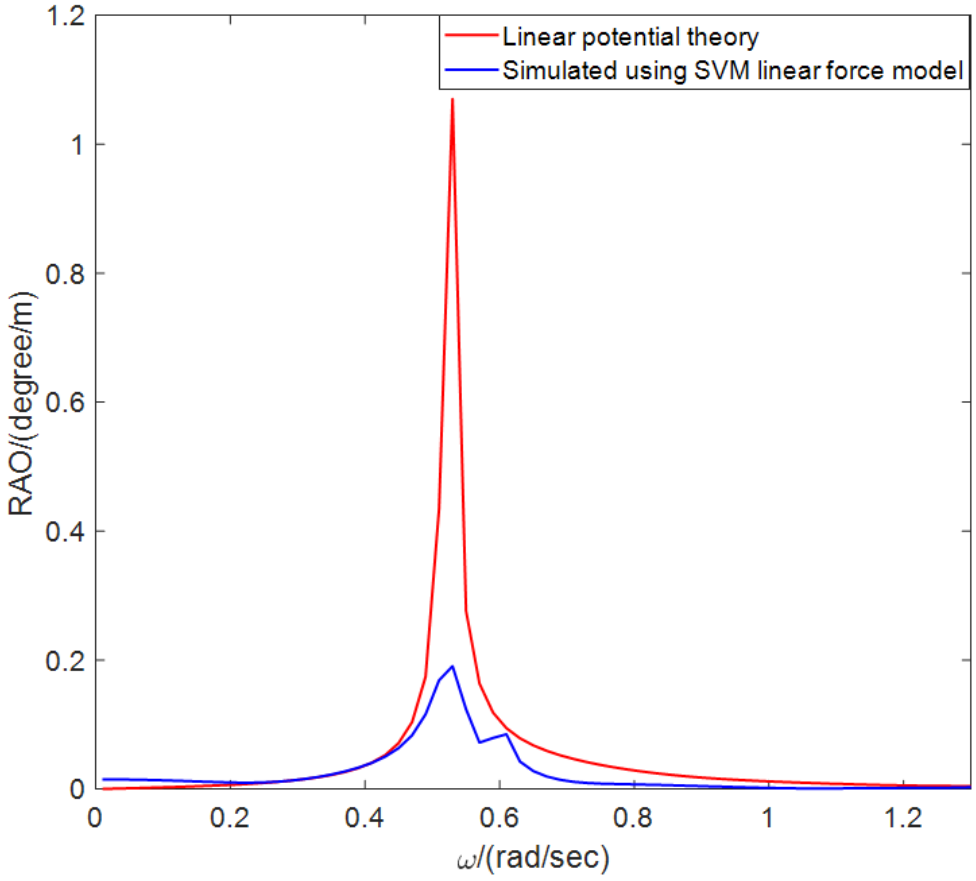

Figure 6-8: Comparison of the transfer function between linear potential theory and that with the linear-kernel-SVM model

Furthermore, the irregular wave spectrum from the CFD simulation is used in (6.13) to calculate the spectrum of the ship roll displacement. The frequency domain result may be converted to time-domain records via the inverse Fourier transform. Figure 6-9 illustrates the comparion of the ship roll displacement between the CFD simulation and the linear-kernel-SVM model in both time-domain and frequency-domain. The difference of the standard deviation of the ship roll displacement is 9.54%.

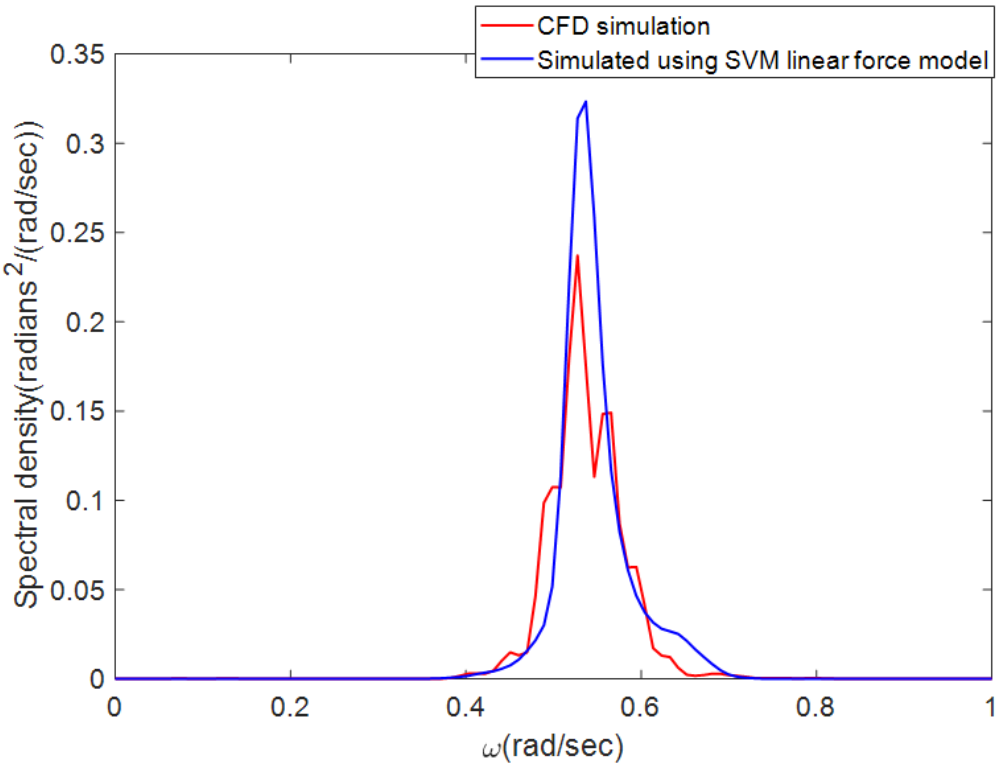

Figure 6-9: Comparison of spectral density of the ship roll displacement between the CFD simulation and the linear-kernel-SVM model

6.4.2 SVM regression model with Gaussian kernel

Having established the SVM model using a linear kernel, we further explored the alternative of using Gaussian kernel with data from irregular wave records. The feature selection and SVM training process are the same with that of the linear kernel. The nonlinear residual force in (6.6) is estimated now by the SVM regression model with a Gaussian kernel. In what follows, the estimated nonlinear residual force in (6.6) is referred to as $F_{SVM,nl}$.

Since the Gaussian kernel (see (2.8)) is a nonlinear function of its arguments, the equation of motion cannot be converted to the frequency domain. In order to validate the feasibility of using the Gaussian-kernel-SVM model, (6.6) with the estimated nonlinear force $F_{SVM,nl}$ is simulated directly in the time-domian.

Figure shows the training and testing results of the hydrodynamic force obtained from the simulation of the Gaussian-kernel-SVM model. Figure shows the spectrum of

the ship kinematics estimated using the Gaussian-kernel-SVM model. The difference of the standard deviation of the ship roll displacement between the CFD simulations and the Gaussian SVM model is 5.67%.

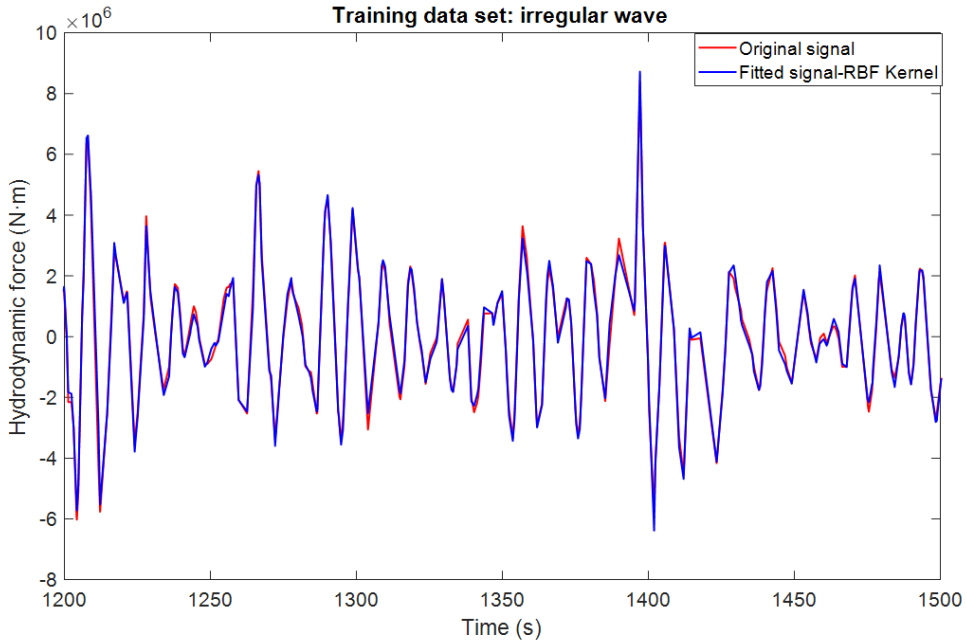

(a) Training results using data from irregular wave case

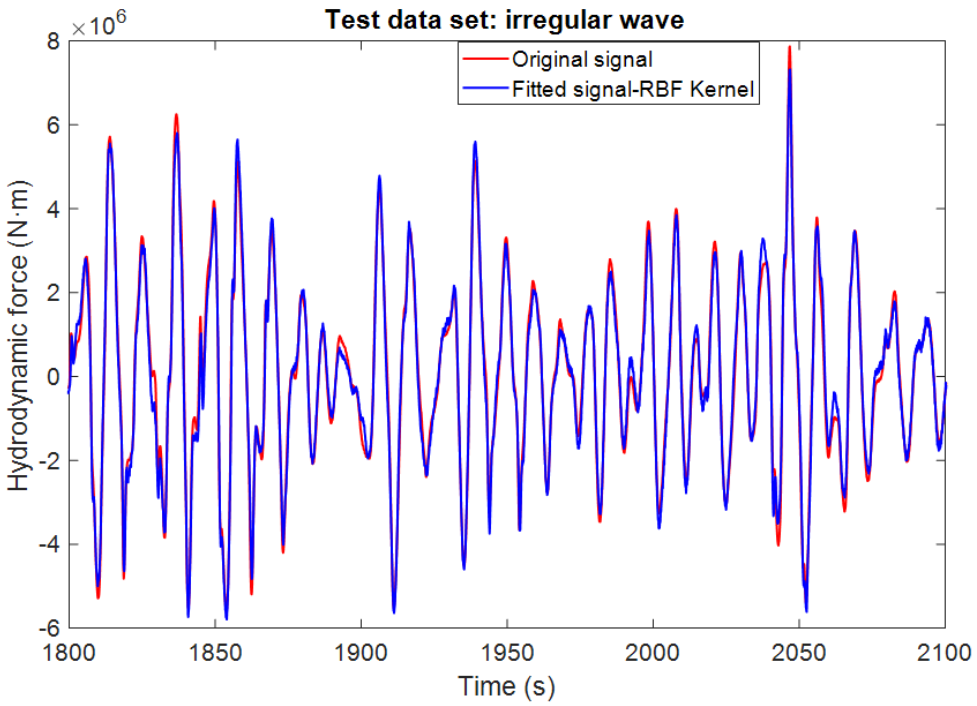

(b) Test results on the irregular wave condition

Figure 6-10: Training and test results with Gaussian kernel under irregular wave conditions

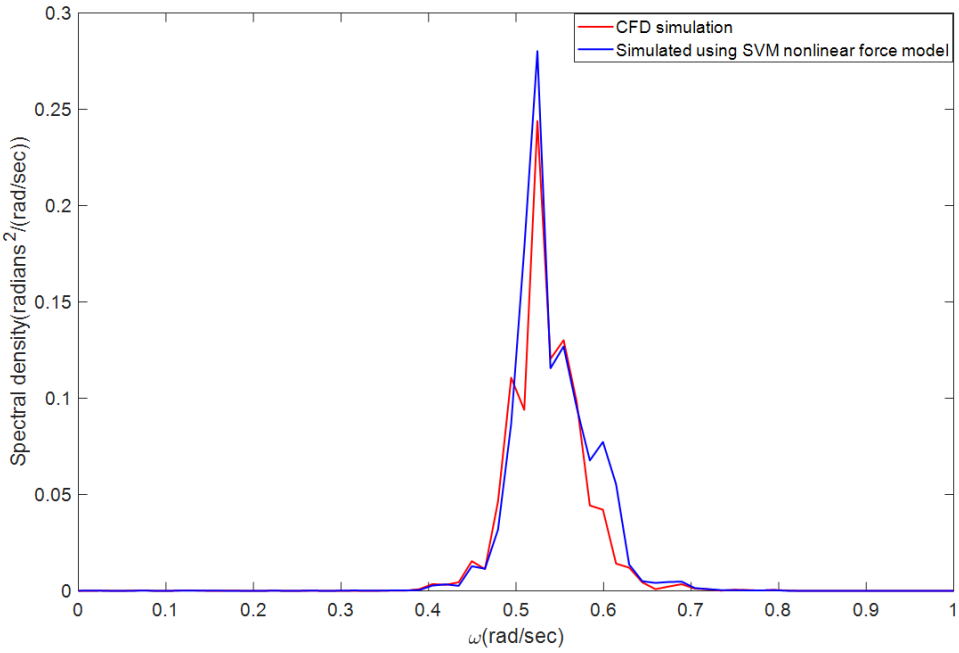

Figure 6-11: Comparison of spectral density of ship roll displacement between CFD simulation and the Gaussian-kernel-SVM model

It may be seen from Figure 6-9 and Figure 6-11 that the SVM model using the nonlinear and more general Gaussian kernel leads an increased accuracy of the spectral density of the roll motion and better agreement with the results obtained from the CFD simulations which are assumed to correctly capture all flow physics. Yet the performance of the SVM model using the linear kernel is satisfactory and readily amenable to the efficient machinery of linear system theory.

6.5 Conclusions and discussions

A series of simulations have been conducted for a rectangular barge with bilge keels using a 2D CFD solver. The CFD simulations are validated by comparing results of free decay tests and regular wave cases with experiments.

On the basis of the data derived from validated CFD simulations, generalized SVM regression models are developed in this chapter that establish the mapping relation between the ship kinematics and wave elevation records and the nonlinear

ship roll hydrodynamic loads. In essence, the kernel maps the association of the features of the target samples to those of the training samples in the hyperspace, and predicts the target value of the quantity being modeled as a function of the kernel arguments which are the target and training features. Therefore, by randomly selecting a set of training samples, the model achieves a very good generalization capability to predict unseen targets through the training process combined with the optimization scheme which determines the width parameter of the kernel and the regularization parameter. In the context of ship roll hydrodynamics, this means that if high-fidelity CFD simulation records of ship roll hydrodynamics and motions in an irregular sea state are available, the SVM regression model established using the methodology presented in this provides a very good estimate of the nonlinear ship roll hydrodynamic loads.

Both the linear kernel and Gaussian kernels are selected and tested in this study. The Gaussian kernel has better accuracy and generalization capability in fitting the force signal. However the linear kernel enables the use of linear frequency domain analysis and renders its use more efficient in design practice.

In a more general context, a stochastic SVM model may be developed which is trained to estimate the probability density function of the quantity being modeled conditional upon knowledge of the features. This extension will enable the modeling of the statistical properties of the nonlinear responses of vessels in a stochastic sea state when they are significantly affected by viscous and nonlinear free surface effects, a topic that will be studied in future research.

Chapter 7

Support Vector Regression Model of the Nonlinear Hydrodynamics of Fixed Cylinders

7.1 Introduction

The modeling of hydrodynamics loads has developed for decades to understand the relevant physics and predict the wave-structure interaction. Linear frequency-domain analysis derived from the panel methods based on potential flow theory is one of the most popular tools because of its efficiency and reliability. However, in many scenarios, the nonlinear effects are not negligible due to large-amplitude body motions, nonlinear resonance etc. Having a better prediction of nonlinear wave loads are critical to evaluate extreme statistics and structural fatigue analysis for offshore structures [74] [56] [52]. Many researchers have published studies on the impact of nonlinear wave loads to the design, safety and maintenance of offshore platforms [89] [31] [49].

In the past decades, a variety of numerical methods have developed to understand and predict the nonlinear wave-structure interactions. The potential flow theory remains the most popular used tools to predict global responses of offshore structures extending the linear theory to nonlinear free surface and body boundary conditions

[75]. The classical boundary element methods are formulated in two different ways using either Rankine panel method or the transient free surface Green function method [7] [57] [16]. Based upon the solution of wave-structure interaction, the hydrodynamic load can be calculated either by integrating the pressure over the body surface which is obtained by Bernoulli's equation [59] or by the time rate of change of the impulse of the velocity potential which is a new methodology recently proposed by Sclavounos [75] as Fluid Impulse Theory. These methods require the discretization of the body surface and some also require the discretization of the free surface, which can be very demanding in both delicate numerical treatment and computational cost. Meanwhile, depending on the surface and body boundary conditions imposed, the numerical schemes can only take account contributions from certain nonlinear aspects to a certain order. Therefore, establishing a direct generalized model for nonlinear wave loads from a data-driven perspective could be very prospective in terms of accuracy and efficiency, which could be further applied in various design and operation practises.

In this chapter, a SVM regression model is trained and validated using experiment and simulation data for a fixed cylinder in shallow water. Different feature and target selections are compared and discussed in this work. Statistics of the nonlinear wave loads by the SVM regression model are compared with the original measurements to show the accuracy of the model, which is critical to further applications in structural design and analysis.

7.2 Baseline data set

In this study, we are interested in establishing SVM regression models for the prediction of the nonlinear wave loads on a fixed cylinder. To establish such a model, experimental data from a model test were used as the baseline data set. Meanwhile, the simulated nonlinear wave loads from fluid impulse theory [75] are also used in the model development as well in order to explore the merits of different feature and target selections.

7.2.1 Wave tank experiment set-up

The experiment was carried out in the wave tank at the Marine Technology Center, NTNU on a bottom fixed cylinder in finite depth water. The wave tank is 28 meters long, 2.5 meters wide and with a depth of 19 meters. The scale ratio of the model is 1:48. The diameter of the cylinder is 6.912 m in full scale. The sketch of the model test facility is shown in Figure 7-1. More details of the experiments can be found in [5] [40].

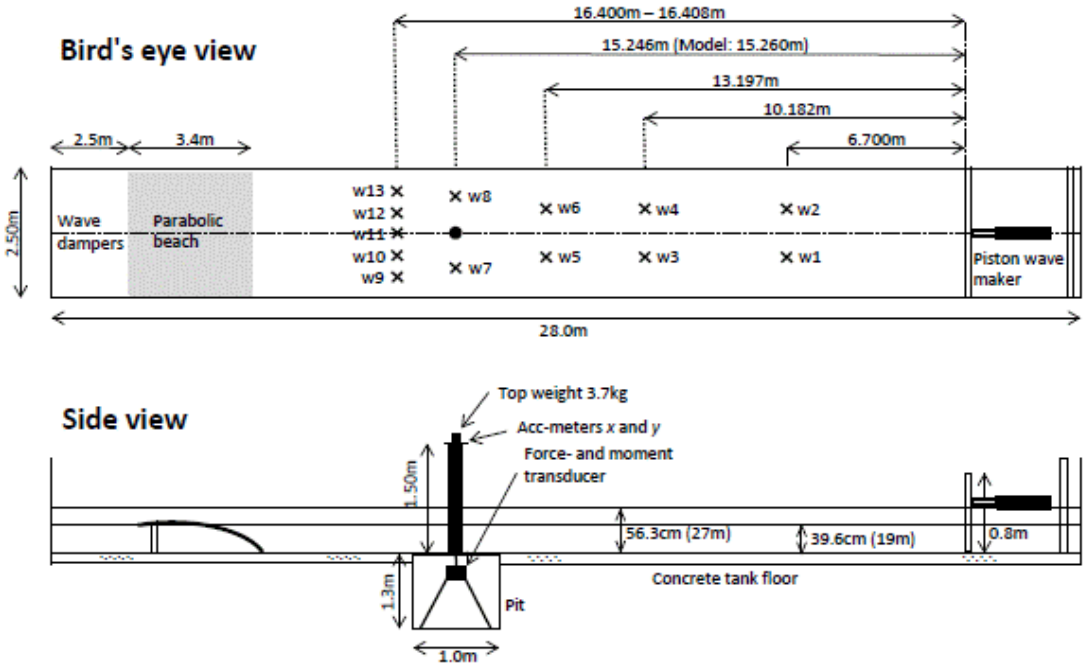

Figure 7-1: Sketch of the model test facility

Three sets of irregular wave cases are used in this study. The irregular wave sea states were generated using the standard Jonswap spectrum with a spectral parameter γ. The parameters of the sea states are summarized in Table 7.1. For each sea state, the experiments were repeated 20 times with independent random seeds. Each realization of the irregular wave sea states was tested and measured for approximately 3.5 hours with a sampling rate 0.0346 s in full scale. During the experiments, the total horizontal force F_x and the mudline bending moment M_y were measured, which are the two physical quantities that this study targets to model. The sketch of the

loading on the fixed cylinder is shown in Figure 7-2.

Table 7.1: Parameters of the irregular wave sea states

Case No.	Tp (s)	Hs (m)	γ
Sea state 1	10.0	6.15	3.04
Sea state 2	11.5	6.7	1.9
Sea state 3	13.2	6.8	1.0

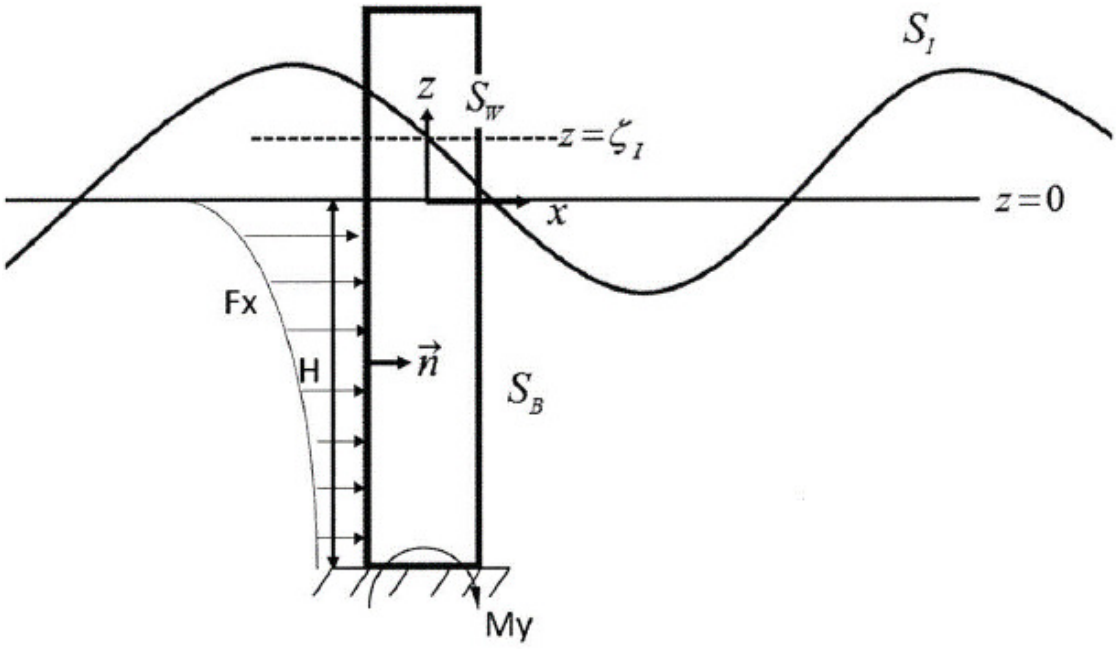

Figure 7-2: Sketch of the loading on the fixed cylinder

7.2.2 Fluid impulse theory

The fluid impulse theory expresses the nonlinear forces and moments as time derivatives of the fluid impulse which circumvents the time-consuming computation of the temporal and spatial derivatives in Bernoulli's equation. In a recent development of the fluid impulse theory, Sclavounos et al. [78] derived an approximation of the exciting force on a vertical cylinder for ambient waves assuming that the wavelength

is large compared to the cylinder diameter and the amplitude is comparable to its diameter. The detailed derivation of the fluid impulse theory is presented in [75] [78].

In this study, the nonlinear wave loads F_x and M_y (defined as in Figure 7-2) for the fixed cylinder take into account the linear component, second-order contribution from the convective terms in the fluid acceleration and a waterline quadratic contribution. They take the form:

$$\begin{aligned} F_x &= 2\pi\rho R^2 \int_{-H}^{0} \dot{u}_1 dz \\ &\quad + 2\pi\rho R^2 \int_{-H}^{0} (u_1 \frac{\partial u_1}{\partial x} + u_3 \frac{\partial u_1}{\partial z}) dz \\ &\quad + 2\pi\rho R^2 \dot{u}_1 \xi_I \end{aligned} \tag{7.1}$$

$$\begin{aligned} M_y &= 2\pi\rho R^2 \int_{-H}^{0} \dot{u}_1 (H+z) dz \\ &\quad + 2\pi\rho R^2 \int_{-H}^{0} (u_1 \frac{\partial u_1}{\partial x} + u_3 \frac{\partial u_1}{\partial z})(H+z) dz \\ &\quad + 2\pi\rho R^2 \dot{u}_1 \xi_I H \end{aligned} \tag{7.2}$$

Where, ρ is the fluid density, R is the radius of the cylinder, H is the draft, u_1, u_3 are the ambient wave velocities in the x, z directions, respectively, ζ_I is the ambient wave elevation and $\dot{u}_1$ is the ambient wave acceleration.

7.3 SVM regression model of the nonlinear wave loads

In this study, we aim to establish a SVM regression model for the nonlinear wave loads using the ambient wave elevations and its kinematics as features. As mentioned in section 7.2.1, three different sea states with 20 random realizations for each sea state were tested in the experiment (see Table 7.1).

To compare the results, the nonlinear wave loads in the same three sea states were also simulated by fluid impulse theory. The ambient wave kinematics, velocity and acceleration were calculated by linear wave theory using the shallow water dispersion

relation. Then the simulated nonlinear wave loads were derived through (3.1) and (3.2).

In the following sections, $F_{x-exp}, F_{x-fit}, M_{y-exp}, M_{y-fit}$ refer to the horizontal force and bending moment measured in the experiment and simulated by fluid impulse theory, respectively. Three different combinations of features have been tested in the study (see Table 7.2). In order to take into account memory effects and the non-causality of the wave excitation forces, a time window of the wave kinematics of finite duration, instead of an instantaneous value, is defined as a feature. The time duration of each feature is $[t - 15s, t + 10s]$, where t refers to the current time. The sampling rate within the feature window is the same as that of the sampling rate in the experiment, which is 0.0346 seconds in full scale. Therefore, the vector length of each feature is 25/0.0346=722.

Table 7.2: Combinations of feature selections

Case No.	Features
Features 1	Ambient wave elevations (η)
Features 2	Ambient wave horizontal velocities (u_1) + accelerations ($\dot{u}_1$)
Features 3	Ambient wave elevations (η) + horizontal velocities (u_1) + accelerations ($\dot{u}_1$)

As is known, the standard deviation and kurtosis are two important statistics of loads, and their magnitude is critical for fatigue analysis and the evaluation of the extreme statistics. The kurtosis of a Gaussian signal is always 3, which is the case for all linear loads and responses within linear wave-structure theory. Therefore the kurtosis of the measured signal is considered to be a measure of nonlinearity in wave / wave-structure interaction problem. The kurtosis of the measured wave loads is listed in Table 7.3 as a measure of the load nonlinearity.

Table 7.3: Kurtosis of the measured wave loads

Force modes	Sea state 1	Sea state 2	Sea state 3
F_x	2.96	2.85	3.06
M_y	3.12	3.29	3.39

Therefore, to evaluate the accuracy of the SVM regression model, the difference of the standard deviation and kurtosis are compared between the measured and SVM predicted signal. The metrics used to evaluate the model are defined as follows:

$$\Delta\sigma = \frac{|\sigma_y - \sigma_{\hat{y}}|}{\sigma_y} \tag{7.3}$$

$$\Delta\kappa = \frac{|\kappa_y - \kappa_{\hat{y}}|}{\kappa} \tag{7.4}$$

Where, y_i is the true value of the signal, $\hat{y}_i$ is the predicted value, σ_y is the standard deviation of the signal, and κ_y is the kurtosis of the signal.

We first have trained the model using the measured wave loads directly as the target. Data from realization 1 in sea state 1 are used as the training data set. The number of training samples is 3000, each sample has a duration of 25 seconds with a sampling rate 0.0346 seconds, and the samples used in the training process have been selected randomly from a long time scale of a 3-hour sea state. The sufficiently long time scale used for the selection of the features guarantees that the samples used for the training of the algorithm have accounted for most of the inherent physical information contained in the training seastate for the purpose of modeling the nonlinear load on the cylinder.

The rest of 19 realizations of sea state 1 and all the 20 realizations of sea state 2 and state 3 are used as the test data set to validate the accuracy and robustness of the model. For each seastate realization, a 3500-second long section is used for testing. The large data set used for testing ensures that the performance of the model is statistically robust and consistent. The results of the training and testing stages are

shown in Figure 7-3 $\sim$ Figure 7-6. For each test sea state, results from one of the realizations with one of the feature selections are shown here as examples. The overall error statistics are listed in Table 7.4 and Table 7.5.

Table 7.4: Error statistics of horizontal force F_x by SVM model

Features	Features 1	Features 2	Features 3
$\Delta\sigma$ for sea state 1	1.47%	1.59%	1.54%
$\Delta\sigma$ for sea state 2	1.82%	1.73%	1.75%
$\Delta\sigma$ for sea state 3	2.61%	1.80%	1.96%
$\Delta\kappa$ for sea state 1	2.70%	3.12%	2.99%
$\Delta\kappa$ for sea state 2	4.03%	3.87%	3.97%
$\Delta\kappa$ for in sea state 3	5.48%	4.51%	4.94%

Table 7.5: Error statistics of bending moment M_y by SVM model

Features	Features 1	Features 2	Features 3
$\Delta\sigma$ for sea state 1	2.41%	2.52%	2.51%
$\Delta\sigma$ for sea state 2	3.34%	3.02%	3.21%
$\Delta\sigma$ for sea state 3	4.58%	3.29%	3.71%
$\Delta\kappa$ for sea state 1	5.18%	5.52%	5.65%
$\Delta\kappa$ for sea state 2	6.72%	6.13%	6.53%
$\Delta\kappa$ for in sea state 3	8.23%	6.59%	7.33%

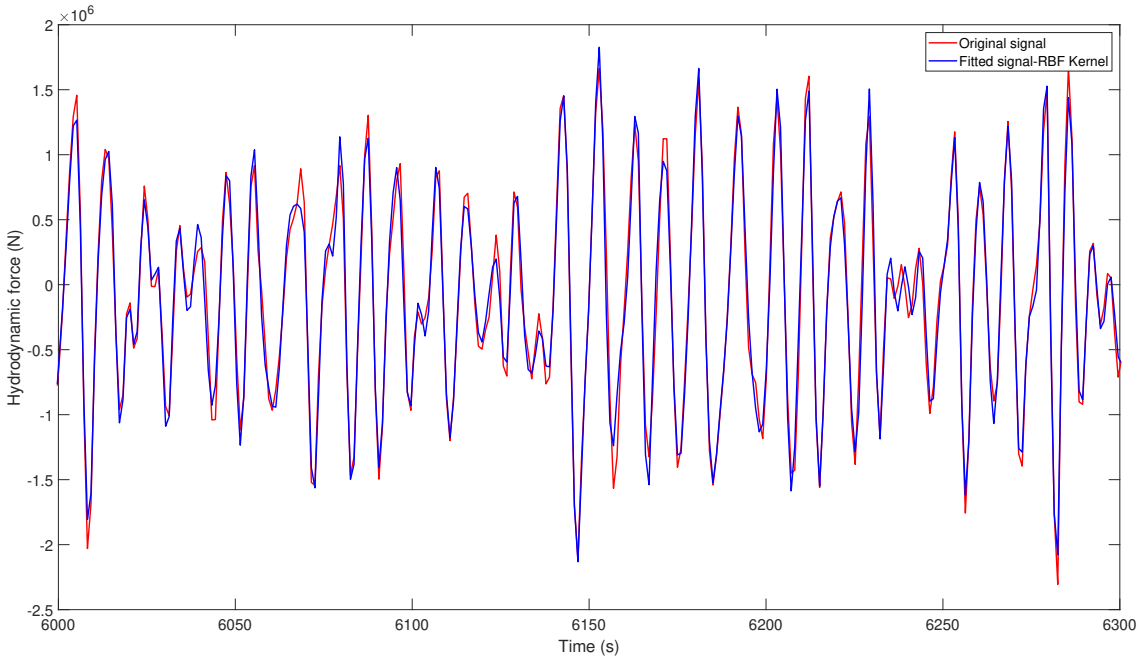

(a) Training results using features 1

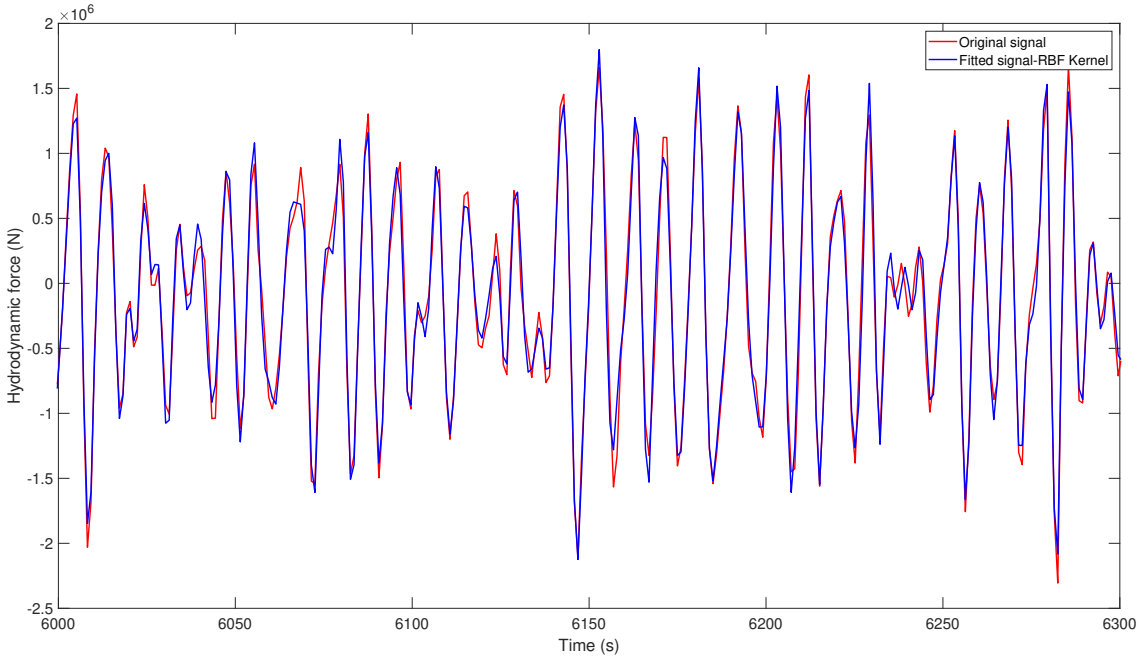

(b) Training results using features 2

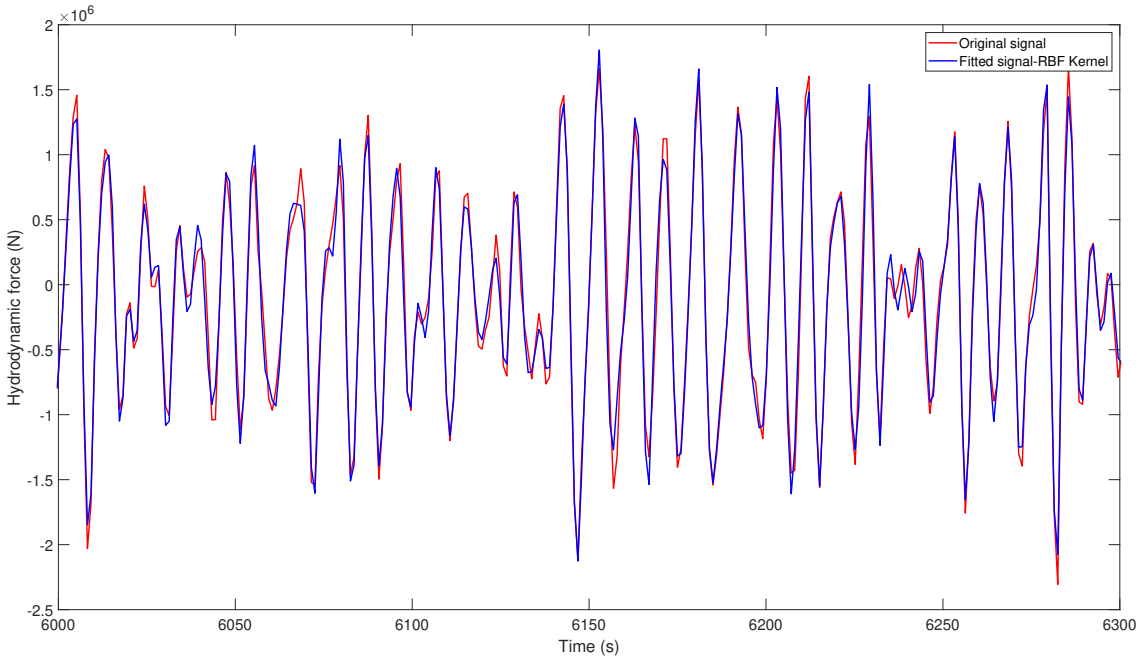

(c) Training results using features 3

Figure 7-3: Comparison of the horizontal force between the measured signal and fitted using SVM: training results

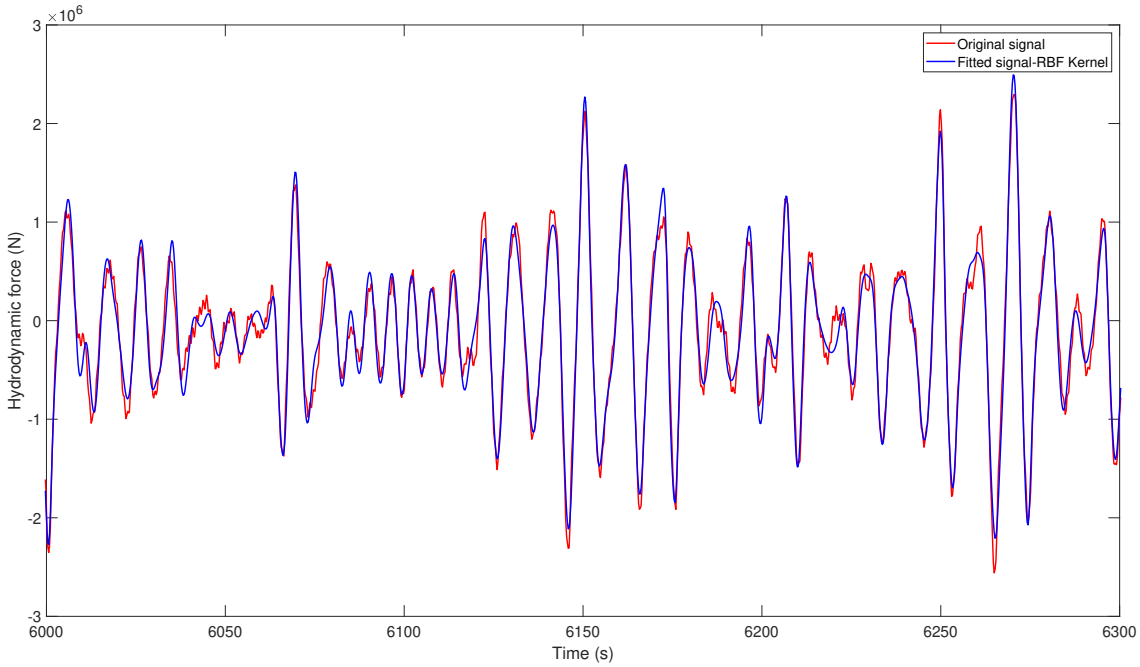

(a) Test results using features 1 in sea state 1

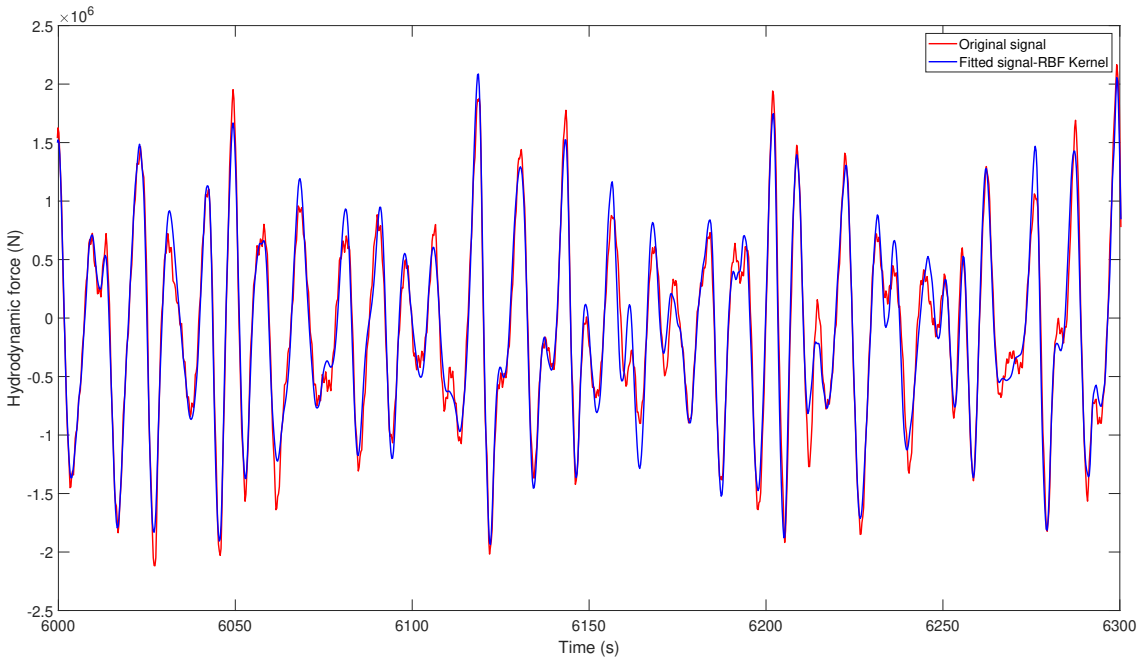

(b) Test results using features 2 in sea state 2

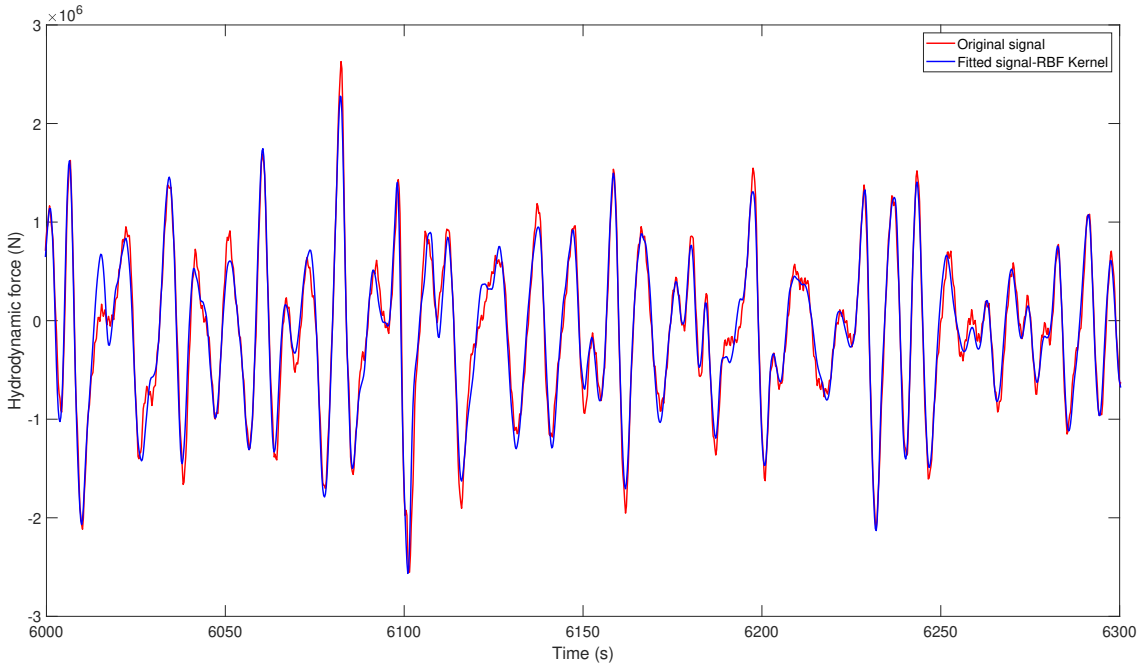

(c) Test results using features 3 in sea state 3

Figure 7-4: Comparison of the horizontal force between the measured signal and fitted using SVM: test results

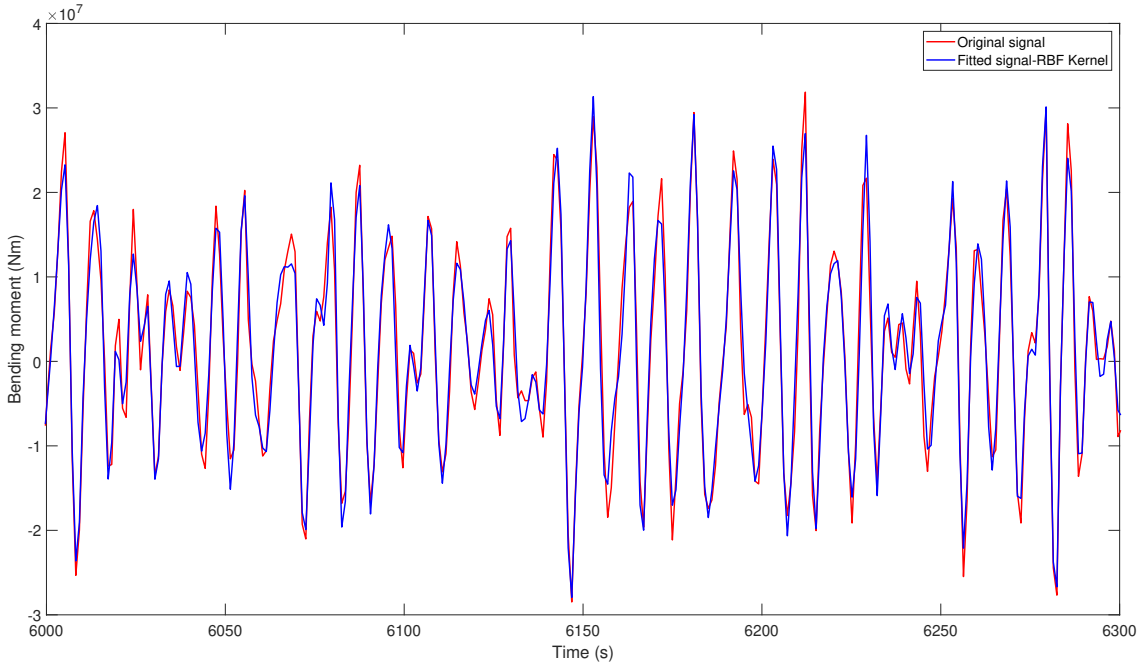

(a) Training results using features 1

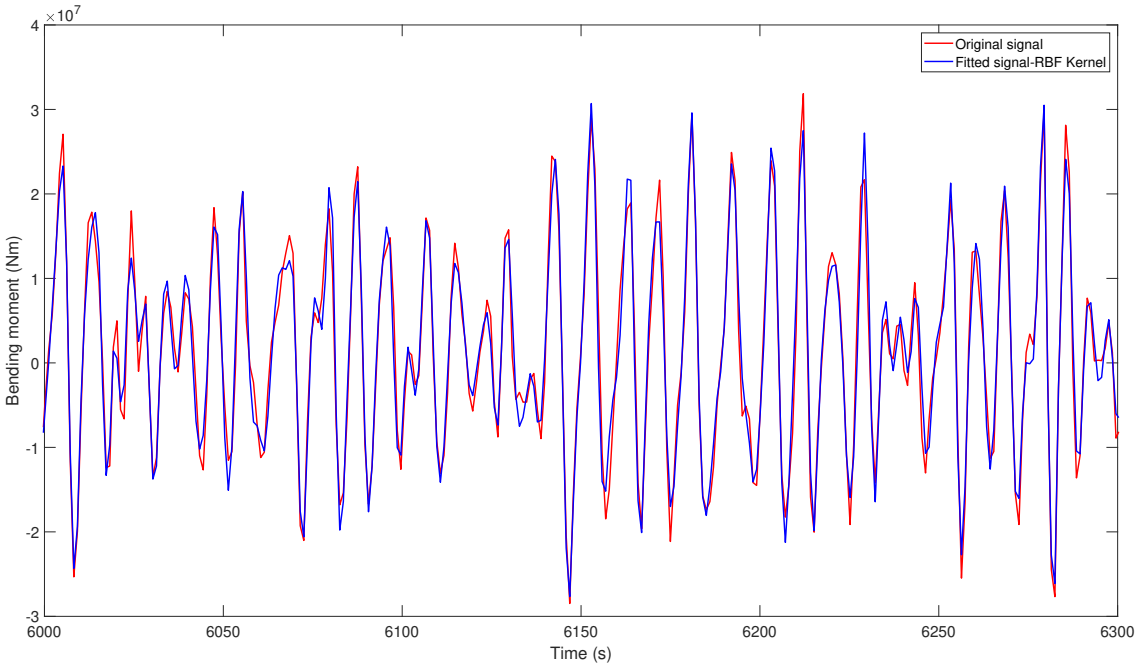

(b) Training results using features 2

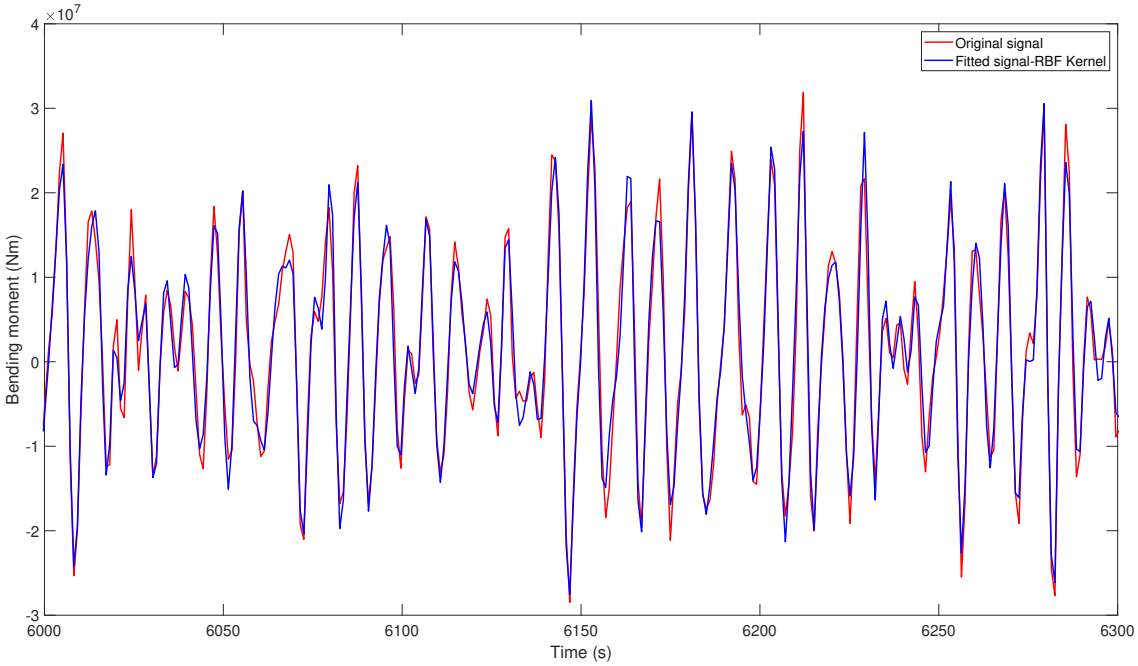

(c) Training results using features 3

Figure 7-5: Comparison of the bending moment between the measured signal and fitted using SVM: training results

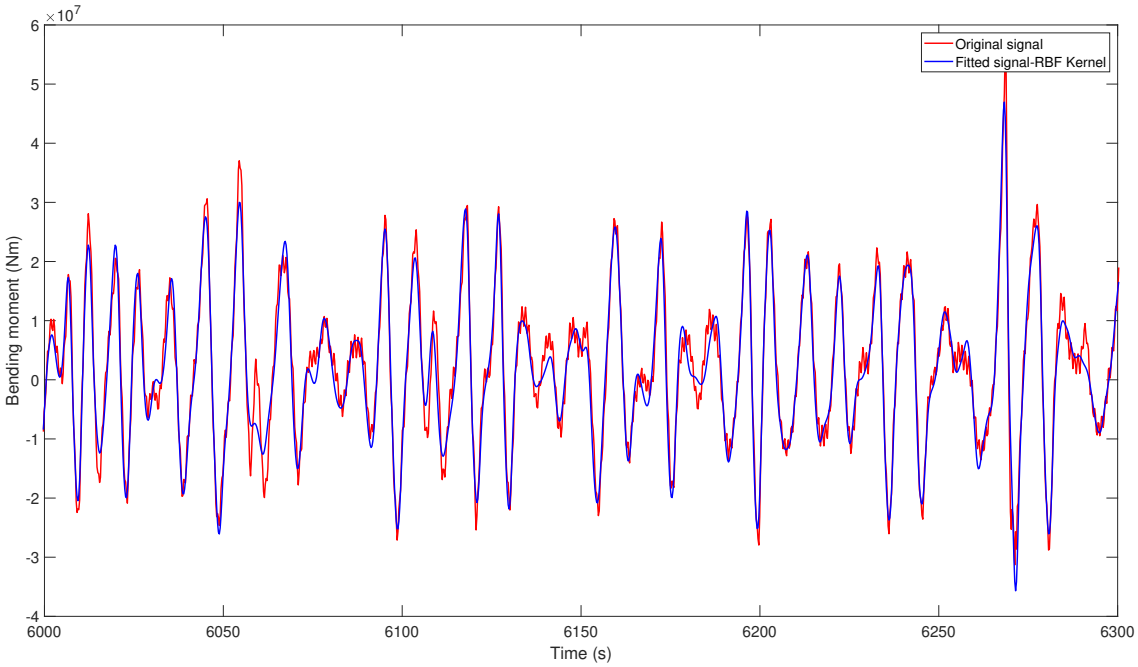

(a) Test results using features 1 in sea state 1

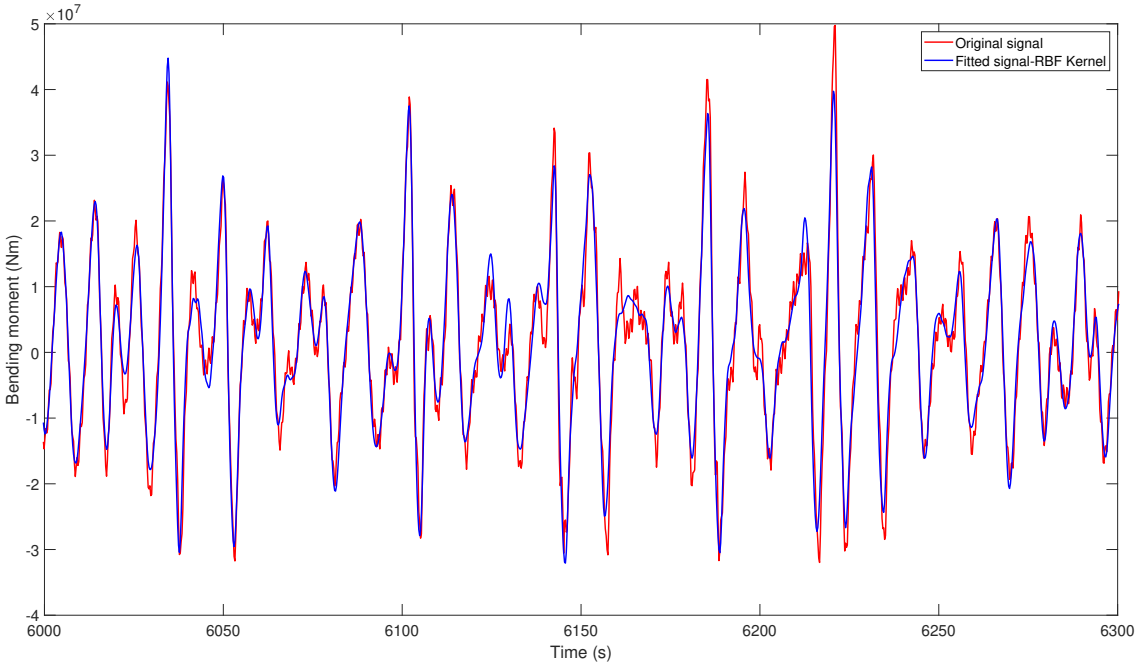

(b) Test results using features 2 in sea state 2

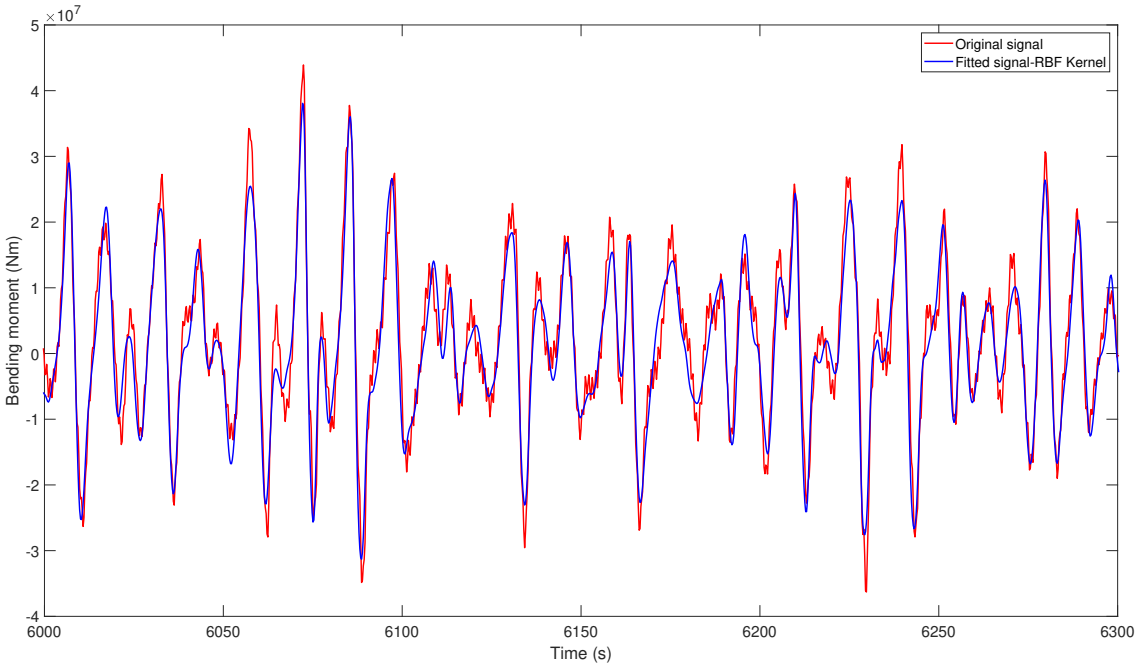

(c) Test results using features 3 in sea state 3

Figure 7-6: Comparison of the bending moment between the measured signal and fitted using SVM: test results

From these results, it can be seen that the SVM regression model has successfully captured the nonlinear physical relation between the features and the targets. The trained model using data from one sea state performs very well in the two other sea states which proves the robustness and generalization capability of the model. Furthermore, the different selection of features among ambient wave elevations or derived velocities and accelerations does not lead to a significant difference in performance. This is expected given the fact that the ambient wave elevations and derived wave kinematics are dependent via a convolution-type operation, intuitively justified by linear wave propagation theory. From the practical perspective, the ambient wave elevations are more accessible by direct measurements in experiments or simulations. In this sense, the SVM regression model effectively establishes a data-driven nonlinear transfer function between the ambient wave elevations and the nonlinear wave loads, derived from experimental measurements.

To further illustrate the performance of this model, Table 7.6 shows the error statistics between the simulated wave loads by fluid impulse theory (3.1) - (3.2)

and the measured experimental data. A comparison of the results of the SVM regression model with that of the FIT simulation in Table 7.4 $\sim$ Table 7.6, shows that the SVM regression model has a much better performance in predicting the overall statistics. The accurate prediction of the nonlinear wave load itself and its overall statistics (standard derivation and kurtosis) suggests that the model is a valuable and efficient tool for further use in design or simulation practice. For certain design or simulation purposes, the SVM regression model can be trained using a custom single representative sea state. Then a well trained SVM regression model can be applied to more realizations of the same sea state or other sea states for structural design or any other demanded analysis. The design of custom representative sea states for the purpose of training SVM nonlinear transfer functions will be the subject of future research.

Table 7.6: Error statistics of simulated wave loads by fluid impulse theory

Force modes	F_x	M_y
$\Delta\sigma$ for sea state 1	11.1%	13.04%
$\Delta\sigma$ for sea state 2	12.26%	11.48%
$\Delta\sigma$ for sea state 3	13.34%	10.16%
$\Delta\kappa$ for sea state 1	11.32%	51.34%
$\Delta\kappa$ for sea state 2	13.88%	55.87%
$\Delta\kappa$ for in sea state 3	18.39%	71.15%

To further explore a possible enhancement of the modeling accuracy of the SVM regression model, we have trained the model against the nonlinear residual force obtained as the difference of the experimental measurement and the simulated values from the fluid impulse theory, defined as:

$$F_{x-res} = F_{x-exp} - F_{x-FIT}, \quad M_{y-res} = M_{y-exp} - M_{y-FIT} \tag{7.5}$$

The training and testing process is exactly the same as the one using measured

experiment data directly as the target, so that we can compare the results. The same error statistics are shown in Table 7.7 and Table 7.8, which are also the statistics of the overall nonlinear wave loads by adding the subtracted fluid impulse theory contributions back. Figure 7-7 $\sim$ Figure 7-10 show examples of the comparison between the original measured signal and the signal with the SVM model of the residual force.

Comparing the results in Table 7.7 $\sim$ Table 7.8 to Table 7.4 $\sim$ Table 7.5, it can be seen that if the target is the residual component after the fluid impulse theory prediction is subtracted, the performance of the SVM model in predicting the overall statistics (both standard deviation and kurtosis) is better than the case when the overall nonlinear hydrodynamics is directly modeled by the SVM algorithm, without invoking the intermediate simulation by the fluid impulse theory. Since the load components accounted for by the fluid impulse theory are the dominant linear and the second-order contributions which have a clear physical origin, by subtracting these components, the SVM regression model is able to learn more complex information from the remaining load component which is dominated by strongly nonlinear free-surface and separated flow physics. It is conjectured that this the reason why fitting the residual components leads to a better predictive performance. The same process may be followed when the SVM algorithm is used to model more complex flows around marine structures. Well understood linear and second-order physics may be initially used via simulation using potential flow methods and subtracted from the overall measured nonlinear load or response being modeled. The residual load would then be modeled by the SVM algorithm along the lines of the present section. This topic will be the subject of a future study.

Table 7.7: Error statistics of horizontal force F_x by fitting the residual components

Features	Features 1	Features 2	Features 3
$\Delta\sigma$ for sea state 1	1.18%	1.05%	1.01%
$\Delta\sigma$ for sea state 2	0.64%	0.48%	0.01%
$\Delta\sigma$ for sea state 3	0.39%	0.30%	0.90%
$\Delta\kappa$ for sea state 1	2.10%	2.36%	1.80%
$\Delta\kappa$ for sea state 2	2.61%	2.43%	1.98%
$\Delta\kappa$ for in sea state 3	1.96%	0.96%	1.13%

Table 7.8: Error statistics of bending moment M_y by fitting the residual components

Features	Features 1	Features 2	Features 3
$\Delta\sigma$ for sea state 1	2.12%	2.31%	2.31%
$\Delta\sigma$ for sea state 2	1.63%	1.76%	1.86%
$\Delta\sigma$ for sea state 3	1.17%	1.03%	1.25%
$\Delta\kappa$ for sea state 1	3.06%	3.94%	3.80%
$\Delta\kappa$ for sea state 2	3.32%	3.43%	3.51%
$\Delta\kappa$ for in sea state 3	3.26%	1.65%	1.96%

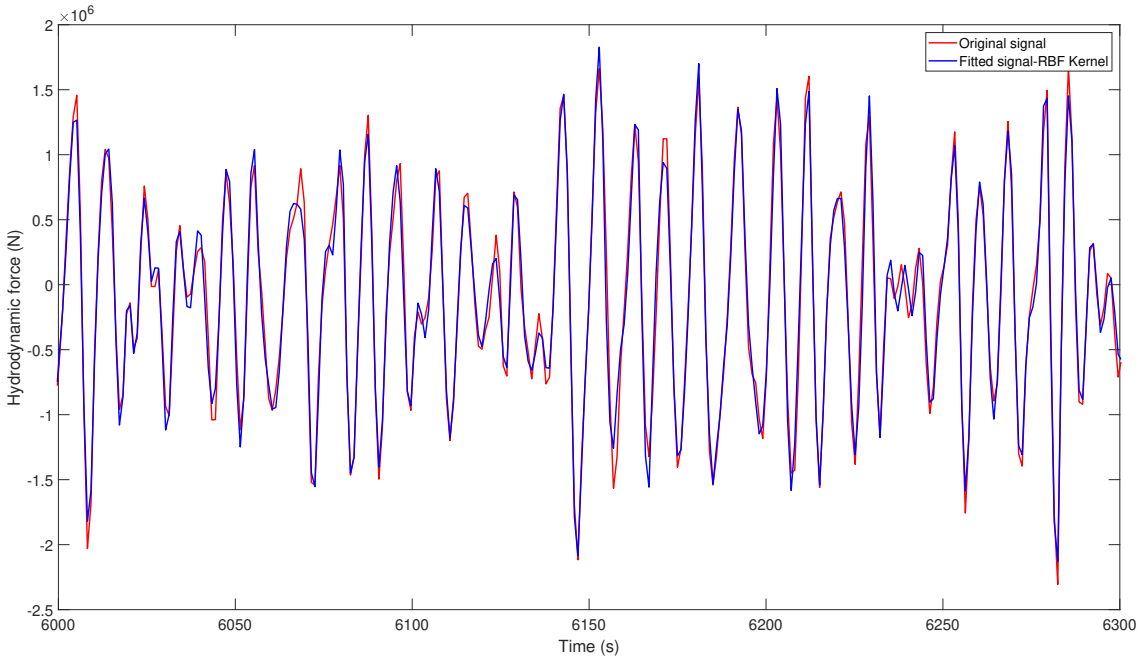

(a) Training results using features 1

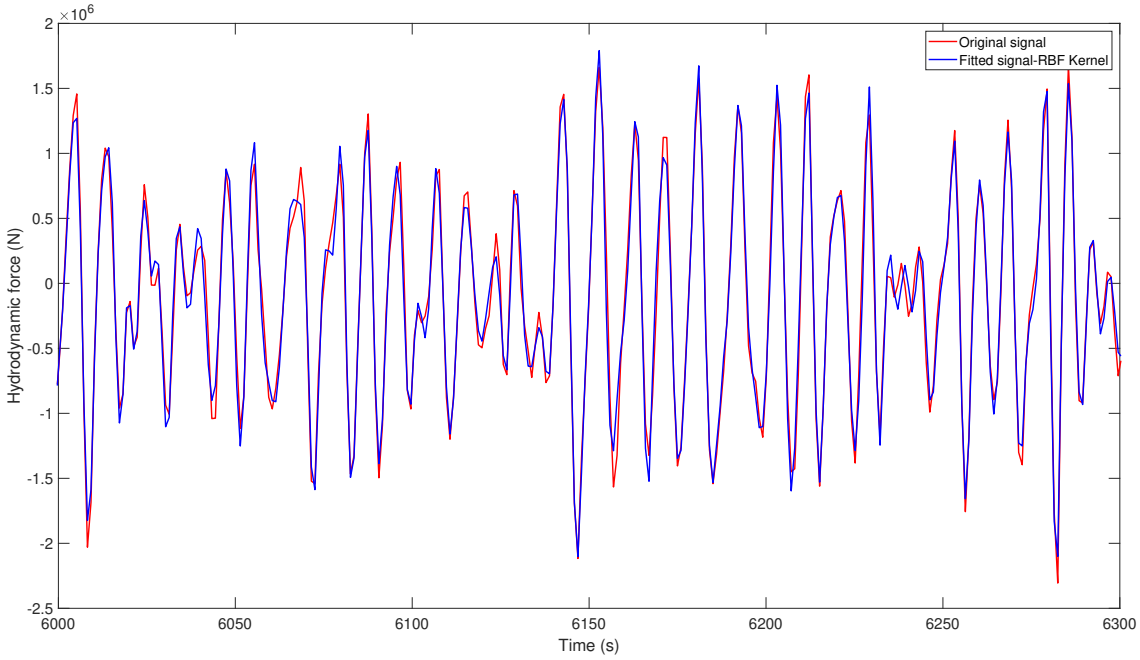

(b) Training results using features 2

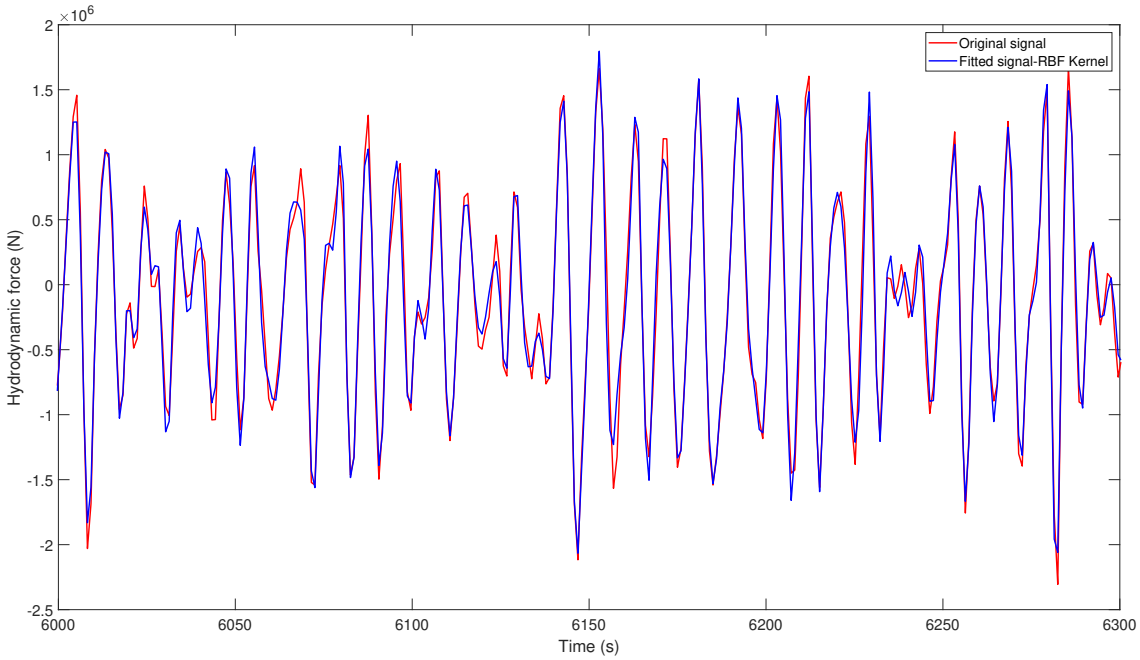

(c) Training results using features 3

Figure 7-7: Comparison of the horizontal force between the measured signal and fitting the residual components via SVM: training results

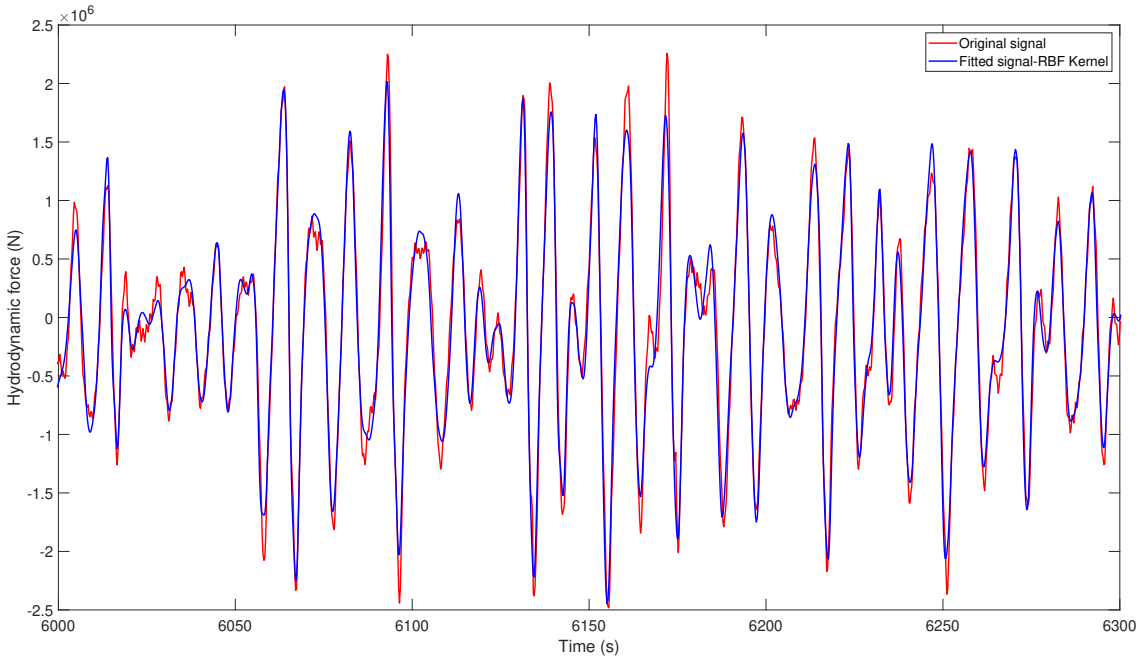

(a) Test results using features 1 in sea state 1

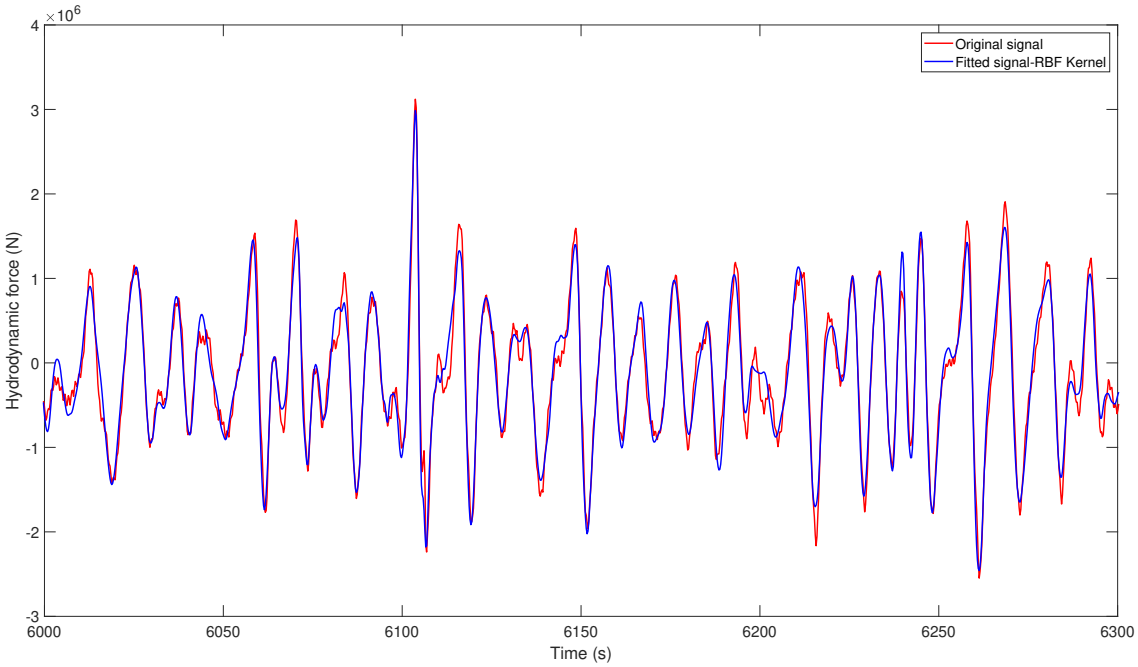

(b) Test results using features 2 in sea state 2

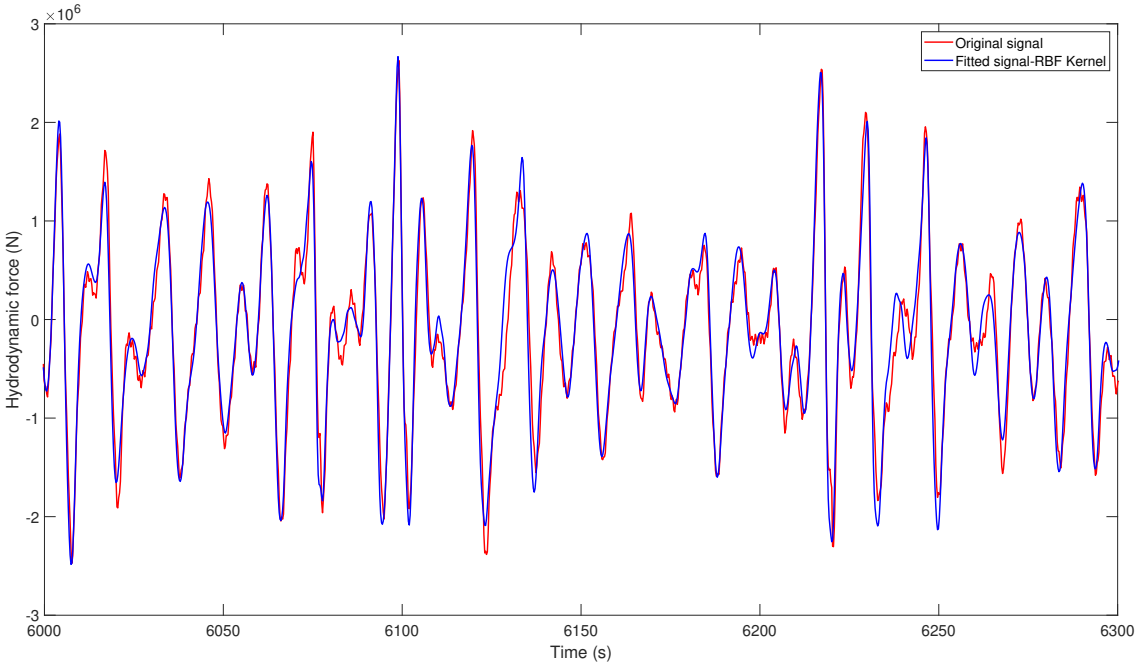

(c) Test results using features 3 in sea state 3

Figure 7-8: Comparison of the horizontal force between the measured signal and fitting the residual components via SVM: test results

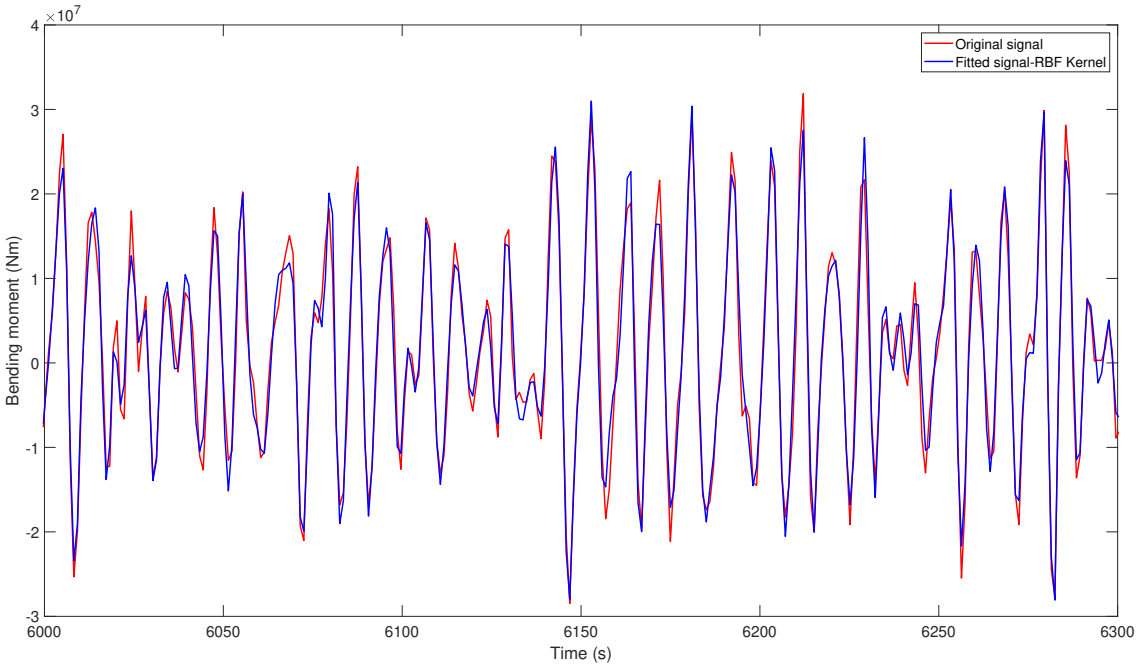

(a) Training results using features 1

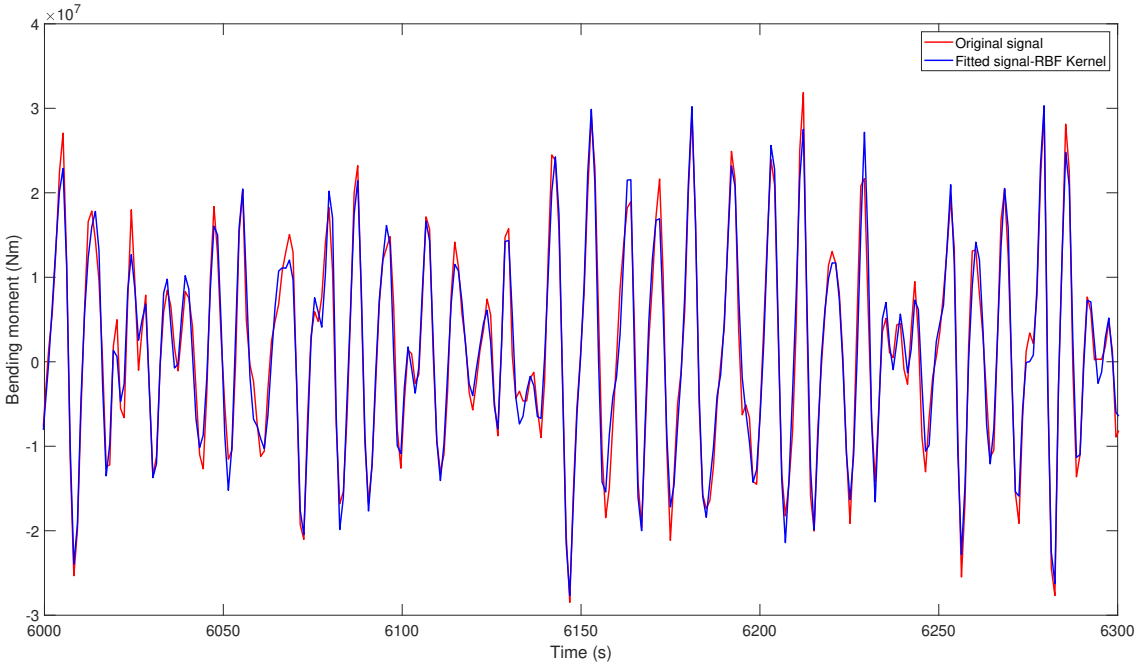

(b) Training results using features 2

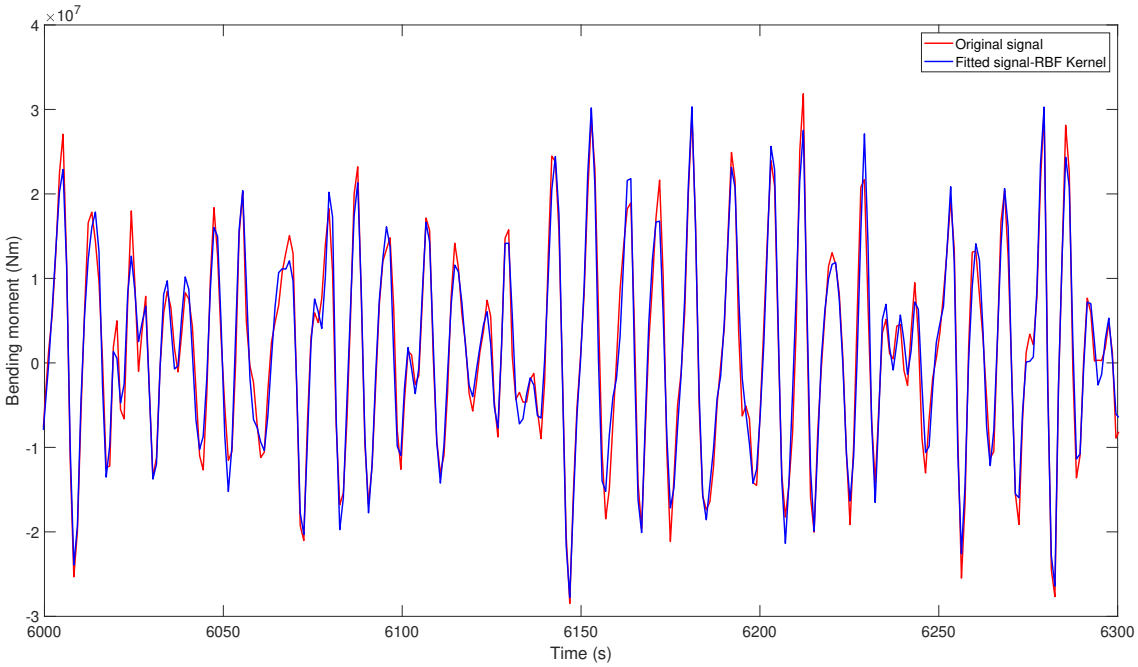

(c) Training results using features 3

Figure 7-9: Comparison of the bending moment between the measured signal and fitting the residual components via SVM: training results

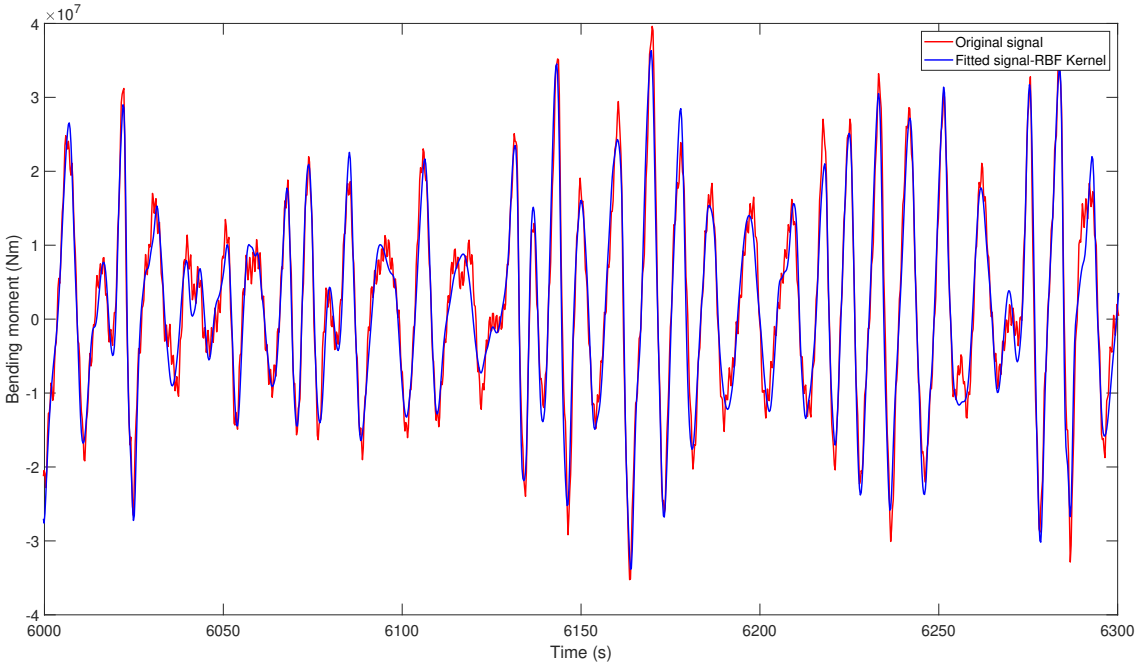

(a) Test results using features 1 in sea state 1

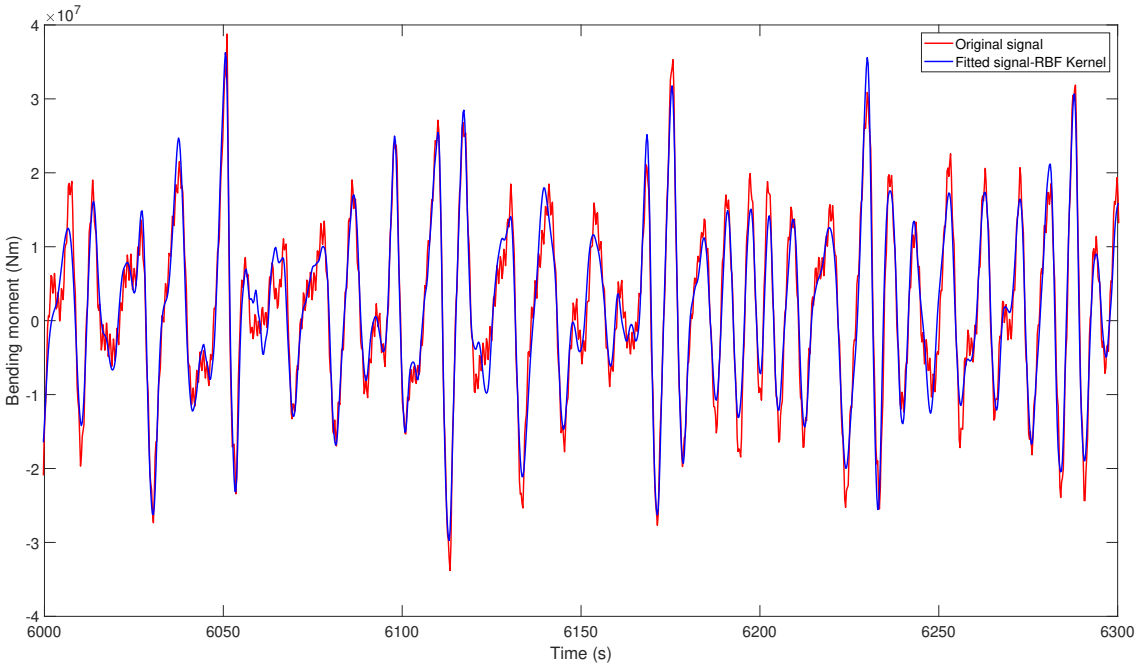

(b) Test results using features 2 in sea state 2

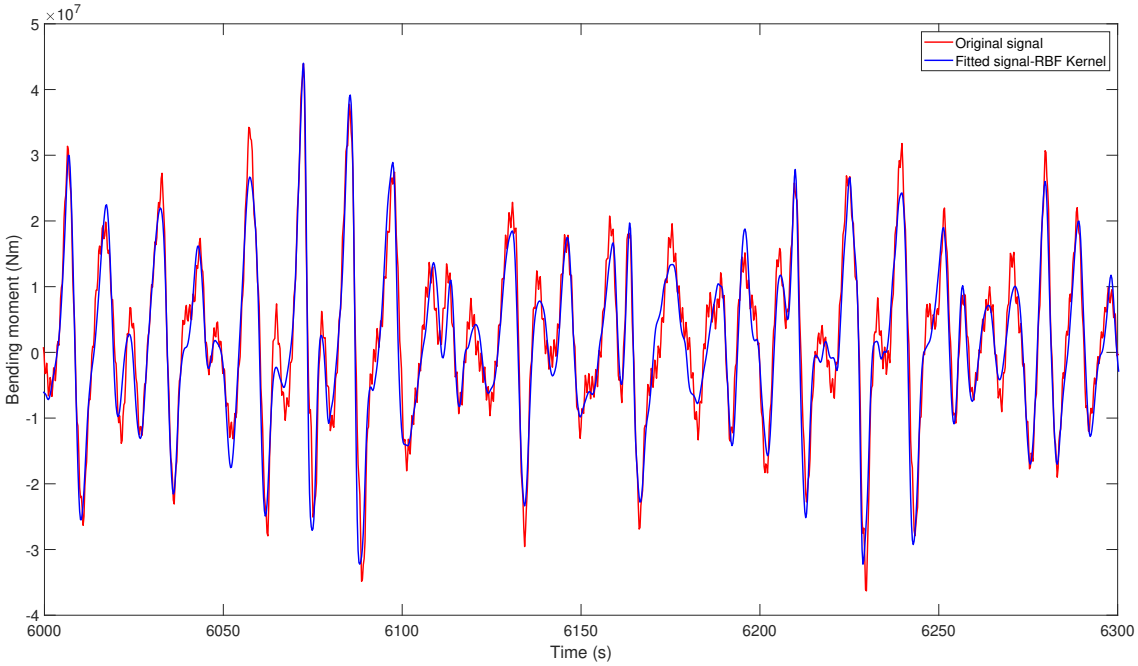

(c) Test results using features 3 in sea state 3

Figure 7-10: Comparison of the bending moment between the measured signal and fitting the residual components via SVM: test results

7.4 Conclusions and discussions

This chapter takes the experimental data for a fixed cylinder in finite depth water as the baseline dataset and considers the modeling of nonlinear wave loads by a machine learning SVM regression algorithm. The SVM regression model successfully establishes a deterministic nonlinear mapping function between the features (ambient wave kinematics in this study) to targets (nonlinear wave loads).

In essence, the kernel maps the association of the features of the target samples to those of the training samples in a hyperspace spanned by a set of basis functions which are the eigenfunctions of a positive definite kernel. The SVM algorithm predicts the target value of the quantity being modeled as a function of the kernel arguments which are the target and the features used during the training of the algorithm. Therefore, by randomly selecting a set of training samples from a representative sea state, the model achieves a very good generalization capability to predict unseen targets through the training process, combined with an optimization scheme which determines the width parameter or variance of the kernel and the regularization parameter which controls the magnitude of the SVM model error.

In this chapter, different combinations of features and targets are tested. The selection of the features, either using ambient wave elevations or derived wave velocities and accelerations or using all of them, does not affect the overall performance significantly. From the practical point of view, ambient wave elevations are a better choice as features since they are easy to measure or simulate in design cases. Furthermore, if some components of the hydrodynamic force are available through a reliable analytical or simulation model, fitting the residual force obtained by subtracting from the experimental measurements the modeled or simulated components, the SVM regression model was found to perform better in predicting the load statistics. This methodology may be extended to the study of a wide range of nonlinear wave-structure interaction problems where experimental measurements are available and potential flow models are not sufficiently accurate. In such cases residual loads may be derived and modeled by a SVM algorithm acting as a nonlinear

transfer function for strongly nonlinear free-surface and separated flow effects. This subject will be the topic of future research.

In this study, the representative sea states in the experiments were designed for ultimate limit state (ULS) tests, and the SVM regression model was established on the basis of available experiment data. However, this can be extended to more general cases if other specific targets are of interest, and specific representative sea states are carefully selected to provide samples to the SVM regression model. The design of the most appropriate representative seastate for the purpose of training a SVM algorithm for a particular application will be considered in a future study. It will enable the use of the algorithm as a nonlinear transfer function over a wide range of test sea states of interest in design practice, mitigating the need for and costs of systematic experiments.

Chapter 8

Conclusions and Future Work

8.1 Conclusions

Support vector machines is a powerful tool to mapping nonlinear relations from pertinent features to targets. The essence of SVM algorithms is to use kernels instead of an explicit set of basis functions in order to establish a more compact and generalized model based upon a set of explanatory variables or features. The selected kernel with optimized hyperparameters encodes the covariance structure between the features, which forms the basis of the learning algorithm that relates the quantity being modeled to the features, from the perspective of statistical learning theory.

This thesis establishes a framework that how we can use data from real-time measurements or data gathered from experiments and simulations to provide an alternative SVM model for physical modeling and practical engineering solutions. Specifically, two kinds of problems in ocean applications have been studied using this data-driven approach: the short-term wave prediction based on real-time measurements and its application to the advanced controls of renewable energy; the modeling of nonlinear hydrodynamics for ships and offshore platforms.

The SVM regression model is developed for real-time short-term forecast of wave elevations and wave excitation forces. The model is trained and validated using measurements from a wave tank test, which is considered as a good representative of the real ocean measurements. The SVM regression model is compared with a

conventional subspace method ESPRIT and proved to have better generalization capability and consistently better performance.

Following the successful prediction of the wave force over a finite horizon into the future, two model predictive control algorithms are then designed for the offshore floating turbines and wave energy converters separately since they target different objectives and have different system characteristics.

For the offshore floating wind turbines, on the basis of the ability to forecast the wave force over a finite horizon into the future, a deterministic finite-horizon LQR controller is designed to reduce the fore-aft tower base bending moment, especially the components excited by the wave force. The performance of the optimal control is effective and robust for the aimed load reduction comparing to the baseline speed regulator.

For the wave energy converters, the objective is to maximize the energy capture under stochastic seas. The objective along with the system dynamics as constraints have formed a convex quadratic programming problem that has been optimized. The cumulative power of the wave energy converter under two different sea states are shown increased significantly under this optimal control.

Furthermore, this thesis has provided an alternative approach using SVM regression to model the nonlinear hydrodynamic loads of ships and offshore platforms.

A series of simulations have been conducted for a rectangular barge with bilge keels using a 2D CFD solver. The CFD simulations are validated by comparing results of free decay tests and regular wave cases with experiments. On the basis of the data derived from validated CFD simulations, generalized SVM regression models are developed in this thesis that establish the mapping relation between the ship kinematics and wave elevation records and the nonlinear ship roll hydrodynamic loads. In essence, the kernel maps the association of the features of the target samples to those of the training samples in the hyperspace, and predicts the target value of the quantity being modeled as a function of the kernel arguments which are the target and training features. Therefore, by randomly selecting a set of training samples, the model achieves a very good generalization capability to predict unseen targets through

the training process combined with the optimization scheme which determines the width parameter of the kernel and the regularization parameter. In the context of ship roll hydrodynamics, this means that if high-fidelity CFD simulation records of ship roll hydrodynamics and motions in an irregular sea state are available, the SVM regression model established using the methodology presented in this provides a very good estimate of the nonlinear ship roll hydrodynamic loads. Both the linear kernel and Gaussian kernels are selected and tested in this study. The Gaussian kernel has better accuracy and generalization capability in fitting the force signal. However the linear kernel enables the use of linear frequency domain analysis and renders its use more efficient in design practice.

Other than CFD simulations, experiment data is also a reliable source to build up the data-driven model. A set of experiments for a shallow water bottom fixed cylinder are studied in the thesis to develop the SVM regression model of the nonlinear wave loads. The SVM regression model successfully establishes a deterministic nonlinear mapping function between the features (ambient wave kinematics in this study) to targets (nonlinear wave loads). Different combinations of features and targets are also tested in the thesis. The selection of the features, either using ambient wave elevations or derived wave velocities and accelerations or using all of them, does not affect the overall performance significantly. From the practical point of view, ambient wave elevations are a better choice as features since they are easy to measure or simulate in design cases. Furthermore, if some components of the hydrodynamic force are available through a reliable analytical or simulation model, fitting the residual force obtained by subtracting from the experimental measurements the modeled or simulated components, the SVM regression model was found to perform better in predicting the load statistics.

8.2 Future work

Using data-driven approach to solve physical-related problems is a promising field under development. It requires a good understanding of the physical problem as well

as the learning theory. A lot of work can be done in the future both in general topics of data-driven approaches or these specific topics that we have worked on.

For the short-term forecast of wave elevations and wave excitation forces, the general predictability of a sea state is a difficult question to answer in principle since real sea states are nonstationary and multi-directional. Therefore, we rely on the performance of the forecast algorithms in our work and do not address the more fundamental question of how forecastable real seastate elevations are. From the results of the two different sea states tested in this thesis, SVM model has pretty consistent performance with regard to different wave spectrum characteristics, but further study can be conducted to systematically explore the forecastability of different sea states under different data measurement qualities. The error in the forecasts generated by the algorithms consist of three components a) algorithm bias b) algorithm variance c) noise. Alternative algorithms introduce different bias vs variance tradeoffs, which is a topic that we do not address in this thesis as well. Ambient noise is unforecastable by any algorithm. The relative magnitude of these three sources of error is only possible after a systematic study among alternative algorithms and parameters within each algorithm. This topic is beyond the scope of the present thesis and will be addressed in the future work.

For the model predictive controls, in future work, more detailed sensitivity studies will be conducted in terms of the effects of the optimization horizon, controller update rate and predictor accuracy. Furthermore, on-line linearization and optimization techniques would be considered for better real-time implementations. The computational effort necessary to generate the forecasted signals needs to be addressed so that the on-line implementation can be achieved efficiently for sequential controller updates.

The control algorithm developed in this thesis for a stiff TLP floating wind turbine may be also implemented with minor modifications for "softer" floating wind turbine concepts like Spars and Semisubmersibles. For example, the effectiveness of blade-pitch controllers has been already demonstrated for the Hywind concept for the mitigation of responses at frequencies well below the peak of the wave spectrum.

Meanwhile, this approach is also promising for different control targets combined with the ability to forecast wind speed.

Similarly, this thesis takes a simple form of a heaving cylinder as an example to illustrate the feasibility and effectiveness of such a model predictive controller with the ability of forecasting the wave excitation force without going deep into the study of specific PTO mechanisms. Future work could be done by applying the same principle of model predictive control to various types of floater designs with different PTO systems.

For the modeling of nonlinear hydrodynamics for ships and offshore platforms, in a more general context, a stochastic SVM model may be developed which is trained to estimate the probability density function of the quantity being modeled conditional upon knowledge of the features. This extension will enable the modeling of the statistical properties of the nonlinear responses in a stochastic sea state when they are significantly affected by viscous and nonlinear free surface effects.

This methodology may also be extended to the study of a wide range of nonlinear wave-structure interaction problems where experimental measurements are available and potential flow models are not sufficiently accurate. In such cases residual loads may be derived and modeled by a SVM algorithm acting as a nonlinear transfer function for strongly nonlinear free-surface and separated flow effects.

In this study, the SVM regression model was established on the basis of available experiment or CFD data. However, this can be extended to more general cases if other specific targets are of interest, and specific representative sea states are carefully selected to provide samples to the SVM regression model. The design of the most appropriate representative seastate for the purpose of training a SVM algorithm for a particular application can be considered in the future. It will enable the use of the algorithm as a nonlinear transfer function over a wide range of test sea states of interest in design practice, mitigating the need for and costs of systematic experiments.

Bibliography

[1] Wave star. Technical report, Wave Star A/S, 2005.

[2] Wavedragon. Technical report, Wave Dragon, 2005.

[3] Pelamis wave. Technical report, Pelamis Wave Power, 2012.

[4] Global wind report 2015. Technical report, Global wind Energy Council, 2015.

[5] E. E. Bachynski, T. Kristiansen, and M. Thys. Experimental and numerical investigations of monopile ringing in irregular finite-depth water waves. *Applied Ocean Research*, 2017.

[6] C.C. Bassler. *Analysis and modeling of hydrodynamic components for ship roll motion in heavy weather*. PhD dissertation, Virginia Tech, 2013.

[7] H.B. Bingham. *Simulating ship motions in the time domain*. PhD dissertation, Massachusetts Institute of Technology, 1994.

[8] C.M. Bishop. *Pattern Recognition and Machine Learning*. Springer, 2006.

[9] B.E. Boser, I.M. Guyon, and V.N. Vapnik. A training algorithm for optimal margin classifiers. In *Proceedings of the Fifth Annual Workshop on Computational Learning Theory*, 1992.

[10] K. De Brabanter, P. Karsmakers, F. Ojeda, C. Alzate, J. De Brabanter, K. Pelckmans, B. De Moor, J. Vandewalle, and J.A.K. Suykens. *LS-SVMlab Toolbox User's Guide*. Katholieke Universiteit Leuven, 2010.

[11] T.K. Brekken. On model predictive control for a point absorber wave energy converter. In *PowerTech*, 2011.

[12] S. Butterfield, W. Musical, J. Jonkman, and P. Sclavounos. Engineering challenges for floating offshore wind turbines. In *2005 Copenhagen Offshore Wind Conference*, 2005.

[13] C.C.B. Casanovas. Advanced controls for floating wind turbines. Master's thesis, Massachusetts Institute of Technology, 2014.

[14] CD-Adapco. *STAR CCM+ User Guide*, 2019.

[15] A. Celisse. Optimal cross-validation in density estimation with the L^2-loss. *The Annals of Statistics*, 2014.

[16] X.B. Chen, L. Diebold, and Y. Doutreleau. New green-function method to predict wave-induced ship motions and loads, 2001.

[17] J.A. Cretel, G. Lightbody, G.P. Thomas, and A.W. Lewis. Maximisation of energy capture by a wave-energy point absorber using model predictive control. In *IFAC Proceedings*, 2011.

[18] N. Cristianini and J. Swane-Taylor. *Support Vector Machines*. Cambridge University Press, .

[19] J. Cross-Whiter, B.B. Ackers, D Arora, A. Wright, P. Fleming, M. Lackner, and S. Park. Load mitigation on floating offshore wind turbines with advanced controls and tuned mass dampers. In *Proceedings of the ASME 2018 1st International Offshore Wind Technical Conference*, 2018.

[20] S. Xavier de Souza, J.A.K. Suykens, J. Vandewalle, and D. Bolle. Coupled simulated annealing. *IEEE Transctions on Systems, Man and Cybernetics*, 2010.

[21] H. Drucker, C.C. Burges, L. Kaufman, and A.J. Smola. Support vector regression machines. *Neural Information Processing Systems*, 1996.

[22] K. Duan, S.S. Keerthi, and A.N. Poo. Evaluation of simple performance measures for tuning SVM hyperparameters. *Neurocomputing*, 2003.

[23] T. Duriez, S.L. Brunton, and B.R. Noack. *Machine learning control-taming nonlinear dynamics and turbulence*, volume 116 of *Fluid Mechanics and Its Applications*. Springer, 2017.

[24] J. Falnes. *Ocean Waves and Oscillating Systems*. Cambridge University Press, 2002.

[25] J. Falnes. Optimum control of oscillation of wave-energy converters. *International Journal of Offshore Polar Engineering*, 2002.

[26] J. Falzarano, A. Somayajula, and R. Seah. An overview of the prediction methods for roll damping of ships. *Ocean Systems Engineering*, 2015.

[27] G.E. Fasshauer and M.J. McCourt. Stable evaluation of gaussian rbf interpolants. *SIAM Journal on Scientific Computing*, 2011.

[28] P.A. Fleming, I. Pineda, M. Rossetti, A.D. Wright, and D. Arora. Evaluating methods for control of an offshore floating turbine. In *ASME 2014 33rd International Conference on Ocean, Offshore and Arctic Engineering*, 2014.

[29] F. Fusco and J.V. Ringwood. Short-term wave forecasting for real-time control of wave energy converters. *IEEE Transactions on Sustainable Energy*, 2010.

[30] N. Golyandina and A. Zhigljavsky. *Singular Spectrum Analysis for Time Series*. Springer, 2013.

[31] X. Gu and T. Moan. Long-term fatigue damage of ship structures under nonlinear wave loads. *Marine Technology*, 2002.

[32] J. Hals, J. Falnes, and T. Moan. Constrained optimal control of a heaving buoy wave-energy converter. *Journal of Offshore Mechanics and Arctic Engineering*, 2011.

[33] T. Hastie, R. Tibshirani, and J. Friedman. *The Elements of Statistical Learning*. Springer, 2009.

[34] G. James, D. Witten, T. Hastie, and R. Tibshirani. *An Introduction to Statistical Learning*. Springer, 2013.

[35] J. Jonkman, S. Buterfield, W. Musial, and G. Scott. Definition of a 5-mw reference wind turbine for offshore system development. Technical report, National Renewable Energy Laboratory, 2009.

[36] J.M. Jonkman and B.J. Jonkman. Fast modularization framework for wind turbine simulation. *Journal of Physics: Conference Series*, 2010.

[37] J.M. Jonkman and M.L. Buhl Jr. *FAST user's guide*. National Renewable Energy Laboratory, 2005.

[38] S.S. Kianejad, H. Enshaei, J. Duffy, N. Ansarifard, and D. Ranmuthugala. Ship roll damping coefficient prediction using cfd. *Journal of Ship Research*, 2019.

[39] A. Korber and R. King. Model predictive control for wind turbines. In *EWEC*, 2010.

[40] T. Kristiansen, E. E. Bachynski, F. Bickert, A. Hniche, V. Kocher, and A. Liandrat. Aspects in model testing of a monopile in steep waves. In *ASME 2017 36th International Conference on Ocean, Offshore and Arctic Engineering*, 2017.

[41] J. Laks, L.Y. Pao, A. Wright, N. Kelley, and B. Jonkman. Blade pitch control with preview wind measurements. In *Proc. 48th AIAA Aerospace Sciences Meeting*, 2010.

[42] J.H. Laks, L.Y. Pao, and A.D. Wright. Control of wind turbines: Past, present, and future. In *2009 American Control Conference*, 2009.

[43] T.J. Larsen and T.D. Hanson. A method to avoid negative damped low frequent tower vibrations for a floating, pitch controlled wind turbine. *Journal of Physcis: Conference Series*, 2007.

[44] C. Lee and J.Y. Lou. A direct boundary-element method for three-D wave diffraction and radiation problems. *Ocean engineering*, 1988.

[45] C.H. Lee and J.N. Newman. *WAMIT User Manual*. WAMIT, Inc, 2006.

[46] G. Li and M.R. Belmont. Model predictive control of sea wave energy converters – part i: A convex approach for the case of a single device. *Renewable Energy*, 2014.

[47] W. Luo, C.G. Soares, and Z. Zou. Parameter identification of ship maneuvering model based on support vector machines and particle swarm optimization. *Journal of Offshore Mechanics and Arctic Engineering*, 2016.

[48] Y. Ma, P.D. Sclavounos, J. Cross-Whiter, and D. Arora. Wave energy conversion using machine learning forecasts and model predictive control. *Renewable Energy*, 2018.

[49] E. Marino, C. Borri, and U. Peil. A fully nonlinear wave model to account for breaking wave impact loads on offshore wind turbines. *Journal of Wind Engineering and Industrial Aerodynamics*, 2011.

[50] S.R. Massel. *Ocean Surface Waves: Their Physics and Prediction*. World Scientific, 1996.

[51] D. Matha. Model development and loads analysis of an offshore wind turbine on a tension leg platform with a comparison to other floating turbine concepts. Master's thesis, University of Colorado - Boulder, 2009.

[52] M.R. Moarefzadeh and R.E. Melchers. Nonlinear wave theory in reliability analysis of offshore structures. *Probabilistic Engineering Mechanics*, 2006.

[53] A.R. Irkal Mohsin, S. Nallayarasu, and S.K. Bhattacharyya. Experimental and CFD simulation of roll motion of ship with bilge keel. In *International Conference on Computational and Experimental Marine Hydrodynamics*, 2014.

[54] A.R. Irkal Mohsin, S. Nallayarasu, and S.K. Bhattacharyya. CFD approach to roll damping of ship with bilge keel with experimental validation. *Applied Ocean Research*, 2016.

[55] P. Naaijen and E. Blondel-Couprie. Reconstruction and prediction of short-crested seas based on the application of a 3D-FFT on synthetic waves: Part1-Reconstruction. In *ASME 2013 31 st International Conference on Ocean, Offshore and Arctic Engineering*, 2012.

[56] A. Naess and T. Moan. *Stochastic dynamics of marine structures*. Cambridge University Press, 2012.

[57] D.E. Nakos. *Ship wave patterns and motions by a three dimensional Rankine panel method*. PhD dissertation, Massachusetts Institute of Technology, 1990.

[58] J.M. Newman and P.D. Sclavounos. The computation of wave loads on large offshroe structures. In *BOSS'88*, 1988.

[59] J.N. Newman. *Marine Hydrodynamics*. MIT press, 1977.

[60] S.R.K. Nielsen, Q. Zhou, M.M. Kramer, B. Basu, and Z. Zhang. Optimal control of nonlinear wave energy point converters. *Ocean Engineering*, 2013.

[61] J. Nocedal and S.J. Wright. *Numerical Optimization*. Springer, 2006.

[62] M.K. Ochi. *Ocean waves: the stochastic approach*. Cambridge University Press, 2005.

[63] E. Oguz, D. Clelland, A.H. Day, A Incecik, J.A. López, G. Sánchez, and G.G. Almeria. Experimental and numerical analysis of a TLP floating offshore wind turbine. *Ocean Engineering*, 2018.

[64] L.Y. Pao and K.E. Johnson. Control of wind turbines. *IEEE Control Systems*, 2011.

[65] V. Pereyra and G. Scherer. *Exponential data fitting and its applications*. Bentham Science Publishers, 2010.

[66] T. Perez and T.I. Fossen. A matlab toolbox for parametric identification of radiation-force models of ships and offshore structures. *Modeling, Identification and Control*, 2009.

[67] D. Potts and M. Tasche. Parameter estimation for exponential sums by approximate prony method. *Signal Processing*, 2010.

[68] A.A.E Price, D.I.M. Forehand, and A.R. Wallace. Time-span of future information necessary for theoretical acausal optimal control of wave energy converters. In *Control Conference*, 2009.

[69] S. Raach, D. Schlipf, F. Sandner, D. Matha, and P.W. Cheng. Nonlinear model predictive control of floating wind turbines with individual pitch control. In *2014 American Control Conference*, 2014.

[70] M. Raissi and G.E. Karniadakis. Hidden physics models: machine learning of nonlinear partial differential equations. *Journal of Computational Physics*, 2017.

[71] M. Raissi, Z. Wang, M.S. Triantafyllou, and G.M. Karniadakis. Deep learning of vortex-induced vibrations. *Journal of Fluid Mechanics*, 2019.

[72] S. Salcedo-Sanz, E.G. Ortiz-Garci, A.M. Perez-Bellido, A. Portilla-Figueras, and L. Prieto. Short term wind speed prediction based on evolutionary support vector regression algorithms. *Expert Systems with Applications*, 2011.

[73] T. Sarpkaya. Force on a circular cylinder in viscous oscillatory flow at low Keulegan-Carpenter numbers. *Journal of Fluid Mechanics*, 1986.

[74] S. Schløer. *Fatigue and extreme wave loads on bottom fixed offshore wind turbines. Effects from fully nonlinear wave forcing on the structural dynamics*. PhD dissertation, Technical University of Denmark, 2013.

[75] P.D. Sclavounos. Nonlinear impulse of ocean waves on floating bodies. *Journal of Fluid Mechanics*, 2012.

[76] P.D. Sclavounos and Y. Ma. Artificial intelligence machine learning in marine hydrodynamics. In *ASME 2018 37th International Conference on Ocean, Offshore and Arctic Engineering*, 2018.

[77] P.D. Sclavounos and Y. Ma. Wave energy conversion using machine learning forecasts and model predictive control. In *33st International Workshop on Water Waves and Floating Bodies*, 2018.

[78] P.D. Sclavounos, Y. Zhang, Y. Ma, and D.F. Larson. Offshore wind turbine nonlinear wave loads and their statistics. *Journal of Offshore Mechanics and Arctic Engineering*, 2019.

[79] J.A. Suykens and J. Vandewalle. Least squares support vector machine classifiers. *Neural Process. Lett*, 1999.

[80] T. Taniguchi, J. Umeda, T. Fujiwara, and H. Goto. Experimental and numerical study on point absorber type wave energy converter with linear generator. In *Proceedings of the ASME 2017 36th International Conference on Ocean, Offshore and Arctic Engineering*, 2017.

[81] T.B. Trafalis and H. Ince. Support vector machine for regression and applications to financial forecasting. In *IJCNN*, 2000.

[82] A. Rodriguez Tsouroukdissian, M. Lackner, J. Cross-Whiter, S.M. Park, P. Pourazarm, W. La Cava, and S. Lee. Smart novel semi-active tuned mass damper for fixed-bottom and floating offshore wind. In *Offshore Technology Conference*, 2016.

[83] L. Vita, G.K.V. Ramachandran, A. Krieger, M.I. Kvittem, D. Merino, J. Cross-Whiter, and B.B. Ackers. Comparison of numerical models and verification against experimental data, using pelastar tlp concept. In *ASME 2015 34th International Conference on Ocean, Offshore and Arctic Engineering*, 2015.

[84] J. Wang, J. Wu, and H. Xiao. Physics-informed machine learning approach for reconstructing reynolds stress modeling discrepancies based on DNS data. *Physical Review Fluids*, 2017.

[85] N. Wang, K.E. Johnson, A.D. Wright, and C.E. Carcangiu. Lidar-assisted wind turbine feedforward torque controller design below rated. In *2014 American Control Conference*, 2014.

[86] S. Wassermann, D.F. Feder, and M. Abdel-Masksoud. Estimation of ship roll damping—a comparison of the decay and the harmonic excited roll motion technique for a post panamax container ship. *Ocean Engineering*, 2016.

[87] E.N. Wayman, P.D. Sclavounos, S. Butterfield, J. Jonkman, and W. Musial. Coupled dynamic modeling of floating wind turbine systems. In *Offshore Technology Conference*, 2006.

[88] J. Yong and X.Y. Zhou. *Stochastic controls: Hamiltonian systems and HJB equations*. Springer, 1999.

[89] Y. Zhang. *Offshore Wind Turbine Nonlinear Wave Loads and Their Statistics*. PhD dissertation, Massachusetts Institute of Technology, 2019.

[90] Q. Zhong and R.W. Yeung. An efficient convex formulation for model-predictive control on wave-energy converters. In *Proceedings of the ASME 2017 36th International Conference on Ocean, Offshore and Arctic Engineering*, 2017.

[91] J. Zhou, J. Shi, and G. Li. Fine tuning support vector machines for short-term wind speed forecasting. *Energy Conversion and Management*, 2011.